

H α imaging of the *Herschel* Reference Survey

The star formation properties of a volume-limited, K-band-selected sample of nearby late-type galaxies^{*}

A. Boselli¹, M. Fossati^{2,3}, G. Gavazzi⁴, L. Ciesla⁵, V. Buat¹, S. Boissier¹, T. M. Hughes⁶

¹ Aix Marseille Université, CNRS, LAM (Laboratoire d'Astrophysique de Marseille) UMR 7326, 13388, Marseille, France e-mail: alessandro.boselli@lam.fr

² Universitäts-Sternwarte München, Schenierstrasse 1, D-81679 München, Germany

³ Max-Planck-Institut für Extraterrestrische Physik, Giessenbachstrasse, 85748, Garching, Germany e-mail: mfossati@mpe.mpg.de

⁴ Università di Milano-Bicocca, piazza della Scienza 3, 20100, Milano, Italy e-mail: Giuseppe.Gavazzi@mib.infn.it

⁵ University of Crete, Department of Physics, Heraklion 71003, Greece e-mail: ciesla@physics.uoc.gr

⁶ Sterrenkundig Observatorium, Universiteit Gent, Krijgslaan 281-S9, Gent 9000, Belgium e-mail: thomas.hughes@ugent.be

ABSTRACT

We present new H α + [NII] imaging data of late-type galaxies in the *Herschel* Reference Sample aimed at studying the star formation properties of a K-band-selected, volume-limited sample of nearby galaxies. The H α + [NII] data are corrected for [NII] contamination and dust attenuation using different recipes based on the Balmer decrement and the 24 μ m luminosities. We show that the H α luminosities derived with different corrections give consistent results only whenever the uncertainty on the estimate of the Balmer decrement is $\sigma[C(H\beta)] \leq 0.1$. We use these data to derive the star formation rate of the late-type galaxies of the sample, and compare these estimates to those determined using independent monochromatic tracers (FUV, radio continuum) or the output of spectral energy distribution (SED) fitting codes. This comparison suggests that the 24 μ m based dust extinction correction for the H α data might be non universal, and that it should be used with caution in all objects with a low star formation activity, where dust heating can be dominated by the old stellar population. Furthermore, because of the sudden truncation of the star formation activity of cluster galaxies occurring after their interaction with the surrounding environment, the stationarity conditions required to transform monochromatic fluxes into star formation rates might not always be satisfied in tracers other than the H α luminosity. In a similar way, the parametrisation of the star formation history generally used in SED fitting codes might not be adequate for these recently interacting systems. We then use the derived star formation rates to study the *SFR* luminosity distribution and the typical scaling relations of the late-type galaxies of the HRS. We observe a systematic decrease of the specific star formation rate with increasing stellar mass, stellar mass surface density, and metallicity. We also observe an increase of the asymmetry and smoothness parameters measured in the H α -band with increasing *SSFR*, probably induced by an increase of the contribution of giant HII regions to the H α luminosity function in star-forming low-luminosity galaxies.

Key words. Galaxies: spiral; galaxies: star formation; galaxies: fundamental parameters; galaxies: luminosity function; galaxies: clusters: general; galaxies: photometry

1. Introduction

Star formation is a key process in the study of galaxy evolution. Stars are formed within giant molecular clouds through the collapse of the gaseous component. Massive stars, once formed, produce and inject metals into the interstellar medium, that later aggregate to form dust (Valiante et al. 2009). The various ingredients of the interstellar medium, including those produced during stellar evolution, all contribute in regulating the matter cycle in galaxies. The formation of the molecular gas occurs primarily on dust grains (Hollenbach & Salpeter 1971; Wolfire et al. 2008). Dust also absorbs the interstellar radiation field, and is thus an important parameter in the cooling process of the gas (Bakes & Tielens 1994; Wolfire et al. 1995; Hollenbach & Tielens 1997). Massive stars can also inject a large amount of kinetic energy into the interstellar medium, favoring the ionisation of the surrounding gas and the dissociation of the molecular component,

but also cloud-cloud collisions important in the process of star formation.

The hydrogen recombination lines are due to the cascade of electrons captured by the hydrogen nucleus once photoionised by the far-UV radiation ($\lambda < 912 \text{ \AA}$) in HII regions. This highly energetic UV radiation is mainly emitted by massive ($m_{star} > 8 M_{\odot}$) O-B stars, whose life on the main sequence is very short ($< 10^7$ yr). Their presence thus indicates recent episodes of star formation. The H α Balmer line ($\lambda 6563 \text{ \AA}$) is the brightest of the hydrogen recombination lines. This line is easily accessible from ground based facilities in local galaxies since it is located in the visible spectral domain. Under specific conditions, its emission is proportional to the number of newly formed stars and can thus be used as a direct tracer of star formation (Kennicutt et al. 1994; Kennicutt 1998; Boselli et al. 2001). Star formation rates are proportional to H α luminosities if the star formation activity of the targets is constant over a timescale at least as long as the time that the ionising stars spend on the main sequence ($\sim 10^7$ yr). Only under these conditions does the number of stars that leave the main sequence equal that of newly formed stars. The

^{*} Tables 1-7 are also available in electronic form at the CDS via anonymous ftp to cdsarc.u-strasbg.fr(130.79.128.5) or via http://cdsweb.u-strasbg.fr/cgi-bin/qcat?J/A+A/

constant of proportionality between the $H\alpha$ luminosity and the star formation rate depends on the initial mass function (IMF), on the metallicity, and on several assumptions in the photoionisation models, and can be estimated using population synthesis models.

$H\alpha$ luminosities, however, can be converted into star formation rates only once corrected for dust attenuation. This is generally done using the Balmer decrement (Lequeux et al. 1981), determined by comparing the observed $H\alpha/H\beta$ flux ratio to the value expected for the typical conditions in HII regions (2.86, Case B; Osterbrock & Ferland 2006). Spectroscopic observations can be used for this purpose. An intermediate spectral resolution ($R \sim 1000$) is required to separate the emission of the $H\alpha$ line from that of the two bracketing [NII] lines ($\lambda\lambda$ 6548, 6584 Å), while good signal-to-noise is necessary to determine the underlying Balmer absorption produced by the stellar atmosphere of young stars. The accurate determination of the Balmer decrement is thus non trivial, in particular in normal nearby galaxies characterised by a relatively low or moderate activity of star formation. Indeed, in these galaxies the intensity of the emission lines, and in particular that of $H\beta$, is relatively low and often comparable to the intensity of the underlying absorption. It is thus fundamental to understand up to which limit in signal-to-noise the Balmer decrement can be accurately determined without introducing systematic errors in the estimate of the star formation rate (Groves et al. 2012). This is also crucial to quantify the uncertainties on the determination of the dust attenuation of galaxies up to $z \sim 1$, which is often estimated using higher order Balmer lines ($H\beta$, $\lambda 4861$ Å; $H\gamma$, $\lambda 4340$ Å; $H\delta$, $\lambda 4101$ Å). These lines are characterised by a lower intensity and a higher underlying absorption with respect to $H\alpha$ (e.g. Momcheva et al. 2013). It is also critical to estimate whether the exclusion of objects with low $H\beta$ emission from the analysis of the star formation properties of complete samples of galaxies does not bias the results. Galaxies with low $H\beta$ emission, indeed, are objects with a low star formation activity and/or high dust attenuation.

To overcome these technical difficulties, different tracers have been proposed in the literature either for correcting the observed $H\alpha$ luminosities or for measuring star formation rates (e.g. Kennicutt 1998; Kennicutt et al. 2009; Hao et al. 2011; Kennicutt & Evans 2012). Using the same arguments as for the $H\alpha$ line, any tracer of the young stellar population can be converted, under some assumptions, into star formation rates. The most widely used tracers are the dust-corrected far-ultraviolet (FUV) and the radio continuum luminosities. At 20 cm, the radio continuum emission of galaxies is mainly due to the synchrotron emission of relativistic electrons spinning in weak magnetic fields (e.g. Lequeux 1971; Condon 1992). These electrons are accelerated in supernovae remnants, and are thus tightly related to the youngest stellar populations of galaxies. The FUV and radio continuum luminosities can be converted into star formation rates whenever the star formation activity of galaxies is constant over $\sim 10^8$ yrs, a timescale ten times longer than necessary when using the $H\alpha$ luminosity, making these tracers more uncertain in objects suddenly changing their star formation activity with time. When multifrequency data are available, the star formation activity of galaxies can also be determined through the fitting of their spectral energy distribution (SED) with specific codes. The accuracy of this technique, which has the advantage of providing a consistent estimate of the contribution of dust attenuation to the stellar emission when UV, optical and infrared data are available, depends on the sampling of the different photometric bands. It also depends

on the chosen parametrisation of the star formation history of the galaxies, which is generally done with simple empirical relations. Compared to monochromatic tracers, this method has the advantage to account for possible variations of the star formation history of galaxies, even though these variations are not easily constrained (e.g. Buat et al. 2014).

The direct comparison of these different tracers is therefore crucial for identifying and quantifying their limits and uncertainties, as well as for understanding whether the use of a specific correction or calibration can introduce important systematic biases in the derived star formation rates (Kennicutt 1998; Kennicutt & Evans 2012; Kennicutt et al. 2009; Calzetti et al. 2007, 2010; Salim et al. 2007; Lee et al. 2009; Boselli et al. 2009). The comparison of these tracers must be carried out on well defined samples of galaxies spanning the widest possible range in the parameter space and having the largest possible data coverage over all wavelengths (e.g. Buat et al. 2014).

The *Herschel* Reference Sample (Boselli et al. 2010) is ideal for this purpose. Composed of 323 nearby galaxies, this sample is volume-limited ($15 \leq dist \leq 25$ Mpc) and K-band-selected, which roughly corresponds to a stellar mass selection (Gavazzi et al. 1996). It also includes galaxies of all morphological types in the stellar mass range $5 \times 10^8 \leq M_{star} \leq 10^{11} M_{\odot}$. The sample has been defined to study the physical properties of the interstellar medium, the star formation process, and the effects of the environment on galaxy evolution in normal galaxies. It thus includes galaxies in different density regions, from the sparse field to the rich core of the Virgo cluster. We have been collecting multifrequency data covering the entire electromagnetic spectrum, including UV *GALEX* and visible SDSS data (Boselli et al. 2011; Cortese et al. 2012), near- (2MASS), mid- and far-IR *WISE* (Ciesla et al. 2014), *Spitzer* (Bendo et al. 2012; Ciesla et al. 2014), and *Herschel* (Ciesla et al. 2012; Cortese et al. 2014) data, while radio continuum data at 20 cm are available from the NVSS survey (Condon et al. 1998). Medium resolution ($R \sim 1000$) integrated spectroscopic data are also available (Boselli et al. 2013), as well as HI and CO data (Boselli et al. 2014a). The purpose of this article is to use this unique sample and set of data to determine and compare different tracers of star formation, derived from both monochromatic luminosities and SED fitting techniques, in order to determine their range of validity, their strengths and limits. We then use these data to trace the statistical properties of the star formation activity of the late-type galaxies of the sample, including their star formation rate distribution, scaling relations, and structural and morphological CAS parameters (Conselice 2003), for both normal and cluster galaxies. There are indeed strong indications that the star formation properties of cluster galaxies are strongly affected by the hostile environment in which they reside (e.g. Boselli & Gavazzi 2006, 2014).

The paper is structured as follows: in section 2 we describe the sample, in section 3 the observations and in section 4 the data reduction. The data are analysed in section 5 and 6, and the conclusions summarised in section 7. In three different appendices, we present the new spectroscopic data determined using the GANDALF code, the radio continuum data at 20 cm taken from the literature and used in the analysis, and we list the recipes used to convert observed luminosities into star formation rates. We limit our analysis to the late-type galaxies of the sample (Sa-Im-BCD). It is indeed known that the $H\alpha$ emission in early-types (E-S0) does not necessary come from the photoionisation of the gas by the young stellar populations (several of these early-type objects are also strong X-ray emitters). Furthermore, their FUV

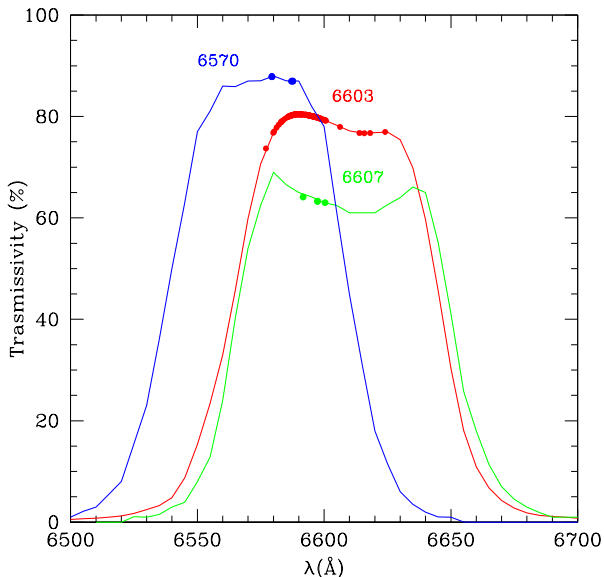


Fig. 1. Transmissivity of the ON-band (6603, 6607, 6570 Å) filters. Points mark the throughput at the wavelength corresponding to the $H\alpha$ line at the redshift of the target galaxies.

emission is generally due to very evolved stars (O’Connell 1999; Boselli et al. 2005) not associated to any event of star formation, while their radio continuum emission might be dominated by the contribution of the central AGN (M87 and M84 are well known powerful radio galaxies).

2. The sample

The observed sample is composed of those HRS late-type galaxies without $H\alpha$ imaging data available in the literature (see Table 1). It also includes a few objects with $H\alpha$ + $[NII]$ data from aperture photometry (Kennicutt & Kent 1983; Romanishin 1990). Combined with $H\alpha$ + $[NII]$ imaging data available in the literature, mostly gathered during our previous survey of the Virgo cluster (Boselli & Gavazzi 2002; Boselli et al. 2002a; Gavazzi et al. 2002, 2006), the HRS sample is now complete at the 87% level, and to 98% if limited to late-type galaxies. Because of the presence of bright stars close to the target, whose reflection causes unwanted extended low surface brightness structures on the images, six objects could not be observed. The HRS sample is listed in Table 1, arranged as follows:

- Column 1: *Herschel* Reference Sample (HRS) name, from Boselli et al. (2010).
- Column 2: Zwicky name, from the Catalogue of Galaxies and of Cluster of Galaxies (CGCG; Zwicky et al. 1961-1968).
- Column 3: Virgo Cluster Catalogue (VCC) name, from Binggeli et al. (1985).
- Column 4: Uppsala General Catalog (UGC) name (Nilson 1973).
- Column 5: New General Catalogue (NGC) name (Dreyer 1888).
- Column 6: Index Catalogue (IC) name (Dreyer 1895).
- Columns 7 and 8: J2000 right ascension and declination, from NED.
- Column 9: Morphological type, from NED, or from our own classification if not available.

- Column 10: Distance, in Mpc. Distances have been determined from the recessional velocity assuming a Hubble constant $H_0 = 70 \text{ km s}^{-1} \text{ Mpc}^{-1}$ for galaxies outside the Virgo cluster, and assumed to be 17 Mpc for galaxies belonging to Virgo, with exception to those located in the Virgo cluster B substructure (23 Mpc; Gavazzi et al. 1999).
- Column 11: Stellar mass, from Cortese et al. (2012a), determined following the prescription of Zibetti et al. (2009) based on the i -band luminosity and $g - i$ mass-to-light ratio. For galaxies without SDSS g and i -band data (11 objects, marked with ^a in Table 1), stellar masses have been computed using the prescription of Boselli et al. (2009) based on the H-band luminosity and $B - H$ mass-to-light ratio.
- Column 12: g -band optical isophotal diameter (24.5 mag arcsec⁻²), from Cortese et al. (2012a). For the HRS galaxies without SDSS images, the g -band isophotal diameter was determined from the relation $r_{24.5}(g) = 0.871(\pm 0.017)r_{25}(B) + 6.041(\pm 2.101)$, where $r_{25}(B)$ is the radius given in NED (Boselli et al. 2014a).
- Column 13: inclination of the galaxy, determined using the prescription based on the morphological type described in Haynes & Giovanelli (1984) and the i -band ellipticity given in Cortese et al. (2012a).
- Column 14: Heliocentric radial velocity (in km s^{-1}), from HI data when available (Boselli et al. 2014a), otherwise from NED.
- Column 15: Cluster or cloud membership, from Gavazzi et al. (1999) for Virgo and Tully (1987) or Nolthenius (1993) whenever available, or from our own estimate (Boselli et al. 2010).
- Column 16: Code to indicate whether $H\alpha$ + $[NII]$ data are available (1) or not (0).

3. Observations

$H\alpha$ + $[NII]$ narrow band imaging of 138 HRS late-type galaxies has been obtained during different observing runs, from 2006 to 2012, with the 2.1m and the 1.5m telescopes at San Pedro Martir (SPM; Baja California, Mexico). These galaxies have been observed as fillers during an $H\alpha$ + $[NII]$ imaging survey of HI selected galaxies in the nearby universe ($H\alpha 3$; Gavazzi et al. 2012; Gavazzi et al. 2015b). All galaxies observed at the 2.1m SPM telescope (133 objects) were observed through the narrow band interferometric filter $\lambda=6603 \text{ \AA}$, $\Delta\lambda 70 \text{ \AA}$ (ON-band frame) whose spectral coverage is optimal for HRS objects with recessional velocity $160 < vel < 3500 \text{ km s}^{-1}$. The 5 galaxies done at the 1.5m telescope have been observed using the $\lambda=6607 \text{ \AA}$, $\Delta\lambda 61 \text{ \AA}$ (ON-band frame) and the $\lambda=6570 \text{ \AA}$, $\Delta\lambda 66 \text{ \AA}$ filters (see Fig. 1). Given the relatively large width of these filters, the present $H\alpha$ images include the contribution from the $[NII]$ lines. The stellar continuum (OFF-band frame) was gathered through a broad-band r -Gunn filter. Typical integration times were 15-20 minutes ON-band, generally split into shorter exposures for cosmic ray removals, and 4 minutes OFF-band. The observations were generally taken during photometric conditions, with a seeing of ~ 1.5 - 3.0 arcsec (see Gavazzi et al. 2012; Gavazzi et al. 2015b). Photometric calibrations were secured with the observation of two standards, Feige34 and Hz44, from the catalogue of Massey et al. (1988), observed every 2-3 hours with integrations of 1-2 minutes. The repeated observations of the standard stars have shown that the photometric accuracy (zero point) was stable within $< 5\%$.

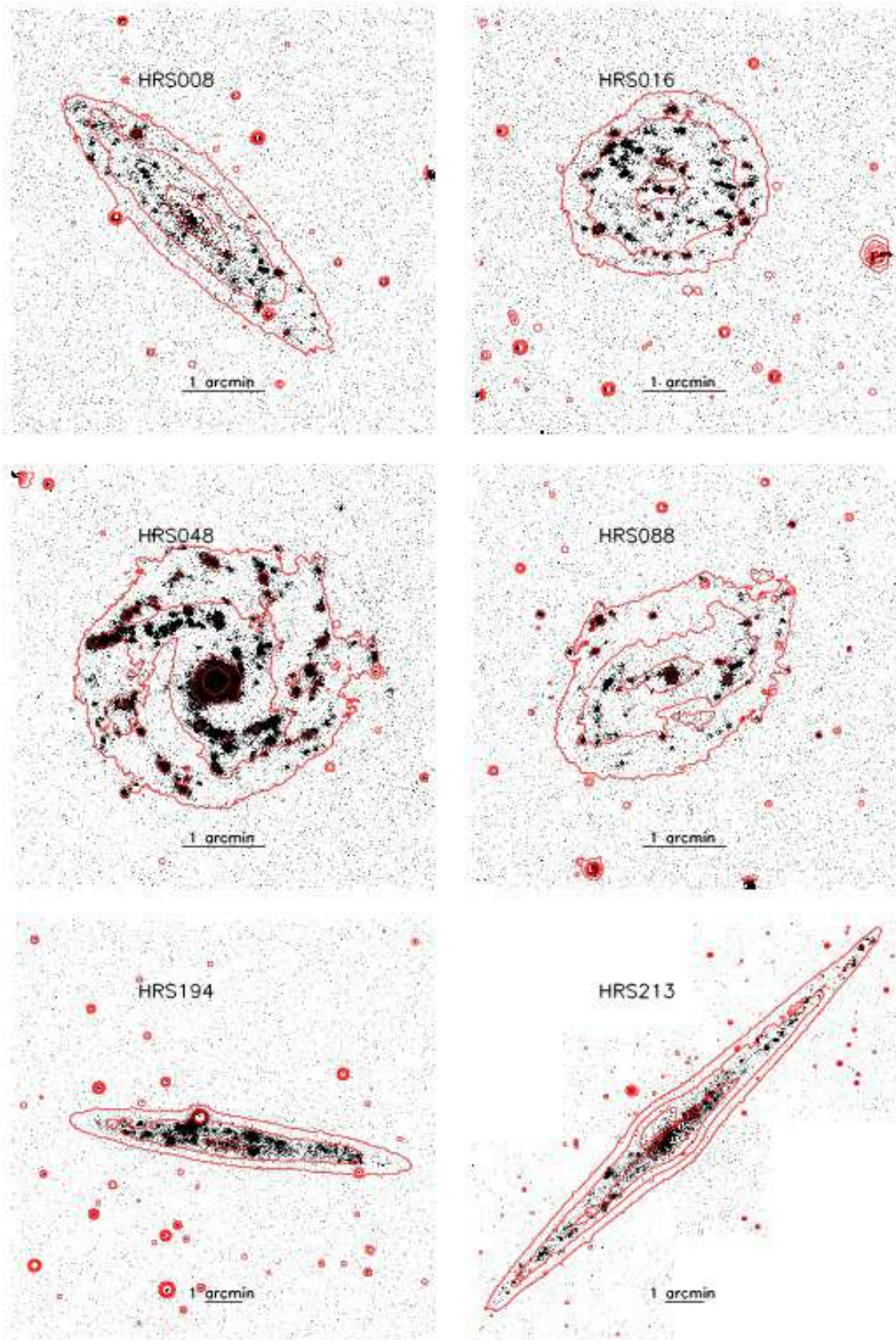


Fig. 2. Images of 6 galaxies observed in $H\alpha$. The OFF-band contours are logarithmically drawn at 3 , 9 , 27 , and $81 \times \sigma$ of the sky background in the OFF frame and the grey scales represent the NET flux intensity between 1 and $5 \times \sigma$ of the sky in the NET frame. A 1 arcmin bar is given on all images. North is up and east is to the left.

4. Data reduction

The obtained frames were reduced following the same procedures as described in our previous papers (e.g. Gavazzi et al. 2002, 2012). These are standard procedures generally used in the literature (e.g. Waller 1990; Koopmann et al. 2001; James et al. 2004; Kennicutt et al. 2008). These procedures are based on IRAF STSDAS¹ reduction packages. Each image was bias subtracted and divided by the median of several flat fields obtained on empty sky regions during twilight. When three images in the same filter were available, a median combination of the images allowed cosmic ray removal. For single images, cosmic ray removal was secured using the COSMICRAY IRAF task and by direct inspection of the frame. Unwanted foreground stars were removed on each ON- and OFF-band frame. The sky background was measured in concentric, uncontaminated annuli around the object, and subtracted from the flat-fielded images.

Total counts in the two frames have been obtained by integrating the pixel counts over the area covered by each galaxy, as derived by the optical major and minor diameters. If C_{ON} and C_{OFF} are the integrated pixel counts in the ON and OFF-band filter respectively, $C_{NET} = C_{ON} - nC_{OFF}$, then the NET flux in the observed $H\alpha+[NII]$ line is given by:

$$F(H\alpha + [NII])_o \quad [\text{erg cm}^{-2}\text{sec}^{-1}] = 10^{Zp} \frac{C_{NET}}{\text{TR}_{ON}(H\alpha)} \quad (1)$$

and the equivalent width by:

$$H\alpha + [NII]E.W._o \quad [\text{\AA}] = \frac{\int R_{ON}(\lambda)d\lambda}{R_{ON}(H\alpha)} \frac{C_{NET}}{nC_{OFF}} \quad (2)$$

where T is the integration time (sec), 10^{Zp} is the ON-band zero point ($\text{erg cm}^{-2}\text{sec}^{-1}$) corrected for atmospheric extinction and $R_{ON}(\lambda)$ is the transmissivity of the ON-filter at the wavelength of the redshifted $H\alpha$ line (Fig. 1). Eq. (2) shows that the $H\alpha$ equivalent width does not depend on Zp , but only on the normalization constant n measured using several stars in both frames, and so it can also be estimated in marginal photometric conditions. The normalisation factor n has been multiplied by ~ 0.95 as indicated by Spector et al. (2012) to account for the fact that field stars are generally redder than the stellar continuum of the observed galaxies.

We corrected for the contamination of the $H\alpha+[NII]$ line emission in the broad band filter (OFF-band) following the prescription given in Boselli et al. (2002a):

$$\begin{aligned} F(H\alpha + [NII])_c &= \\ &= F(H\alpha + [NII])_o \left(1 + \frac{\int R_{ON}(\lambda)d\lambda}{\int R_{OFF}(\lambda)d\lambda}\right) \end{aligned} \quad (3)$$

and

$$\begin{aligned} H\alpha + [NII]E.W._c &= \\ &= H\alpha + [NII]E.W._o \left(1 + \frac{H\alpha + [NII]E.W._o}{\int R_{OFF}}\right) \times \\ &\quad \left(1 + \frac{\int R_{ON}(\lambda)d\lambda}{\int R_{OFF}(\lambda)d\lambda}\right) \end{aligned} \quad (4)$$

¹ IRAF is distributed by the National Optical Astronomy Observatory, which is operated by the Association of Universities for Research in Astronomy (AURA) under cooperative agreement with the National Science Foundation.

where $F(H\alpha + [NII])_o$ and $H\alpha + [NII]E.W._o$ are the observed values (from eq. (1) and (2)), $F(H\alpha + [NII])_c$ and $H\alpha + [NII]E.W._c$ the corrected ones, and R_{ON} and R_{OFF} the transmissivity of the ON band and r -Gunn filters.

For extended sources, the dominant source of error is the variation of the background on angular scales similar to the size of the source on the plane of the sky. The error thus depends primarily on the quality of the flat-fielding. We measured the background in several regions comparable with the size of the galaxies and determined that its fluctuation (per pixel) is 10 % of the purely statistical rms on the individual pixels. The total uncertainty on the ON and OFF counts is thus proportional to the area A (in pixels) covered by each galaxy, estimated from the optical major and minor axes, a and b :

$$\sigma_{ON} = 0.1 \text{ rms}_{ON} A$$

$$\sigma_{OFF} = 0.1 \text{ rms}_{OFF} A$$

which add up to:

$$\sigma_{NET} = \sqrt{(\sigma_{ON})^2 + (\sigma_{OFF})^2 + (0.1 C_{NET})^2}$$

The term $(0.1 C_{NET})^2$ accounts for the uncertainty on the photometric calibration.

The errors on the $H\alpha + [NII]$ flux σ_F and equivalent width $\sigma_{E.W.}$ are finally:

$$\sigma_F = \frac{F(H\alpha)}{C_{NET}} \sigma_{NET} \quad (5)$$

$$\sigma_{E.W.} = \frac{\int R_{ON}(\lambda)d\lambda}{R_{ON}(H\alpha)(nC_{OFF})^2} \sqrt{(nC_{OFF})^2 \sigma_{ON}^2 + C_{ON}^2 \sigma_{OFF}^2} \quad (6)$$

We recall that equations 5 and 6 do not take into account the uncertainty on the normalisation factor n which might depend on the colour of each galaxy and can be as large as 10-30% (Spector et al. 2012). The derived parameters of the observed galaxies are listed in Table 2, arranged as follows:

- Column 1: *Herschel* Reference Sample (HRS) name.
- Column 2: ON-band filter.
- Column 3: Telescope.
- Column 4: used CCD.
- Column 5: Pixel size, in arcseconds.
- Column 6: Observing run.
- Column 7: Number of exposures.
- Column 8: ON band exposure time per pose, in seconds.
- Column 9: Air mass.
- Column 10: Photometric quality of the sky: 1 stands for photometric conditions, 0 unclear conditions (thin cirrus).
- Column 11: Zero point of the observations, in $\text{erg cm}^{-2} \text{s}^{-1}$.
- Column 12: Normalisation factor n between the ON- and the OFF-band (r -Gunn) filter.

A few galaxies have been observed during different observing runs. For these galaxies Table 2 gives a mean value.

4.1. $H\alpha+[NII]$ data for HRS galaxies

We combine the new set of $H\alpha+[NII]$ imaging data with those collected in the literature. With our new observations, 281 of the 323 galaxies of the sample now have $H\alpha+[NII]$ imaging data. The sample is almost complete if limited to late-type systems (254/260 objects, 98 %). Table 3 lists the $H\alpha+[NII]$ equivalent widths and fluxes for the whole HRS sample. Table 3 is arranged as follows:

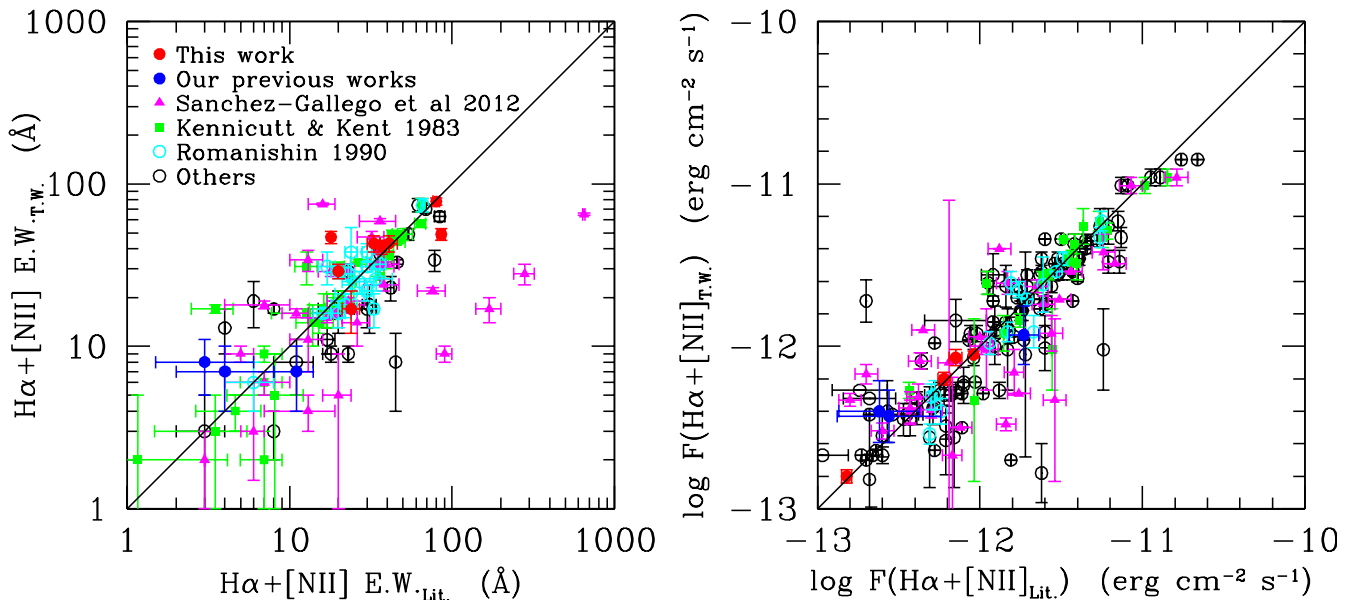


Fig. 3. Comparison of the $H\alpha$ + $[NII]$ equivalent widths (left) and fluxes (right) of the HRS galaxies with independent measurements available in the literature. Red filled dots indicate galaxies with multiple observations done in this work, blue filled dots galaxies with data already published by our team (Boselli & Gavazzi 2002; Boselli et al. 2002a; Gavazzi et al. 2002, 2006), magenta, green, cyan, and black symbols $H\alpha$ + $[NII]$ measurements from Sanchez-Gallego et al. (2012), Kennicutt & Kent (1983) (corrected by a factor of 16% as suggested by Kennicutt et al. 1994), Romanishin (1990) or from other references in the literature, respectively. The solid line shows the 1:1 relation.

- Column 1: *Herschel* Reference Sample (HRS) name.
- Column 2 and 3: $H\alpha$ + $[NII]$ equivalent width and error, in Å.
- Column 4 and 5: observed $H\alpha$ + $[NII]$ flux and error, in $\text{erg cm}^{-2} \text{s}^{-1}$.
- Column 6: Reference to the data. When two references are given, the first refers to the equivalent width, the second to the flux. References are coded as follows: TW: this work, 1: Boselli & Gavazzi (2002), 2: Boselli et al. (2002a), 3: Gavazzi et al. (2002), 4: Gavazzi et al. (2006), 5: Koopmann et al. (2001), 6: Young et al. (1996), 7: Kennicutt et al. (1987), 8: Macchetto et al. (1996), 9: James et al. (2004), 10: Hameed et al. (2005), 11: Koopmann & Kenney (2006), 12: Usui et al. (1998), 13: Domingue et al. (2003), 14: Trinchieri & Di Serego Alighieri (1991), 15: Finkelman et al. (2010), 16: Kim (1989), 17: Martel et al. (2004), 18: Shields (1991), 19: Singh et al. (1995), 20: Kennicutt & Kent (1983), 21: Romanishin (1990), 22: Sanchez-Gallego et al. (2012).
- Column 7: Alternative references, if available.
- Column 8: Notes to individual objects: *c* indicates that the flux of the galaxy has been determined by indirectly calibrating the image using the published flux of the companion galaxy, *m* indicates that the published value is a mean value of two independent measurements, *v* is for vignetted images where the total flux cannot be properly extracted.

We also determined the $H\alpha$ + $[NII]$ CAS (concentration, asymmetry and clumpiness; Conselice 2003) structural parameters for all galaxies with available images. These parameters have been determined following the same procedures described in Fossati et al. (2013) in both the NET- and the *r*-band images. These parameters are given in Table 4, arranged as follow:

- Column 1: *Herschel* Reference Sample (HRS) name.
- Columns 2-4: *r*-band, $H\alpha$ + $[NII]$ and $EW_{H\alpha+[NII]}$ effective radii, in arcsec.

- Columns 5-7: Concentration, asymmetry, and clumpiness (CAS) parameters from the *r*-band images.
- Columns 8-10: Concentration, asymmetry, and clumpiness (CAS) parameters from the $H\alpha$ + $[NII]$ narrow band images.

Figure 2 shows the $H\alpha$ + $[NII]$ image of six representative galaxies of the sample. All the Tables presented in this work, as well as the $H\alpha$ + $[NII]$ images of the whole sample, will be made available to the community through the HRS dedicated database (<http://hedam.lam.fr>).

4.2. Comparison with the literature

Independent sets of data are available for several HRS galaxies (see Table 8). In order to check the quality of our own measurements and of those collected from the literature, in Fig. 3 we compare the different sets of published data. A comparison between the equivalent width of the $H\alpha$ + $[NII]$ line determined from this set of imaging data with that obtained from integrated spectroscopy has been already presented in Boselli et al. (2013). Figure 3 and Table 8 indicate that the different sets of imaging data give results consistent within $\approx 20\%$ for the equivalent widths and $\approx 10\%$ for the fluxes. The agreement with the spectroscopic data of Boselli et al. (2013) is within $\approx 5\%$ (see their Fig. 10). The agreement is good between our independent measurements, or with those obtained by our team during previous observing runs (Boselli & Gavazzi 2002; Boselli et al. 2002a; Gavazzi et al. 2002, 2006). Our new set of data is also consistent with the measurements of Kennicutt & Kent (1983) (corrected by a factor of 16% as suggested by Kennicutt et al. (1994) to take into account a possible contamination of a telluric line in their narrow band filters) and Romanishin (1990) done using aperture photometry. They are also fairly consistent with the data recently published by Sanchez-Gallego et al. (2012) or with a few other data collected from the literature from a large variety of refer-

ences. Figure 3 and Table 8 also show that the uncertainty on the data is generally underestimated using standard error propagation (as recipes given in eq. 5 and 6). One possible reason is because these recipes do not take into account the contribution from correlated noise (which is realistically expected to be a factor of 2-3). Other possible reasons are the photometric uncertainties on the zero point determination and uncertainties in the continuum subtraction. Overall, the uncertainty on $H\alpha$ + $[NII]E.W.$ over the whole HRS dataset is of the order of $\sim 66\%$, while that on the $H\alpha$ + $[NII]$ flux $\sim 60\%$.

5. Determination of the SFR

5.1. Dust attenuation correction

As mentioned in the introduction, the $H\alpha$ emission of late-type star forming galaxies not dominated by an AGN is due to the gas ionised by the youngest and most massive O-B stars (Kennicutt 1998; Boselli et al. 2001). Under some assumptions on the shape of the IMF and on the star formation history, $H\alpha$ data can be used to measure the present day star formation activity of galaxies. To do this, the $H\alpha$ + $[NII]$ data listed in Table 3 must be corrected to remove the contribution of the two $[NII]$ lines in the narrow band filter and to account for both the Galactic and internal dust attenuation. We first correct the observed $H\alpha$ + $[NII]$ for the $[NII]$ contamination using an updated version of the long slit integrated spectroscopic data of the HRS galaxies published in Boselli et al. (2013) (see Appendix A). We then correct them for Galactic extinction using the Schlegel et al. (1998) extinction map combined with the Galactic extinction curve of Fitzpatrick & Massa (2007):

$$A_G(H\alpha) = 2.517 \times E(B - V)_G \quad (7)$$

The same set of spectroscopic data is used to estimate the Balmer decrement:

$$C(H\beta) = \frac{\log(2.86) - \log\left[\frac{F(H\alpha)}{F(H\beta)}\right]_{obs}}{f(H\alpha)} \quad (8)$$

based on $H\alpha$ -to- $H\beta$ flux ratio and the Galactic extinction law ($f(H\alpha)=-0.297$). The attenuation in the $H\alpha$ line is then simply given by the relation:

$$A(H\alpha) = 1.754 \times C(H\beta) \quad (9)$$

To allow a direct comparison with other works in the literature, we do not apply any further correction for the escape fraction of ionising photons nor for the absorption of the ionising radiation by dust (see Boselli et al. 2009 for details).

The attenuation in the $H\alpha$ emission can also be determined using the $24\ \mu\text{m}$ emission combined with one of the several prescriptions given in the literature (Kennicutt et al. 2007, 2009; Calzetti et al. 2007, 2010; Zhu et al. 2008)². These relations have been calibrated using nearby samples of galaxies with available narrow band $H\alpha$ + $[NII]$ imaging data, integrated spectroscopy, and mid-infrared data. These data are also available for the HRS sample: *WISE* $22\ \mu\text{m}$ data for the whole HRS have been recently published by Ciesla et al. (2014). These data can be converted into $24\ \mu\text{m}$ flux densities by multiplying them by a factor of 1.22, as prescribed in Ciesla et al. (2014) (see also Boselli et al. 2014d).

² $H\alpha$ fluxes must be first corrected for Galactic extinction and $[NII]$ contamination as mentioned above.

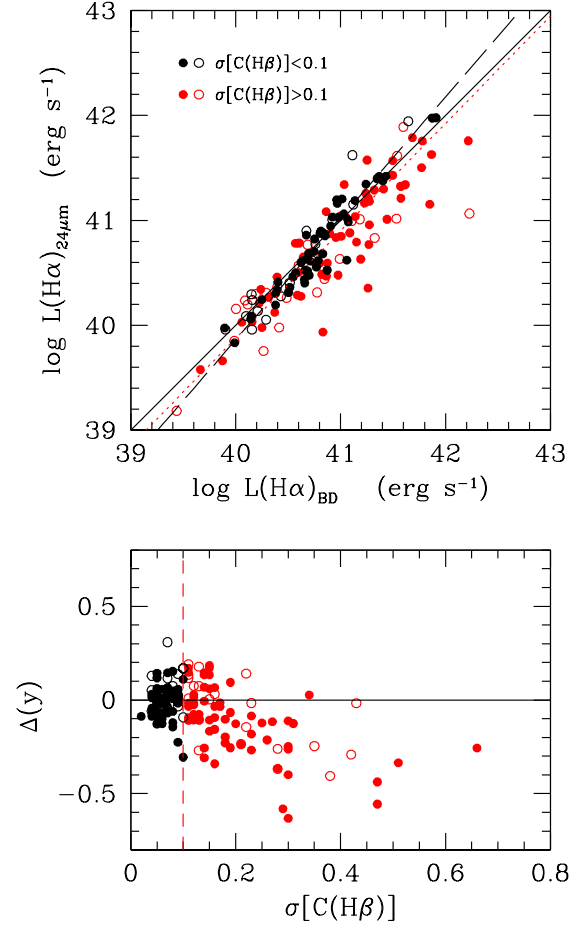


Fig. 4. Upper panel: relationship between the $H\alpha$ luminosity corrected for dust attenuation using the $24\ \mu\text{m}$ luminosity and the prescription of Calzetti et al. (2010) and the $H\alpha$ luminosity corrected using the Balmer decrement. Black symbols are for galaxies with a $\sigma[C(H\beta)] \leq 0.1$, red symbols for $\sigma[C(H\beta)] > 0.1$. Filled dots are for galaxies with a normal gas content ($HI - def \leq 0.4$), empty symbols for gas-poor objects ($HI - def > 0.4$). The black solid line shows the 1:1 relation, the black long-dashed line the bisector fit (Isobe et al. 1990) determined using the best quality sample ($\sigma[C(H\beta)] \leq 0.1$), while the red dotted line the best fit determined using the whole sample. Lower panel: relationship between the distance from the $L(H\alpha)_{24\mu}$ vs. $L(H\alpha)_{BD}$ relation and the uncertainty on the Balmer decrement estimate $\sigma[C(H\beta)]$. The vertical red dashed line shows the limit in $\sigma[C(H\beta)] = 0.1$ above which data are asymmetrically distributed in $\Delta(y)$.

5.1.1. Limits in the Balmer decrement determination

Figure 4 shows the relationship between the $H\alpha$ luminosity corrected for dust attenuation using the $24\ \mu\text{m}$ emission with the prescription of Calzetti et al. (2010) and the $H\alpha$ luminosity corrected using the Balmer decrement. Only galaxies detected at $22\ \mu\text{m}$ and with an available estimate of the $[NII]/H\alpha$ ratio and of the Balmer decrement are included. The two dependent variables are obviously strongly related. The determination of the Balmer decrement, however, is very uncertain in those objects with a weak Balmer emission, since the contamination of the underlying stellar absorption can be dominant. The lower panel of

Fig. 4 shows the relationship between the perpendicular distance from the $L(H\alpha)_{24\mu\text{m}}$ vs. $L(H\alpha)_{BD}$ relation and the uncertainty on the Balmer decrement estimate $\sigma[C(H\beta)]$ given in column 12 of Table 7. Figure 4 shows that the points are symmetrically distributed around the mean relation for $\sigma[C(H\beta)] \lesssim 0.1$, while they systematically drop below this relation for larger uncertainties on the estimate of the Balmer decrement.

To understand whether this trend is due to a systematic bias in the $24\mu\text{m}$ -based dust attenuation correction or in the Balmer decrement-based correction, we compare $L(H\alpha)_{BD}$ and $L(H\alpha)_{24\mu\text{m}}$ to the radio continuum luminosity at 20 cm, which is an independent tracer of the star formation activity in galaxies (e.g. Kennicutt 1998; Bell 2003). At this frequency, the radio continuum emission of galaxies is primarily due to the synchrotron emission of relativistic electrons spinning around weak magnetic fields. These electrons are accelerated in supernova remnants, and are thus a direct tracer of the young stellar population (e.g. Boselli 2011). Radio continuum data at 20 cm (1.49 GHz), collected from the literature as explained in Appendix B, are available for 169 (65%) late-type galaxies³. Figure 5 shows that the 20 cm luminosity of the HRS galaxies is tightly correlated with the $H\alpha$ luminosity. The relation with the $H\alpha$ luminosity corrected for dust attenuation using the $24\mu\text{m}$ band (right panel, $\sigma = 0.15$) is less dispersed than the one determined correcting $H\alpha$ using the Balmer decrement (left panel, $\sigma=0.20$; see Table 9)⁴. Figure 5 shows, however, that as for the $L(H\alpha)_{24\mu\text{m}}$ vs. $L(H\alpha)_{BD}$ relation shown in Fig. 4, the points are symmetrically distributed around the $L(20\text{cm})$ vs. $L(H\alpha)_{BD}$ relation only whenever $\sigma[C(H\beta)] \lesssim 0.1$, while they drop below the mean relation for larger values of $\sigma[C(H\beta)]$. On the opposite, the dispersion in the $L(20\text{cm})$ vs. $L(H\alpha)_{24\mu\text{m}}$ relation is symmetric. Figures 4 and 5 consistently indicate that the Balmer decrement is systematically overestimated by ≈ 0.2 dex ($A(H\alpha) \approx 0.5$ mag) whenever $\sigma[C(H\beta)] \gtrsim 0.1$.

5.1.2. Limits in the $24\mu\text{m}$ dust attenuation correction

The analysis presented in the previous section indicates that $H\alpha$ luminosities can be accurately corrected for dust attenuation using the Balmer decrement only whenever $\sigma[C(H\beta)] \lesssim 0.1$. This, however, might introduce systematic biases, in particular in the comparison with the $24\mu\text{m}$ dust attenuation corrected $H\alpha$ luminosities. Indeed, as shown in Boselli et al. (2013), the Balmer decrement $C(H\beta)$ is tightly related with the $H\beta$ E.W., thus omitting galaxies with low $H\beta$ emission (thus those with low signal-to-noise in $H\beta$ or equivalently with a large uncertainty on $C(H\beta)$, see Appendix A) might strongly bias the sample towards low attenuated objects. The $H\beta$ emission is also tightly connected to the specific star formation rate. The exclusion of galaxies with small values of $H\beta$ might thus bias the sample towards star-forming, low-mass systems. It is well known that in these systems the dust heating sources are mainly young massive stars, while in more quiescent and massive objects the contribution to the dust heating of the

older stellar component might be very important (e.g. Boselli et al. 2006, Cortese et al. 2008, Salim et al. 2009, Bendo et al. 2010, 2012; Boquien et al. 2011; Boselli et al. 2012). Thus, the calibration of dust attenuation based on the $24\mu\text{m}$ emission, taken here as proxy for the total far-infrared luminosity, might not be representative for the most quiescent objects of the sample. To test whether this strong assumption might introduce a systematic bias in the results, we plot in Fig. 6 the relationship between the perpendicular distance from the $L(H\alpha)_{24\mu\text{m}}$ vs. $L(H\alpha)_{BD}$ relation observed in Fig. 4 and different variables characterising the physical properties of the interstellar radiation field of the HRS galaxies. The L_{TIR} , U_{min} , and γ parameters give respectively the total infrared luminosity, the intensity of the general interstellar radiation field responsible for the heating of the diffuse dust component and the fraction of dust mass in PDRs heated by the energetic radiation produced by OB associations (Draine et al. 2007). They have been determined by Ciesla et al. (2014), by fitting the infrared SED of the HRS galaxies using the models of Draine & Li (2007). L_{TIR}/L_{FUV} is a direct tracer of the dust attenuation in galaxies, whereas the γ parameter, the $H\beta$ equivalent width, and the FUV-to-H-band colour index are tracers of the hardness of the radiation field heating the dust. The L_{24}/L_{TIR} quantifies the contribution of the hot dust component to the total far infrared dust emission of galaxies, and is thus tightly connected to the shape of the SED and to the activity of star formation.

Figure 6 shows that, when all galaxies are considered regardless of the uncertainty on the Balmer decrement (black and red symbols together), $\Delta(y)$ is barely anticorrelated with L_{TIR}/L_{FUV} and $(FUV - H)_c$ ⁵ and shows a bimodal distribution when plotted vs. $H\beta$ E.W., L_{24}/L_{TIR} , and γ . In these plots, galaxies with $\Delta(y) \lesssim -0.3/-0.4$ all have low values of $H\beta$ E.W. ($\lesssim 5 \text{ \AA}$), $L_{24}/L_{TIR} (\lesssim 0.1)$, and $\gamma (\lesssim 10^{-2})$. They also have red $(FUV - H)_c$ colours ($\gtrsim 4$ mag) and high L_{TIR}/L_{FUV} ratios ($\gtrsim 5$). All these properties consistently indicate that galaxies located below the standard $L(H\alpha)_{24\mu\text{m}}$ vs. $L(H\alpha)_{BD}$ relation are relatively quiescent objects where the dust heating is dominated by the evolved stellar population and where dust attenuation is probably important. If confirmed, these trends would indicate a systematic residual in the $H\alpha$ luminosity correction based on the $24\mu\text{m}$ emission, making eq. B.2-B.3 non universal since they are valid only for active star forming galaxies. We notice, however, that if the same analysis is restricted to those objects with a low uncertainty on the Balmer decrement ($\sigma[C(H\beta)] \leq 0.1$, black symbols in Fig. 6), only the trend with L_{24}/L_{TIR} is still statistically significant (the probability that the two variables are correlated is $P > 99\%$). As mentioned above, however, limiting the analysis to galaxies with low uncertainty on the Balmer decrement, thus with high signal-to-noise in the $H\alpha$ and $H\beta$ lines, might severely bias the sample towards active galaxies. It is thus hard to conclude whether there is a statistically significant indication that the proposed calibration varies with the properties of galaxies. However, it is clear that, as first stressed by Kennicutt et al. (2009), the dust attenuation correction of the $H\alpha$ emission based on monochromatic far infrared tracers should be used with extreme caution in quiescent massive spiral galaxies.

³ We consider in the following analysis only galaxies with high-quality radio data (flag 1 in Table 5).

⁴ The less dispersed relation between the radio continuum emission and the $H\alpha$ luminosity corrected using the $24\mu\text{m}$ emission than with the Balmer corrected $H\alpha$ luminosity might result from the tight connection between the radio and far infrared emission of galaxies (far infrared-radio correlation, de Jong et al. 1985; Condon et al. 1991; Yun et al. 2001; Bell 2003).

⁵ the probability that the two variables are correlated is $99 < P < 99.9\%$

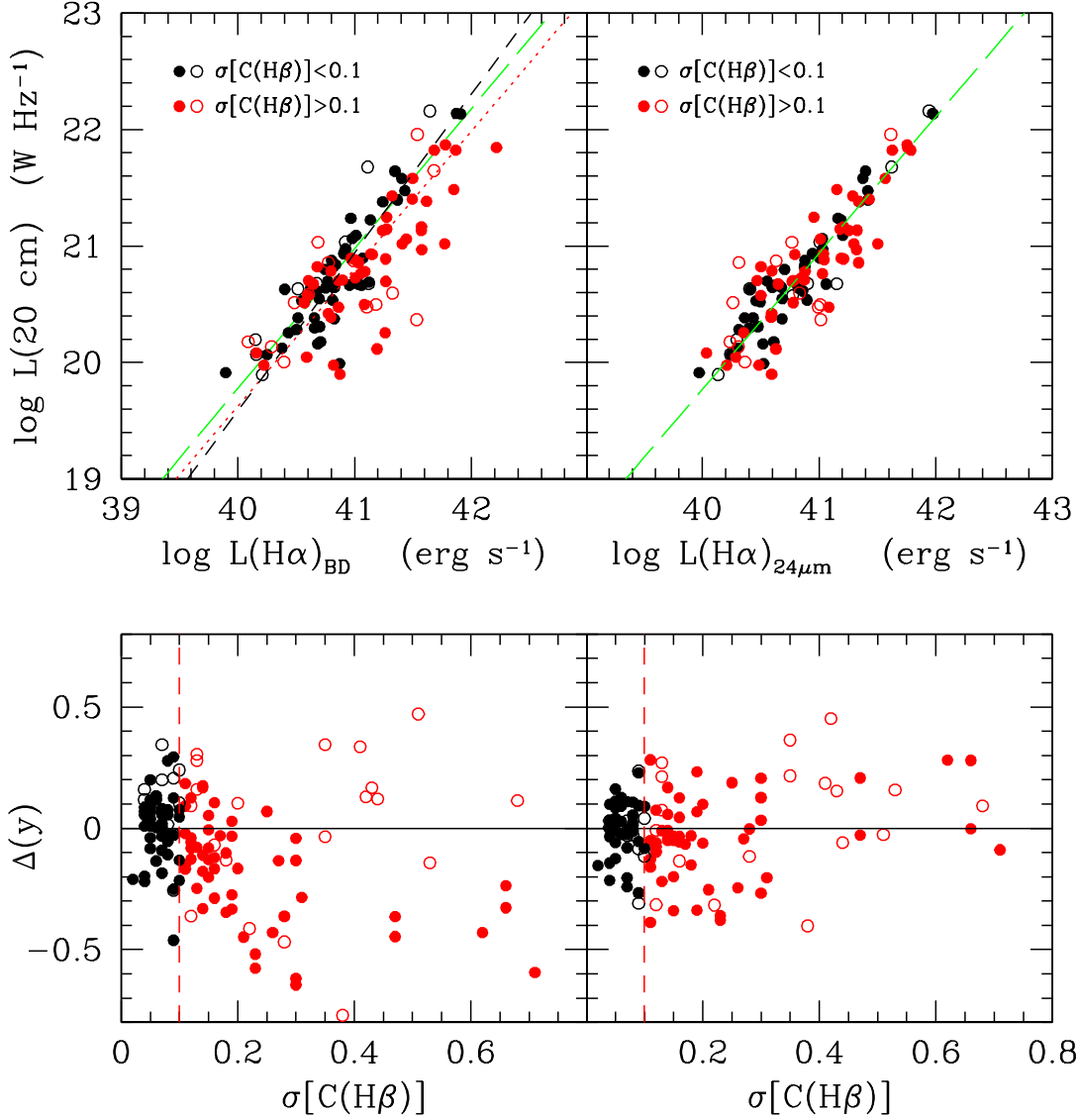


Fig. 5. Upper panels: relationship between the 20 cm radio luminosity and the $H\alpha$ luminosity corrected for dust attenuation using the Balmer decrement (left) and the $24\ \mu\text{m}$ luminosity following the prescription of Calzetti et al. (2010) (right). Black symbols are for galaxies with a $\sigma[C(H\beta)] \leq 0.1$, red symbols for $\sigma[C(H\beta)] > 0.1$. Filled dots are for galaxies with a normal gas content ($HI - def \leq 0.4$), empty symbols for gas-poor objects ($HI - def > 0.4$). The black short-dashed line in the left panel shows the bisector fit determined using the best quality sample ($\sigma[C(H\beta)] \leq 0.1$), while the red dotted line the best fit determined using the whole sample. The green long-dashed line gives the bisector fit in the $L(20\text{cm})$ vs. $L(H\alpha)_{24\mu\text{m}}$ relation determined using all galaxies in the right panel. When plotted in the left panel, this fit is close to the one traced by the black dashed line. Lower panels: relationship between the distance from the $L(20\text{cm})$ vs. $L(H\alpha)_{BD}$ (left) and the $L(20\text{cm})$ vs. $L(H\alpha)_{24\mu\text{m}}$ relations (right) and the uncertainty on the Balmer decrement estimate $\sigma[C(H\beta)]$.

5.1.3. Comparison between different $A(H\alpha)$ and $A(FUV)$ estimators

Different recipes have been proposed in the literature to correct $H\alpha$ luminosities using the $24\ \mu\text{m}$ emission. Figure 7 shows the relationship between different $H\alpha$ attenuations determined using these recipes (Calzetti et al. 2010, 2007, and Kennicutt et al. 2009 from top to bottom), and the $H\alpha$ attenuations determined using the Balmer decrement (left column). All recipes

give $A(H\alpha)_{24\mu\text{m}} \lesssim A(H\alpha)_{BD}$ regardless of the quality of the spectroscopic data. Among these corrections, however, the one proposed by Calzetti et al. (2010), which uses two different coefficients, one for a starburst regime and one for normal star forming regions, gives values closest to the 1:1 relation. Whenever the Balmer decrement cannot be determined with high accuracy ($\sigma[C(H\beta)] \leq 0.1$), we adopt this correction in the following analysis. Figure 7 also shows the relationship between $A(H\alpha)_{24\mu\text{m}}$

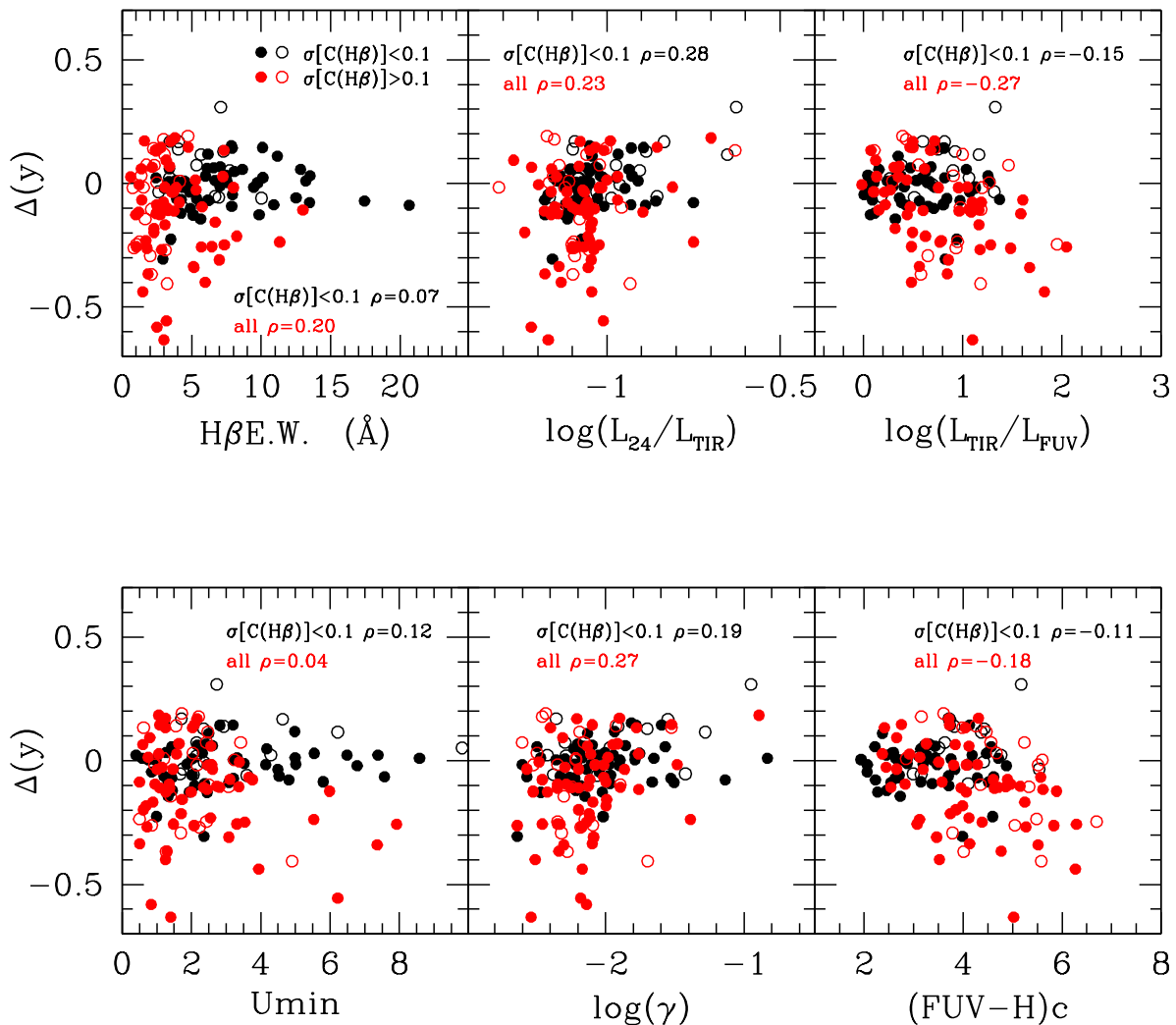


Fig. 6. Relationship between the distance from the $L(H\alpha)_{24\mu}$ vs. $L(H\alpha)_{\text{BD}}$ relation and different parameters characterising the physical properties of the target galaxies, determined as described in the text. Filled dots are for galaxies with a normal gas content ($HI - def \leq 0.4$), empty symbols for gas-poor objects ($HI - def > 0.4$). Black symbols are for galaxies with $\sigma[C(H\beta)] \leq 0.1$, red symbols for $\sigma[C(H\beta)] > 0.1$. ρ gives the Spearman correlation coefficient for each panel for the whole sample (black and red; 152 objects) or for galaxies with high signal-to-noise in the spectroscopic data ($\sigma[C(H\beta)] \leq 0.1$; black; 69 objects).

and $A(FUV)_{24\mu\text{m}}$ determined using the prescription of Hao et al. (2011). $A(H\alpha)_{24\mu\text{m}}$ is generally $\lesssim A(FUV)_{24\mu\text{m}}$ (see however Buat et al. 2002), which is another good reason to prefer the $H\alpha$ to the FUV luminosity as a star formation tracer, given that it is less affected by attenuation. The relation between $A(H\alpha)_{24\mu\text{m}}$ and $A(FUV)_{24\mu\text{m}}$ is steeper than the one expected for a simple screen model combined with a Milky Way attenuation curve (blue dotted-dashed line). This relation is also slightly steeper than the widely used Calzetti’s law (Calzetti 2001, $A(FUV) = 1.86 \times A(H\alpha)$, green dashed line) when the $H\alpha$ attenuation is measured using the prescriptions of Calzetti et al. (2007, 2010),

whereas they are in agreement when the $H\alpha$ attenuation is determined using the prescription of Kennicutt et al. (2009).

5.2. SFR

5.2.1. Comparison between different tracers

Once corrected for dust attenuation, $H\alpha$ luminosities can be transformed into star formation rates (SFR, in $M_{\odot} \text{ yr}^{-1}$) using a factor which depends on the assumed IMF and stellar model⁶:

⁶ As mentioned above, we do not apply any correction for any possible escape fraction of the ionising radiation, nor for the absorption by

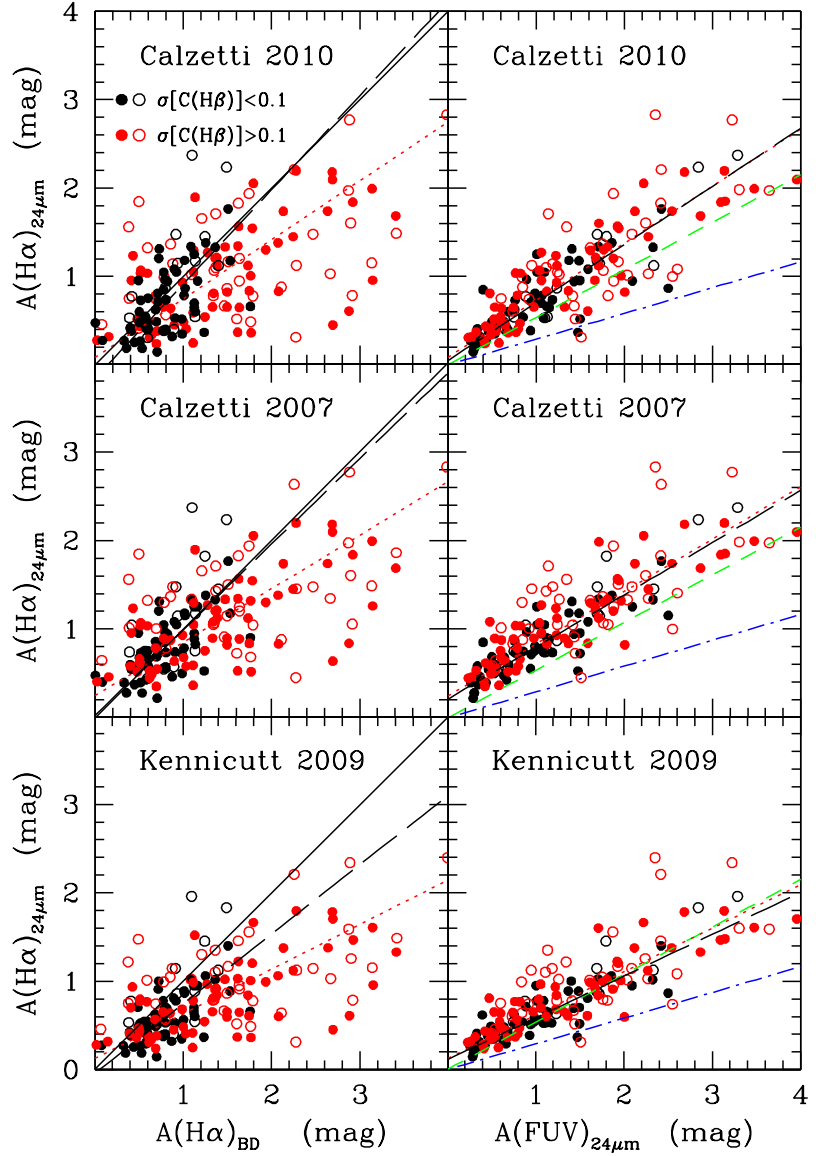


Fig. 7. Left column: comparison of $A(H\alpha)_{24\mu m}$, the attenuation of the $H\alpha$ measured using different recipes based on the $H\alpha$ over $24\mu m$ flux ratio, and that determined using the Balmer decrement. Black symbols are for galaxies with $\sigma[C(H\beta)] \leq 0.1$, red symbols for $\sigma[C(H\beta)] > 0.1$. Filled dots are for galaxies with a normal gas content ($HI - def \leq 0.4$), empty symbols for gas-poor objects ($HI - def > 0.4$). The black solid lines show the 1:1 relation, the black long-dashed line the bisector fit determined using the best quality sample ($\sigma[C(H\beta)] \leq 0.1$), while the red dotted line the best fit determined using the whole sample. Right: comparison of $A(H\alpha)_{24\mu m}$ and the attenuation $A(FUV)_{24\mu m}$ determined in the *GALEX* FUV band using the prescription of Hao et al. (2011) based on the $24\mu m$ emission band. The blue dotted-dashed line shows the relation expected for a screen model and the Galactic extinction law of Fitzpatrick & Massa (2007), the green short-dashed line the Calzetti attenuation law (Calzetti 2000), and the red dotted line the bisector fit to the data for all galaxies.

$$SFR = k(H\alpha) \times L(H\alpha)_{cor} \quad (10)$$

We recall that this relation is valid only under the assumption that the mean star formation activity of the emitting galaxies is constant over a timescale of a few Myr, roughly comparable to

dust of ionising photons before the ionisation of the gas (see Boselli et al. 2009).

the typical time spent by the stellar population responsible for the ionisation of the gas on the main sequence (Boselli et al. 2009; Boissier 2013; Boquien et al. 2014). The ionising stars are O and early-B stars, whose typical age is $\leq 10^7$ years. The stationarity condition is generally satisfied in massive, normal, star forming galaxies undergoing a secular evolution. In these objects the total number of OB associations is significantly larger than the number of HII regions under formation and of OB stars

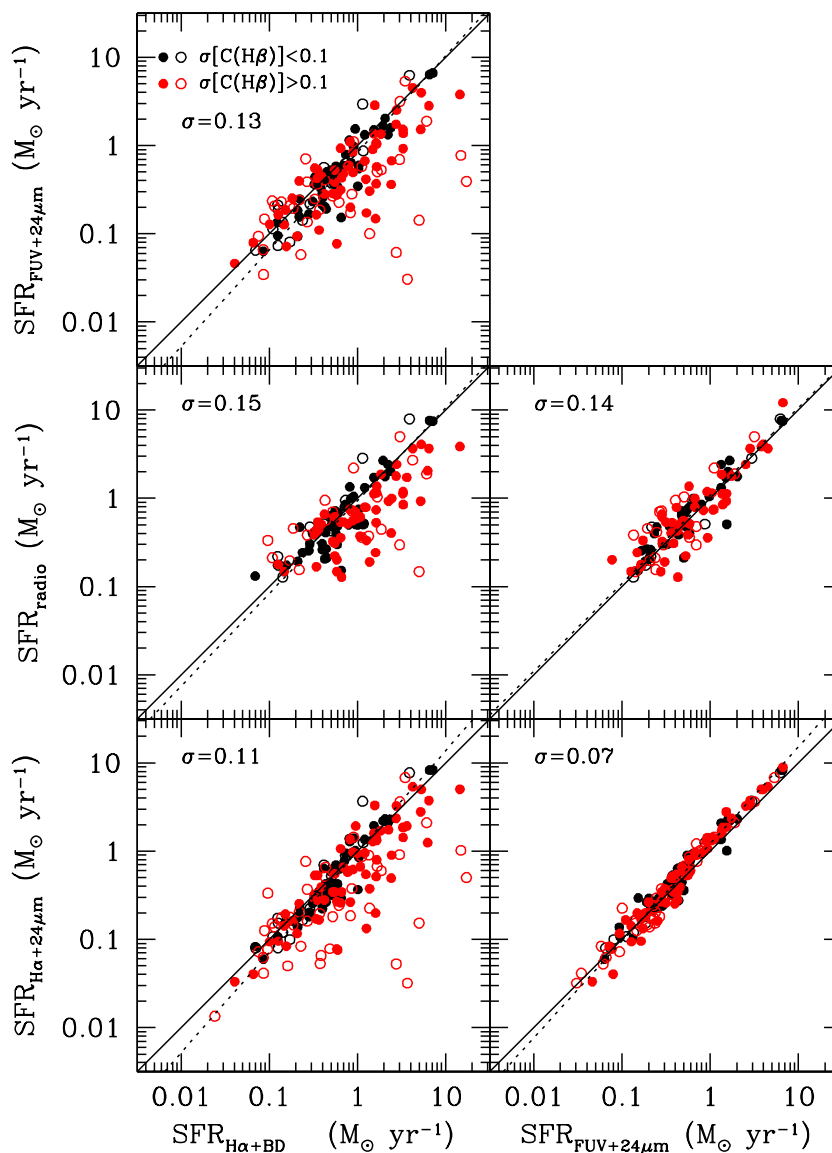


Fig. 8. Comparison between the star formation rate determined using different tracers. $SFR_{H\alpha+BD}$ stands for star formation rates determined using $H\alpha$ luminosities corrected for Balmer decrement (using the GANDALF dataset), $SFR_{H\alpha+24\mu m}$ corrected using the prescription of Calzetti et al. (2010) based on the $24\mu m$ emission. $SFR_{FUV+24\mu m}$ have been determined using *GALEX* FUV data corrected for dust attenuation using the $24\mu m$ emission following Hao et al. (2011), and SFR_{radio} using the 20 cm radio emission following Bell (2003) (see Appendix C). Black symbols are for galaxies with a spectroscopic $\sigma[C(H\beta)] \leq 0.1$, red symbols for galaxies with $\sigma[C(H\beta)] > 0.1$. Filled dots are for galaxies with a normal gas content ($HI - def \leq 0.4$), empty symbols for gas-poor objects ($HI - def > 0.4$). The black solid line shows the 1:1 relation, the black dotted line the bisector fit (and σ its dispersion) determined using the best quality sample ($\sigma[C(H\beta)] \leq 0.1$).

reaching the final stage of their evolution, thus their total $H\alpha$ luminosity is fairly constant with time. This might not be the case in strongly perturbed systems or in dwarf galaxies, where the total star formation activity can be dominated by individual giant HII region (Boselli et al. 2009; Weisz et al. 2012) and the IMF is only stochastically sampled (Lee et al. 2009; Fumagalli et al. 2011; da Silva et al. 2014). The HRS sample is dominated by relatively massive galaxies undergoing a secular evolution. For these objects, eq. (10) can thus be applied. The sample, however,

also includes galaxies in the Virgo cluster region, where the perturbation induced by the cluster environment might have affected their star formation rate (e.g. Boselli & Gavazzi 2006; 2014). Models and simulations have shown that in these objects the suppression of star formation occurs on timescales of the order of a few hundreds Myr (Boselli et al. 2006, 2008a,b, 2014d). These timescales are relatively long compared to the typical age of O-B stars. The recent work of Boquien et al. (2014) has clearly shown that the Lyman continuum emission tightly follows the

rapid variations of the star formation activity of simulated galaxies down to timescales of a few Myrs. We can thus safely consider that the linear relation between the $H\alpha$ luminosity and the star formation rate given in eq. 10 is satisfied in the HRS sample.

Figure 8 shows the relationship between the star formation rate determined using different tracers: the $H\alpha$ luminosity, corrected for dust attenuation using both the Balmer decrement and the $24\ \mu\text{m}$ emission, the FUV *GALEX* luminosities corrected using the $24\ \mu\text{m}$ emission, and the 20 cm radio continuum luminosity. For consistency all *SFR* have been measured using the Kennicutt (1998) prescriptions based on a similar IMF (Salpeter in the stellar mass range $0.1 < m_{\text{star}} < 100 M_{\odot}$). For the radio continuum we use the Bell (2003) calibration, which is consistent with those used in the other bands (see Appendix C). The different values of *SFR* are listed in Table 6.

The different SFR calibrations give similar results once determined for star forming galaxies with low uncertainties in $C(H\beta)$. This result is consistent with what was found in the previous section. When compared to $SFR_{FUV+24\mu\text{m}}$, the dispersion is different when different tracers are used: it is very small when compared to $SFR_{H\alpha+24\mu\text{m}}$ and gradually increases with $SFR_{H\alpha+BD}$ (when limited to $\sigma[C(H\beta)] \leq 0.1$) and SFR_{radio} (see Table 10). This increase of the dispersion in the relations can be naturally explained by considering that some variables are not fully independent. The dispersion in the relation with the radio continuum tracer might also be affected by other physical factors. In fact, the radio continuum emission can be affected by the presence of an AGN. There is also some indication that the radio continuum emission of cluster galaxies is, on average, stronger than that of similar objects in the field (Gavazzi et al. 1991; Gavazzi & Boselli 1999a,b). The increase of the radio continuum activity of cluster galaxies has been interpreted as due to the compression of the magnetic field during their interaction with the dense intergalactic medium (e.g. Boselli & Gavazzi 2006).

Out of the 260 late-type galaxies in the HRS sample, 196 have more than one empirical determination of the *SFR*. Figure 9 shows that the typical dispersion σ in the different tracers is of the order of 24%, while the statistical error σ/\sqrt{N} in the final *SFR* is of the order of 14%⁷. Beside the uncertainty in the data, a part of this scatter can be due to the fact that the *SFR* tracers based on the FUV and radio luminosities can be seriously affected by the fact that the stationarity conditions necessary to transform luminosities into star formation rates are not always satisfied, as clearly indicated by Boquien et al. (2014).

5.2.2. Comparison with SED fitting estimates

The star formation activity of galaxies can also be estimated by fitting their observed spectral energy distribution with stellar population synthesis models. An energetic balance between the absorbed stellar radiation and the energy emitted in the far infrared domain quantifies dust attenuation, allowing the determination of several physical parameters of the studied galaxies, such as the stellar mass and the star formation rate (GRASIL, Silva et al. 1998; MAGPHYS, da Cunha et al. 2008; CIGALE, Noll et al. 2009). SED fitting has several advantages with respect to the star formation rate determination based on monochromatic fluxes used in the previous section. First of all, it uses simultaneously several spectrophotometric bands, thus significantly reducing the observational uncertainty on the data. Thanks to a self consistent determination of the dust attenuation, SED fit-

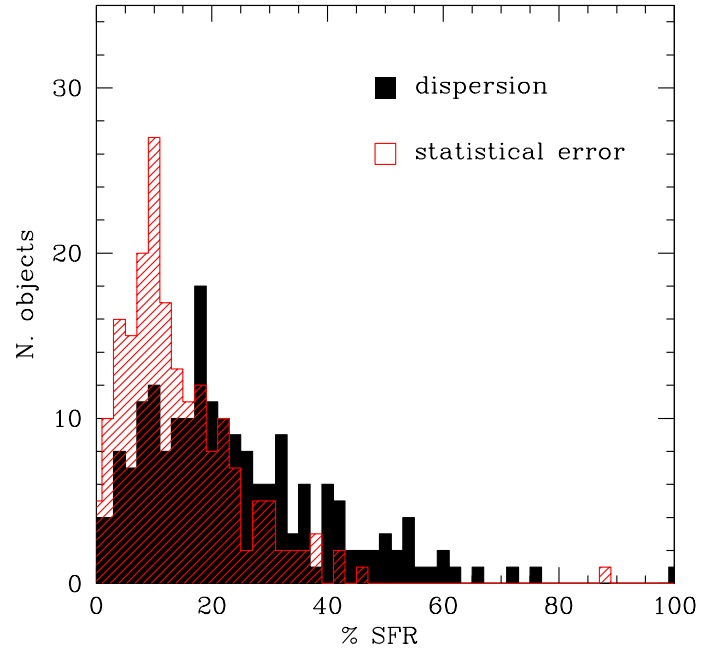


Fig. 9. Distribution of the dispersion σ in the different *SFR* tracers (black histogram) and the statistical error (σ/\sqrt{N}) when more than one estimator is available (red histogram).

ting also provides several physical parameters (*SFR*, M_{star} , Z , ...) suitable for any kind of statistical analysis. The SED fitting technique, however, also has several weaknesses. First of all, the output of the SED fitting depends on the star formation history of the galaxy, which is parametrised using simple analytic prescriptions. These are typically not optimised to reproduce the abrupt truncation of the star formation activity occurred in cluster galaxies (e.g. Boselli & Gavazzi 2006; 2014). SED fitting is generally done assuming a constant (and fixed) metallicity. The star formation rate derived by SED fitting also depends on the adopted population synthesis models and IMF, as in the case of the monochromatic-based estimates.

It is thus worth comparing the star formation rate determined using a SED fitting code to the one derived directly from monochromatic fluxes as described in the previous section. To do this, we run the CIGALE code (Noll et al. 2009; Burgarella et al. in prep. Boquien et al. in prep.) on all the HRS galaxies. The far infrared part of the spectrum is fitted using the Draine & Li (2007) dust models, as extensively described in Ciesla et al. (2014). The UV-visible-near infrared part of the spectrum is fitted using Bruzual & Charlot (2003) stellar population models, and assuming a Salpeter IMF and solar metallicity, consistent with our approach for the monochromatic determinations. The HRS sample is ideally suited for SED fitting since multifrequency data (including 15 photometric bands) are available for the vast majority of the galaxies. For the present work, we limit the comparison to those galaxies with available *GALEX* FUV data. Although nebular emission lines can be added to the stellar continuum emission, we do not use them in the present fit, because we want to be representative of the typical data generally used in the SED fitting of galaxies extracted from cosmological surveys.

To remove any possible dependence on short timescale variations of the star formation activity of cluster galaxies, we use the $H\alpha$ luminosity as a monochromatic tracer (Boquien et al. 2014). Whenever possible ($\sigma[C(H\beta)] \leq 0.1$) we correct it for dust attenuation using the Balmer decrement, otherwise using the 24

⁷ This number underestimates the statistical error since it is based on non fully independent values of *SFR*.

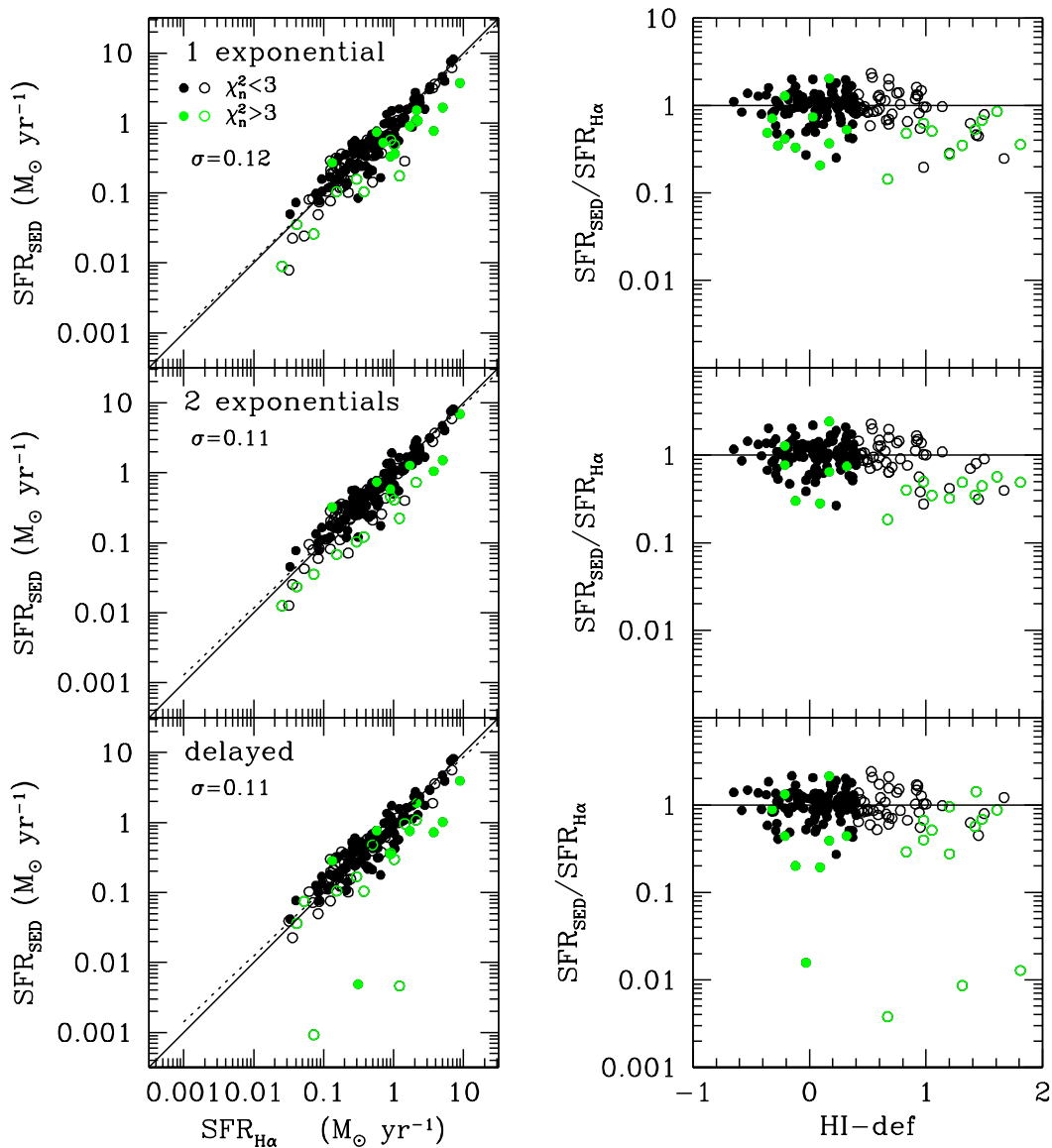


Fig. 10. Left panels: The comparison between the star formation rate determined using a SED fitting technique and that determined using the $H\alpha$ emission. For the SED fitting determination, all galaxies are assumed to be 13 Gyr old. Three different parametric star formation histories are assumed: exponential (upper panel), double exponential (middle), and delayed (lower). Green symbols indicate those objects where the normalised $\chi_n^2 > 3$, black symbols those with $\chi_n^2 < 3$. Filled symbols are for HI-normal galaxies, empty symbols for HI-deficient objects ($HI - def \leq 0.4$). The black solid line shows the 1:1 relation, the black dotted line the bisector fit (and σ its dispersion) determined using galaxies with $\chi_n^2 < 3$. Right panels: relationship between the $SFR_{SED}/SFR_{H\alpha}$ ratio and the HI-deficiency parameter.

μm emission. A $24\ \mu\text{m}$ based correction might indeed introduce systematic age effects since the dust emitting at this wavelength might be heated by stars older than those responsible for the ionisation of the gas (e.g. Bendo et al. 2012). The variable $SFR_{H\alpha}$ is available for 196/260 of the late-type galaxies of the sample.

Figure 10 shows the relationship between the star formation rate determined using the SED fitting procedure and that derived from the $H\alpha$ luminosity. The SED fitting estimates have been determined using three commonly-used parametrisations of the

star formation history of galaxies: a single exponentially declining law

$$SFR(t) \propto \exp(-t/\tau_1) \quad [0.5 \leq \tau_1 \leq 100 \text{ Gyr}] \quad (11)$$

a double exponentially declining law

$$SFR(t) = \begin{cases} \exp(-t/\tau_1) & \text{if } t < t_1 - t_2 \\ \exp(-t/\tau_1 + k \times \exp(-t/\tau_2)) & \text{if } t \geq t_1 - t_2 \end{cases} \quad (12)$$

[$0.5 \leq \tau_1 \leq 20 \text{ Gyr}$; $\tau_2 \rightarrow \infty$]

and a delayed star formation history

$$SFR(t) \propto t \times \exp(-t/\tau_1) \quad [0.5 \leq \tau_1 \leq 20 \text{ Gyr}] \quad (13)$$

where τ are the folding times. These star formation rates are given in Table 6. For the three fits we make the reasonable assumption that galaxies are coeval (13 Gyrs old). Overall the three star formation rate estimates determined with the SED fitting code give results consistent with those determined using $H\alpha$, as already found in other samples of local or high- z galaxies (e.g. Wuyts et al. 2009; Pforr et al. 2012; Buat et al. 2014)⁸. This is expected for several reasons: first of all, the single exponentially declining and delayed star formation histories are smooth with respect of time and do not have major changes in the last hundreds of Myrs. They thus correspond to the stationarity condition ($SFH = \text{constant}$) assumed for the monochromatic determination. Second, the HRS galaxies are mainly massive galaxies which underwent a secular evolution. The sample, indeed, does not include strong starbursts or recent mergers, where the star formation activity might have changed abruptly with time. We notice, however, that the SED fitting derived star formation activities of the most HI-deficient galaxies are generally smaller than those determined using $H\alpha$ luminosities. These are also objects where the quality of the fit is lower than the average (normalised $\chi_n^2 > 3$).

As extensively discussed in Boselli & Gavazzi (2006; 2014), Boselli et al. (2006, 2014c, 2014d), Hughes & Cortese (2009), Cortese & Hughes (2009) and Gavazzi et al. (2013b), the HI-deficiency parameter is tightly connected to the perturbation that affected cluster galaxies. The gas removal resulting from this interaction quenched the activity of star formation on relatively short timescales, in particular in low-mass systems (~ 100 Myr). On these timescales, the $H\alpha$ luminosity can still be used as an accurate tracer of the star formation rate of the perturbed galaxies (Boquien et al. 2014). On the contrary, the parametric star formation histories adopted for the fit are not optimised to reproduce this rapid truncation of the star formation activity in the gas stripped cluster galaxies. It is thus conceivable that in these objects the SED fitting gives less accurate SFR than in unperturbed systems ($HI - def \leq 0.4$). Intuitively, however, we would expect an opposite effect since the adopted smooth star formation history would overestimate, rather than underestimate the present day star formation rate. Tests and simulations done so far on observed or mock catalogues of galaxies consistently indicate that the star formation rates determined using SED fitting codes are accurate regardless the use of different parametrisations or the bursty nature of their evolution (Wuyts et al. 2009; Pforr et al. 2012; Buat et al. 2014; Ciesla et al. 2015). The departure of the HI-deficient galaxies from the 1-to-1 relation might thus be due to other reasons. Indeed, these are quiescent objects characterised by red colours and weak Balmer emission lines, where the contribution of the old stellar population to the dust heating is important. As discussed in sect. 5.1, the recipes used to determine the $H\alpha$ attenuation based on the $24 \mu\text{m}$ emission might introduce systematic effects in the data. To further investigate this intriguing topic, we are planning to use parametric star formation histories ad hoc defined to reproduce the truncated star formation activity of cluster galaxies. The results of this analysis will be presented in a forthcoming paper (Ciesla et al. in prep.).

⁸ In these works composite star formation histories (exponentially declining plus burst) are often adopted.

6. SFR properties of the HRS

The complete nature of the HRS, which is volume-limited and K-band-selected, makes it the ideal sample for determining the typical statistical properties of galaxies in the local universe. The completeness in the $H\alpha$ band has been reached in the late-type systems (Sa-Im-BCD, 98%), hence we can derive their statistical properties. The following analysis is thus limited to these star forming objects. Keeping in mind all the systematic biases in the different tracers analysed in the previous sections, we decided to use in the following analysis the star formation rate determined, whenever possible, by averaging the different monochromatic estimates ($SFR_{H\alpha+BD}$, $SFR_{H\alpha+24\mu\text{m}}$, $SFR_{FUV+24\mu\text{m}}$, SFR_{radio}), otherwise using the only one available among them. We define this variable SFR_{MED} . In this way we increase the number of galaxies with an available estimate of the SFR from 196/260 ($SFR_{H\alpha}$) to 236/260 (SFR_{MED}), making the sample complete to 91%. We checked that the results presented in the following section are robust versus the use of different star formation rate tracers.

6.1. The SFR distribution

The completeness of the sample allows us to estimate the star formation rate distribution of the HRS. This can be done by counting the number of galaxies in 0.5 dex bins of $\log SFR$ (Figure 11). The normalisation factor is determined assuming that the volume covered by the HRS survey is of 4539 Mpc^3 , consistently with Boselli et al. (2014b) and Andreani et al. (2014). This volume has been calculated considering that, according to the selection criteria described in Boselli et al. (2010)⁹, we selected galaxies in the volume between 15 and 25 Mpc over an area of 3649 sq.deg . We recall that this is a star formation rate distribution and not a luminosity function since galaxies are first selected in the K-band and then counted in bins of SFR . We determined the star formation rate distribution for the whole sample and separately for HI-normal ($HI - def \leq 0.4$) and HI-deficient ($HI - def > 0.4$) galaxies. The former can be considered as typical field sources, while the latter are cluster perturbed objects (e.g. Boselli & Gavazzi 2006). The star formation rate distribution is compared to several field (Gallego et al. 1995; Tresse & Maddox 1998; Perez-Gonzalez et al. 2003; Gunawardhana et al. 2013) star formation rate luminosity functions determined for local galaxies. $H\alpha$ luminosity functions have been transformed into star formation rates adopting the same calibration for a Salpeter IMF and assuming $H_0 = 70 \text{ km s}^{-1} \text{ Mpc}^{-1}$.

Figure 11 shows that the shape of the HRS star formation rate distribution for the whole or for the unperturbed sample is very similar to most of the luminosity functions measured for local galaxies in the literature (maybe with the exception of Perez-Gonzalez et al. 2003) for $\log SFR \gtrsim -0.5 \text{ M}_\odot \text{ yr}^{-1}$. For lower values of SFR , the HRS star formation rate distribution drastically drops with respect to the star formation rate luminosity functions published in the literature. This effect is similar to the one observed in the molecular gas mass distribution (Boselli et al. 2014b) of the HRS, and can be explained by the incompleteness of the sample at low $H\alpha$ luminosities. Being less than unity the slope of the SFR vs. M_{star} relation (Fig. 12 and Table 13), a stellar mass selection (which roughly corresponds to a K-band-selection) excludes low mass star forming objects. Using the

⁹ The selection conditions are: high Galactic latitude ($b > +55^\circ$) and low Galactic extinction ($A_B < 0.2 \text{ mag}$) to avoid Galactic cirrus contamination.

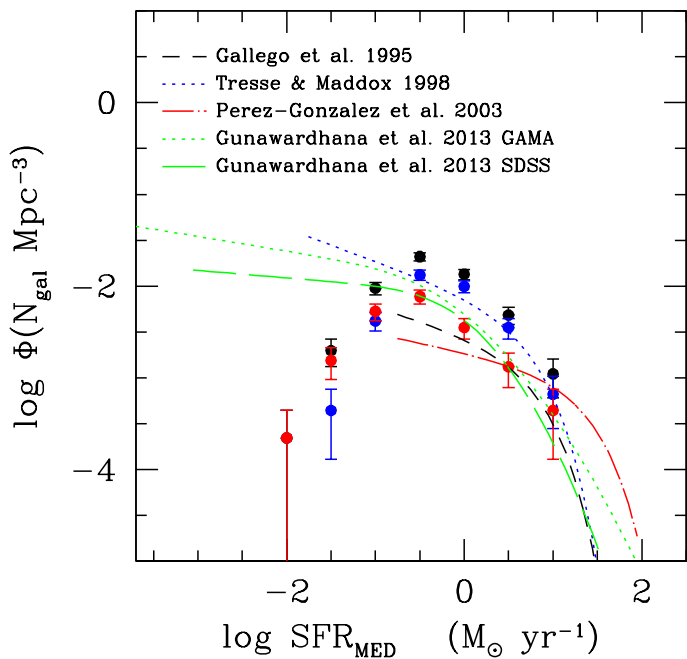


Fig. 11. Distribution of the SFR in number of galaxies Mpc^{-3} for the whole HRS late-type galaxies (black dots) and for the subsample of HI-normal ($HI - def \leq 0.4$; blue dots) and HI-deficient ($HI - def > 0.4$; red dots) galaxies. The distribution is compared to several SFR luminosity function derived from $H\alpha$ measurements for the general field. SFR have been determined using the calibration used in this work for a Salpeter IMF.

SFR distribution of mock samples, it has been shown that the star formation rate distribution of a mass-selected sample does not follow the typical Schechter function, but it is better represented by a double Gaussian function with a form close to the one depicted in Fig. 11 (Salim & Lee 2012). A decrease at the faint end of the $H\alpha$ luminosity function for Coma, A1367, and Virgo cluster galaxies has been found by Iglesias-Paramo et al. (2002).

Figure 11 also shows that the distribution of the HI-normal, unperturbed objects is above that drawn by the HI-deficient, cluster galaxies. This observational evidence can be easily explained by the quenching of star formation activity in late-type galaxies entering the cluster. Their interaction with the surrounding medium efficiently removes their atomic and molecular gas component, reducing the amount of gas available to form new stars (e.g. Boselli & Gavazzi 2006, 2014; Cortese & Hughes 2009; Hughes & Cortese 2009; Gavazzi et al. 2013a,b; Boselli et al. 2014c,d). This transformation is particularly efficient in dwarf systems where the shallow gravitational potential well cannot retain the gaseous component anchored to the disc (Boselli et al. 2008a,b; Boselli et al. 2014d; Boselli & Gavazzi 2014). Curiously, the distribution of the HI-deficient cluster galaxies above $SFR \approx 1 M_{\odot} \text{ yr}^{-1}$ is similar to the one determined from the GAMA and SDSS sample of Gunawardhana et al. (2013). We recall, however, that the determination of the total volume sampled by the HRS is quite uncertain, thus if the shape of the luminosity distribution is robustly determined, a shift in the Y-axis can not be totally excluded.

6.2. SFR scaling relations

We trace the typical star formation rate scaling relations of the HRS. These relations can be compared to those already determined on the same sample for the optical and UV structural parameters (Cortese et al. 2012a), for the atomic (Cortese et al. 2011), molecular, and total gas content (Boselli et al. 2014b), and for the dust component (Cortese et al. 2012b). For a fair comparison with these works, we use in the following section the same scaling parameters: the stellar mass M_{star} (taken from Cortese et al. 2012a), the stellar mass surface density μ_{star} , the metallicity $12+\log(O/H)$, and the specific star formation rate $SSFR$. The star formation rates given in Table 6 have been divided by a factor 1.58 to convert them into the Chabrier (2003) IMF. Stellar masses have been determined using i -band luminosities and $g-i$ colours combined with the prescription of Zibetti et al. (2009). Their typical uncertainty is 0.15 dex¹⁰. The stellar surface density μ_{star} is the total stellar mass divided by the circular area defined by the i -band effective radius (the radius enclosing 50% of the total light). Its typical uncertainty is 0.20 dex. Metallicities are taken from Hughes et al. (2013), and are determined using the PP04 O3N2 calibration on [NII] and [OIII] emission lines (Pettini & Pagel 2004), with an uncertainty of 0.13 dex. Specific star formation rates $SSFR$ are defined as the ratio of the star formation rate per unit stellar mass. They correspond to the birthrate parameter b once the typical age of galaxies (here assumed to be of 13 Gyr) and a constant returned gas fraction R of 0.3 (Boselli et al. 2001) is taken into account. The typical uncertainty on this variable is 0.25 dex.

Figure 12 shows the relationship between the star formation rate and the stellar mass for all the HRS galaxies. This scaling relation is often referred in the literature as the main sequence (e.g., Guzman et al. 1997; Brinchmann & Ellis 2000; Bauer et al. 2005; Bell et al. 2005; Papovich et al. 2006; Reddy et al. 2006; Noeske et al. 2007; Salim et al. 2007; Elbaz et al. 2007; Daddi et al. 2007; Pannella et al. 2009; Rodighiero et al. 2010, 2011; Peng et al. 2010; Karim et al. 2011; Whitaker et al. 2012, 2014; Speagle et al. 2014). This relation is expected since it links two variables that scale with the size of galaxies. What is interesting in this relation is the determination of its slope and intercept and of its dispersion (see Tables 13 and 14). The bisector fit derived for the HRS (black solid line) is similar to the one determined by Peng et al. (2010) for a large sample of SDSS local galaxies (green dotted-dashed line), whereas the best linear fit (black dotted line) is similar to that determined for the HRS by Ciesla et al. (2014) using different definitions of M_{star} and SFR (yellow dashed line). Figure 12 shows a systematic shift in the relation between HI-normal field (filled dots, solid black line) and HI-deficient cluster galaxies (empty circles, solid red line). The relations determined for the two subsamples have a very similar slope, but the shift in the Y-axis is as large as 0.65 dex. The shift in the main sequence as a function of gas content is consistent with what is observed in higher redshift samples by Tacconi et al. (2013). This trend is predictable from the Schmidt law and is a further confirmation that the activity of star formation is quenched in galaxies stripped of their gaseous content in dense environments (e.g. Boselli & Gavazzi 2006, 2014). This evidence, however, contradicts the results of Peng et al. (2010), who found that there is no significant change in the

¹⁰ We choose to use these stellar masses instead of those determined from SED fitting, which are probably more accurate, because we want to be consistent with all the previous HRS papers presenting the stellar (Cortese et al. 2012a), gas (Cortese et al. 2011; Boselli et al. 2014b), and dust (Cortese et al. 2014) scaling relations.

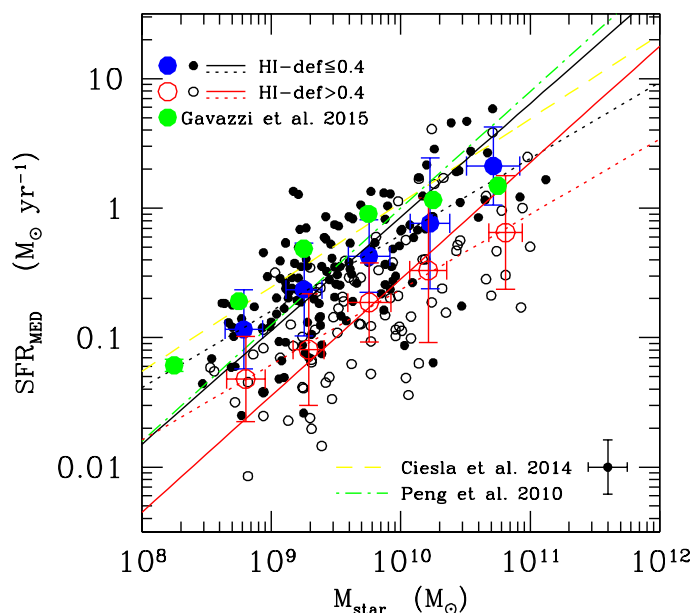


Fig. 12. Relationship between the star formation rate and the stellar mass for the HRS late-type galaxies. Filled dots are for HI-normal ($HI - def \leq 0.4$) field galaxies, empty circles for HI-deficient ($HI - def > 0.4$) cluster objects. The large filled blue and empty red circles give the mean values and the standard deviations in different bins of stellar mass determined in this work. The large green filled dots indicate the mean values of Gavazzi et al. (2015). The bisector fit for HI-normal and HI-deficient galaxies are given by the solid black and red lines, the linear direct fits by the dotted lines. The linear best fit of Ciesla et al. (2014) is marked with a yellow dashed line, the best fit of Peng et al. (2010) by the green dotted-dashed line. The error bar shows the typical uncertainty on the data.

slope and intercept of the main sequence drawn by galaxies belonging to different density environments. The sample of Peng et al. (2010), however, is composed of star forming galaxies as defined in Brinchmann et al. (2004), which includes galaxies with high signal-to-noise ($SN > 3$) in the $H\alpha$ and $H\beta$ lines. This selection criterion obviously favors active star forming objects as those located in the field but excludes the typical HI-deficient galaxies in clusters, where the activity of star formation is significantly quenched by the lack of gas. It is indeed known that these objects mainly populate the green valley and are thus, in terms of star formation, intermediate between normal star forming discs and passive early-type galaxies (Boselli et al. 2008a; Hughes & Cortese 2009; Cortese & Hughes 2009; Gavazzi et al. 2013a,b; Boselli et al. 2014c,d).

Figure 13 shows the relationship between the specific star formation rate and the morphological class in late-type systems. Figure 13 shows that the specific star formation rate is fairly constant with morphological type (e.g. Kennicutt et al. 1994). It also shows that gas-deficient galaxies have, on average, lower specific star formation rates than similar objects in the field. The mean value of the specific star formation rate of HI-normal galaxies is $SSFR = -10.01 \pm 0.41 \text{ yr}^{-1}$, while that of HI-deficient objects is $SSFR = -10.52 \pm 0.49 \text{ yr}^{-1}$. Mean values for each morphological class and standard deviations are given in Table 12. Again, these results are fully consistent with what previously found from the $H\alpha$ imaging survey of nearby cluster galaxies (Gavazzi et al. 2002, 2006).

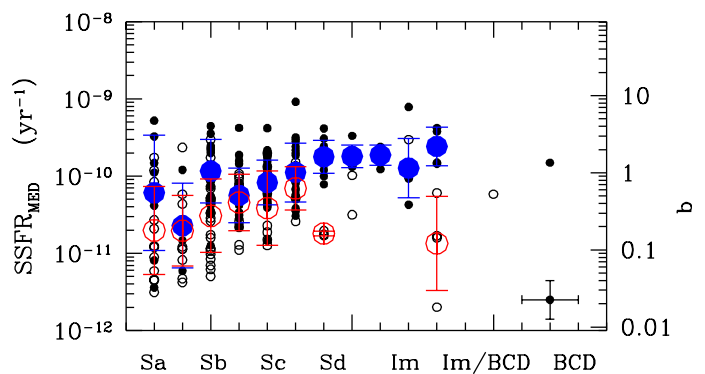


Fig. 13. Relationship between the specific star formation rate and the morphological type for HI-normal ($HI - def \leq 0.4$; filled dots) and HI-deficient ($HI - def > 0.4$; empty circles) galaxies. The large filled blue dots indicate the mean values per each morphological class for normal gas-rich systems, the empty red ones for cluster HI-deficient galaxies. For the large symbols the error bar shows the standard deviation of the distribution. The small error bar shows the typical uncertainty on the data.

Figure 14 and Tables 13 and 14 show that the specific star formation rate decreases with increasing stellar mass, stellar surface density, and metallicity (the probability that these variables are correlated is in all cases $P > 99.9\%$). The decrease of the specific star formation rate as a function of the stellar mass has already been noticed in Gavazzi et al. (1998) and explained in the framework of a secular evolution of galaxies in Boselli et al. (2001). It also matches the trend observed in the SDSS for local galaxies (e.g. Brinchmann et al. 2004). The observed trends with the stellar mass surface density and the metallicity are due to the fact that M_{star} , μ_{star} , and $12 + \log(O/H)$ are tightly connected variables (e.g. Brinchmann et al. 2004; Boselli et al. 2008b; Tremonti et al. 2004). As for Fig. 13, HI-deficient cluster galaxies have, on average, specific star formation rates smaller than similar field objects with a normal HI gas content (Gavazzi et al. 2002, 2006).

6.3. Morphological properties

We can also study how the morphological properties of the HRS late-type galaxies traced by the CAS parameters determined both in the broad band r filter and in the narrow band $H\alpha + [NII]$ filter are related to the scaling parameters used in the previous section (Figs. 15 and 16). Figure 15 shows that the asymmetry A_r and clumpiness S_r parameters measured in the r -band do not change as a function of stellar mass, stellar surface density, and metallicity of galaxies. The concentration parameter C_r , instead, is fairly constant for galaxies of stellar mass $M_{star} \lesssim 10^{9.5} M_{\odot}$, and increases at higher mass. An increase of the concentration index with stellar mass, generally attributed to the presence of a dominant bulge, has been already noticed in the past (e.g. Gavazzi et al. 1996; Fossati et al. 2013). A similar increase of C_r with stellar mass surface density and metallicity is also present, and expected given that all these scaling variables are tightly connected. The three CAS parameters also do not change significantly with the specific star formation rate of galaxies. We notice, however, a very moderate increase of A_r with $SSFR$.

The same parameters measured in the $H\alpha + [NII]$ band show much more dispersed distributions and do not show any evident trend when plotted against the stellar mass, stellar mass surface density, and metallicity. Contrary to the r -band, the concentra-

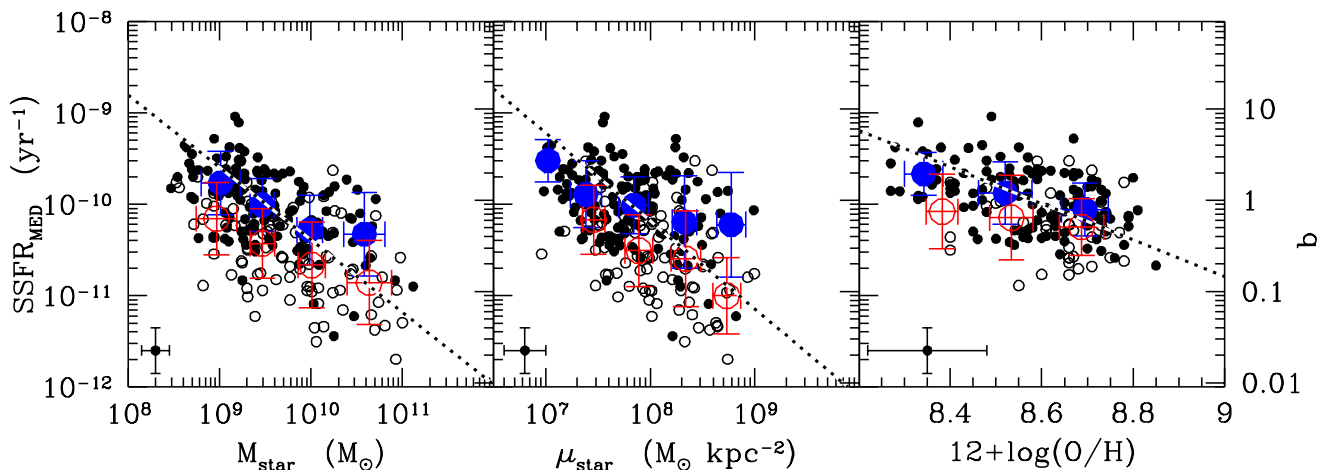


Fig. 14. Relationship between the specific star formation rate and the total stellar mass (left), the stellar mass surface density (centre), and the metallicity (right) for HI-normal ($HI - def \leq 0.4$; filled dots) and HI-deficient ($HI - def > 0.4$; empty circles) galaxies. The large filled blue dots indicate the mean values per each morphological class for normal gas-rich systems, the empty red ones for cluster HI-deficient galaxies. For the large symbols the error bar shows the standard deviation of the distribution. The dotted line shows the bisector fit determined for HI-normal galaxies. The small error bar shows the typical uncertainty on the data.

tion parameter $C_{H\alpha}$ is fairly constant over the whole stellar mass range covered by the sample, consistent with the fact that the star formation activity of galaxies is mainly localised on the disc. Furthermore, the mean values of the three CAS parameters measured in the $H\alpha$ + $[NII]$ band are systematically shifted with respect to those estimated in the r -band, as already noticed by Fossati et al. (2013). A similar increase of the CAS parameters with decreasing wavelength has been also observed by Lauger et al. (2005) and Taylor-Mager et al. (2007) in $z \sim 1$ galaxies. The CAS parameters are often used to quantify the merging rate of different samples of galaxies (e.g. Conselice 2014). None of the 205 galaxies with available CAS parameters in the r -band satisfies the condition:

$$(A > 0.35) \ \& \ (A > S) \quad (14)$$

proposed to identify mergers (Conselice 2014). In the $H\alpha$ band this condition is satisfied by 7/202 objects (HRS 12, 27, 31, 189, 237, 256, 265), but the clumpy nature of the star forming regions makes the condition given in eq. 14 probably not valid in this band.

The asymmetry and clumpiness parameters increase systematically with the specific star formation rate $SSFR$. Galaxies with the highest specific star formation rate, thus those objects which are forming most of their stars at the present epoch, have a strongly asymmetric distribution of the star forming regions over their disc. They have also a clumpy structure in $H\alpha$ + $[NII]$ indicating that their star formation activity is mostly due to giant HII regions sporadically distributed over their discs (distance and blending problems should not introduce strong systematic effects since galaxies are all at \sim the same distance, Thilker et al. 2000, Liu et al. 2013). This result can be explained if the HII region luminosity function and the contribution of the diffuse emission change in galaxies of different stellar mass or morphological type, as first suggested by Kennicutt et al. (1989), Caldwell et al. (1991), and Youngblood & Hunter (1999). These studies have shown that in early-type massive spirals the bulk of the star formation occurs in several small HII regions, whilst late-type, low-mass systems form most of their massive stars in a few giant HII regions. These results, however, still need to be confirmed on large homogeneous samples

with high-quality imaging data (Thilker et al. 2002; Helmboldt et al. 2005; Schombert et al. 2013; Liu et al. 2013). Nevertheless, since the number of HII regions decreases with the decreasing size of galaxies, and that their distribution over the disc is random, we expect an increase of the asymmetry parameter in dwarf systems. Variations of the clumpiness index S as a function of the $H\alpha$ equivalent width, which is a proxy for the $SSFR$, have been already reported by Conselice (2003), while that of the asymmetry parameter A with the $B-V$ colour index by Conselice et al. (2000).

The CAS parameters can also be plotted against the HI-deficiency parameter, often taken as a direct tracer of the perturbation induced by the hostile environment in cluster galaxies (e.g. Boselli & Gavazzi 2006). Figure 17 shows that while the CAS parameters measured in the r -band are fairly constant, $A_{H\alpha}$ and $S_{H\alpha}$ systematically decrease with increasing HI-deficiency. Given that HI-deficient galaxies have, on average, lower $SSFR$ s than unperturbed systems, this observed decrease might result from the $A_{H\alpha}$ and $S_{H\alpha}$ increase with $SSFR$ observed in Fig. 16.

7. Conclusions

We present new $H\alpha$ + $[NII]$ narrow band imaging observations of late-type galaxies in the *Herschel* Reference Survey done with the 2.1 m San Pedro Martir telescope. Combined with those already available in the literature, $H\alpha$ + $[NII]$ data are now available for 281/323 galaxies of the sample, and for 254/260 of the late-type systems. These data are used to extract fluxes and equivalent widths, as well as the CAS morphological parameters, with the aim of studying the star formation properties of a volume-limited, K-band-selected complete sample of nearby late-type (Sa-Im-BCD) galaxies. The $H\alpha$ + $[NII]$ imaging data are first corrected for $[NII]$ contamination and dust attenuation using the integrated spectroscopy and the $24 \mu\text{m}$ flux densities available for this sample. We then compare the star formation rate determined using either independent monochromatic star formation tracers ($H\alpha$, FUV *GALEX*, radio continuum luminosities) or the output of the CIGALE SED fitting code done under different assumptions. The comparison of the different tracers shows that:

1) All tracers are strongly correlated with each other (e.g.

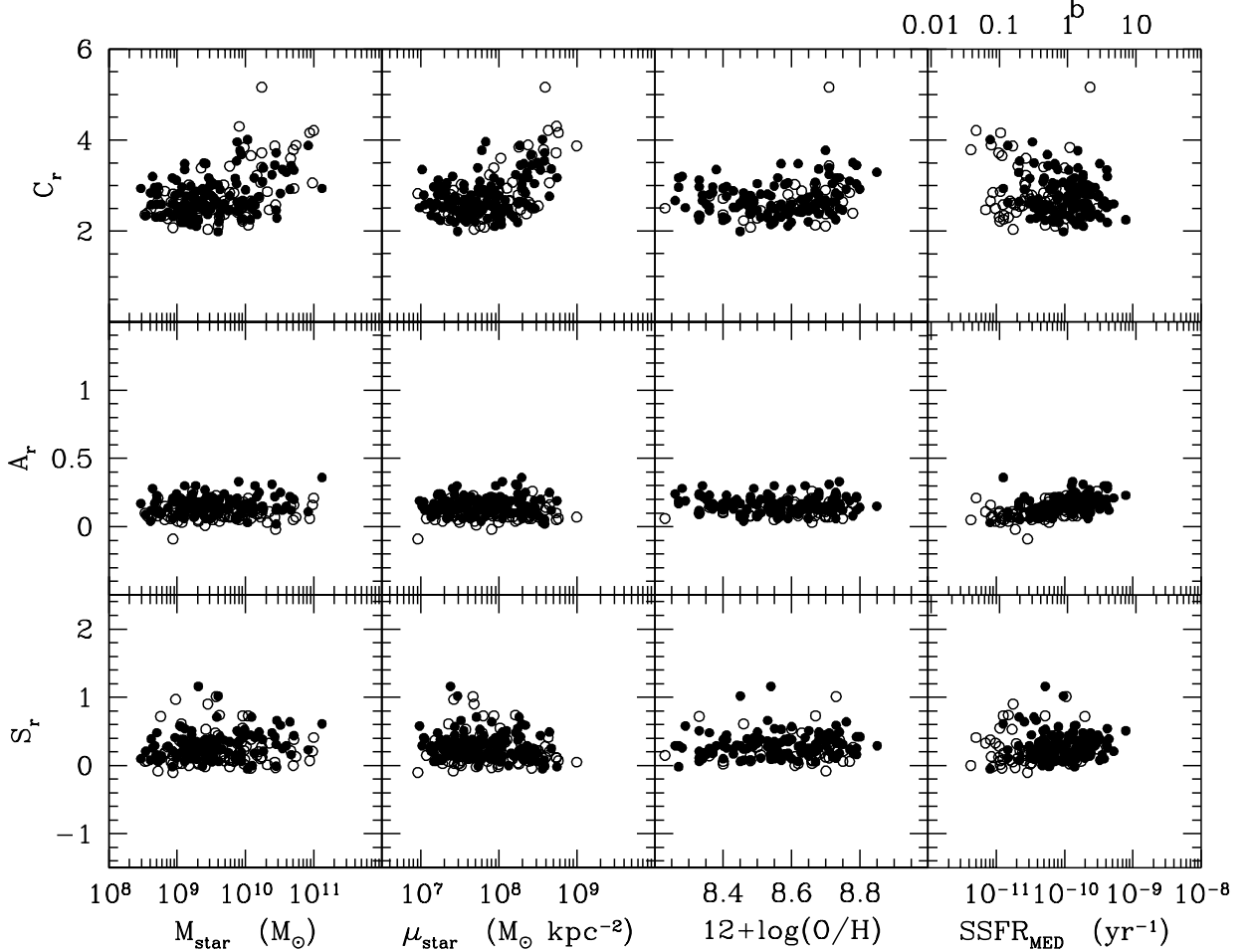


Fig. 15. Relationship between the CAS parameters determined in the r -band and the total stellar mass (left), the stellar mass surface density (centre left), the metallicity (centre right), and the specific star formation rate (right) for HI-normal ($HI - def \leq 0.4$; filled dots) and HI-deficient ($HI - def > 0.4$; empty circles) galaxies.

Calzetti et al. 2007, 2010; Kennicutt et al. 2009). The typical dispersion in the derived star formation rates is of the order of 24%. This value, however, should be considered as a lower limit for the uncertainty of the SFR determination since it has been determined on non fully independent variables and making similar assumptions on the IMF and on the star formation history of the target galaxies.

2) The $H\alpha$ luminosities corrected for dust attenuation using the Balmer decrement and the $24 \mu\text{m}$ emission give consistent results only whenever the Balmer decrement is determined with an accuracy $\sigma[C(H\beta)] \leq 0.1$. The most distant objects from the $L(H\alpha)_{BD}$ vs. $L(H\alpha)_{24\mu\text{m}}$ relation all have physical properties typical of quiescent galaxies. This observational evidence suggests that the $24 \mu\text{m}$ based attenuation correction derived

for star forming galaxies could be non universal and, as pointed out by Kennicutt et al. (2009), should be used with extreme caution in massive galaxies characterised by a low activity of star formation, where the heating of the dust is done also by the evolved stellar populations.

3) The comparison of the star formation rates determined using monochromatic tracers and UV-to-far infrared SED fitting codes gives consistent results in unperturbed late-type systems (e.g. Wuyts et al. 2009; Pforr et al. 2012; Buat et al. 2014), while small but systematic differences in the two tracers are present in HI-deficient cluster galaxies. These differences cannot be explained by a non optimised parametrisation of the star formation history of cluster galaxies that is unable to reproduce an abrupt truncation of their activity once entered into the cluster.

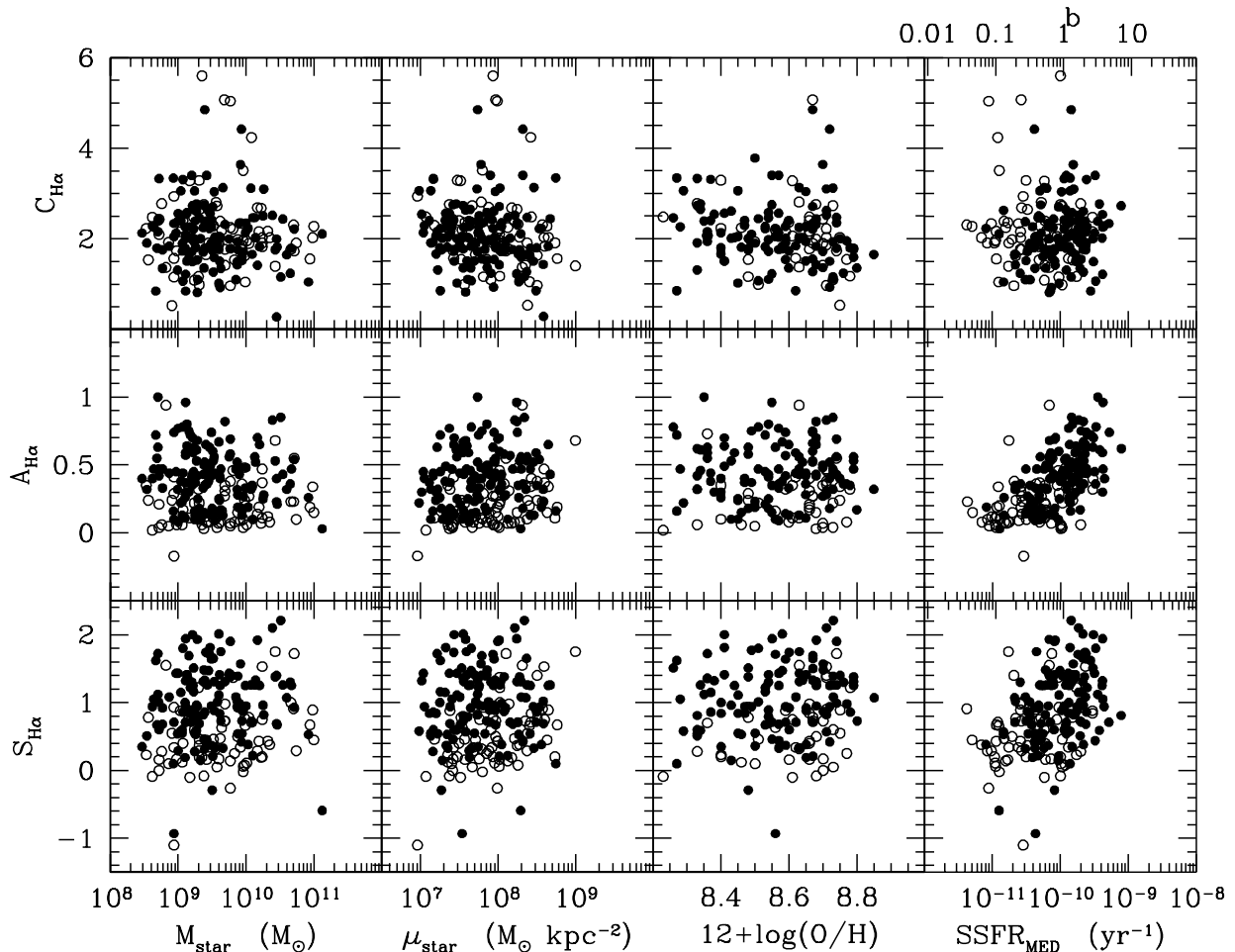


Fig. 16. Relationship between the CAS parameters determined in the $H\alpha$ + $[NII]$ narrow band filter and the total stellar mass (left), the stellar mass surface density (centre left), the metallicity (centre right), and the specific star formation rate (right) for HI-normal ($HI - def \leq 0.4$; filled dots) and HI-deficient ($HI - def > 0.4$; empty circles) galaxies.

They might be a further indication that the prescription used to correct the $H\alpha$ for dust attenuation based on the $24 \mu m$ emission are not valid in red and quiescent spirals, where the dust heating comes primarily from the evolved stellar population.

The new set of data is used to trace the star formation rate distribution of a K-band-selected, volume-limited sample of nearby galaxies and to derive the typical scaling relations between the specific star formation rate and the morphological type, the stellar mass and stellar surface density, the metallicity, and the CAS parameters for the late-type systems. The specific star formation rate is anticorrelated with the stellar mass (e.g. Boselli et al. 2001), the stellar mass surface density, and the metallicity of galaxies in the range sampled by these param-

eters, while it is fairly constant with the morphological type (e.g. Kennicutt et al. 1994). All relations show a systematic difference between cluster and isolated galaxies confirming the quenching of the star formation activity in high density environments (e.g. Boselli & Gavazzi 2006, 2014). They also show a clear relation between the asymmetry and clumpiness parameters and the specific star formation rate. This relation can be explained if the HII luminosity function of low-mass actively star forming galaxies is dominated by a few giant HII regions while that of massive and quiescent systems by several HII region of intermediate-to-low luminosity, a result that still needs to be confirmed observationally.

Acknowledgements. We are grateful to the referee for constructive comments and suggestions, and to Luca Cortese for his long term collaboration on the

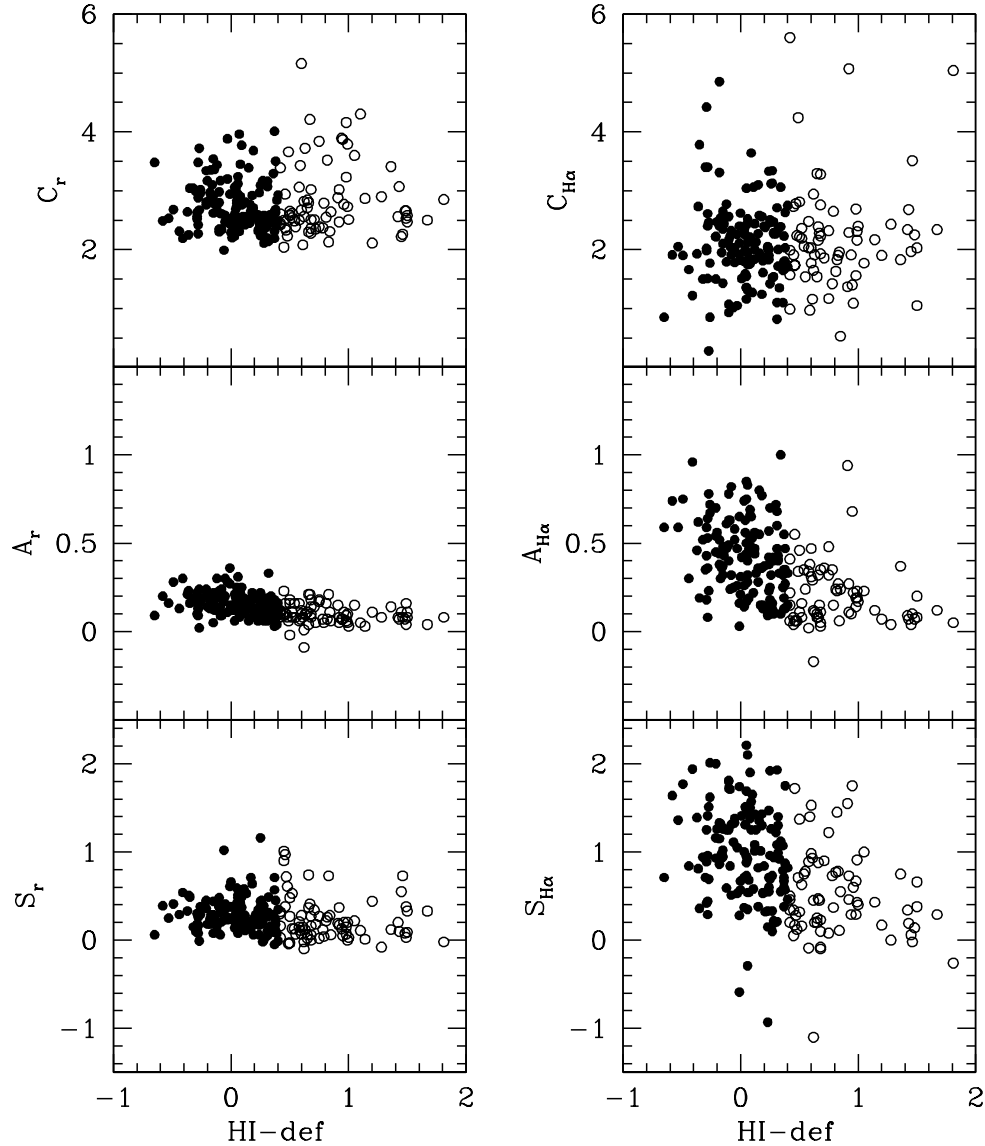


Fig. 17. Relationship between the CAS parameters determined in the r (left) and $H\alpha$ + $[NII]$ narrow band filter (right) and the HI-deficiency parameter for HI-normal ($HI - def \leq 0.4$; filled dots) and HI-deficient ($HI - def > 0.4$; empty circles) galaxies.

HRS project. This research has made use of data from the HRS project. HRS is a Herschel Key Programme utilising guaranteed time from the SPIRE instrument team, ESAC scientists and a mission scientist. The HRS data was accessed through the Herschel Database in Marseille (HeDaM - <http://hedam.lam.fr>) operated by CeSAM and hosted by the Laboratoire d'Astrophysique de Marseille. We acknowledge financial support from Programme National de Cosmologie and Galaxies (PNCG) of CNRS/INSU, France. MF acknowledges the support of the Deutsche Forschungsgemeinschaft via Project ID 387/1-1. The $H\alpha$ + $[NII]$ images of the Virgo cluster galaxies belonging to the HRS have been taken from the GOLDMine database (Gavazzi et al. 2003).

References

- Argence, B., & Lamareille, F. 2009, *A&A*, 495, 759
 Bakes, E. L. O., & Tielens, A. G. G. M. 1994, *ApJ*, 427, 822
 Bauer, A. E., Drory, N., Hill, G. J., & Feulner, G. 2005, *ApJ*, 621, L89
 Becker, R. H., White, R. L., & Helfand, D. J. 1995, *ApJ*, 450, 559
 Bell, E. F. 2003, *ApJ*, 586, 794
 Bell, E. F., Papovich, C., Wolf, C., et al. 2005, *ApJ*, 625, 23
 Bendo, G. J., Wilson, C. D., Pohlen, M., et al. 2010, *A&A*, 518, LL65
 Bendo, G. J., Boselli, A., Dariush, A., et al. 2012, *MNRAS*, 419, 1833
 Bigiel, F., Leroy, A., Walter, F., et al. 2008, *AJ*, 136, 2846
 Binggeli, B., Sandage, A., & Tammann, G. A. 1985, *AJ*, 90, 1681
 Boissier, S. 2013, *Planets, Stars and Stellar Systems. Volume 6: Extragalactic Astronomy and Cosmology*, 141
 Boselli, A. 2011, *A Panchromatic View of Galaxies*, by Alessandro Boselli. - Practical Approach Book - ISBN-10: 3-527-40991-2. ISBN-13: 978-3-527-40991-4 - Wiley-VCH, Berlin 2011. XVI, 324pp, Hardcover,
 Boselli, A., & Gavazzi, G. 2002, *A&A*, 386, 124
 Boselli, A., & Gavazzi, G. 2006, *PASP*, 118, 517
 Boselli, A., & Gavazzi, G. 2014, *A&A Rev.*, 22, 74
 Boselli, A., Gavazzi, G., Donas, J., & Scodreggio, M. 2001, *AJ*, 121, 753
 Boselli, A., Iglesias-Páramo, J., Vilchez, J. M., & Gavazzi, G. 2002a, *A&A*, 386, 134
 Boselli, A., Lequeux, J., & Gavazzi, G. 2002b, *A&A*, 384, 33
 Boselli, A., Cortese, L., Deharveng, J. M., et al. 2005, *ApJ*, 629, L29
 Boselli, A., Boissier, S., Cortese, L., et al. 2006, *ApJ*, 651, 811

- Boselli, A., Boissier, S., Cortese, L., & Gavazzi, G. 2008, *ApJ*, 674, 742
- Boselli, A., Boissier, S., Cortese, L., & Gavazzi, G. 2008, *A&A*, 489, 1015
- Boselli, A., Boissier, S., Cortese, L., et al. 2009, *ApJ*, 706, 1527
- Boselli, A., Eales, S., Cortese, L., et al. 2010, *PASP*, 122, 261
- Boselli, A., Boissier, S., Heinis, S., et al. 2011, *A&A*, 528, AA107
- Boselli, A., Ciesla, L., Cortese, L., et al. 2012, *A&A*, 540, AA54
- Boselli, A., Hughes, T. M., Cortese, L., Gavazzi, G., & Buat, V. 2013, *A&A*, 550, A114
- Boselli, A., Cortese, L., & Boquien, M. 2014a, *A&A*, 564, AA65
- Boselli, A., Cortese, L., Boquien, M., et al. 2014b, *A&A*, 564, AA66
- Boselli, A., Cortese, L., Boquien, M., et al. 2014c, *A&A*, 564, AA67
- Boselli, A., Voyer, E., Boissier, S., et al. 2014d, *A&A*, 570, AA69
- Boquien, M., Calzetti, D., Combes, F., et al. 2011, *AJ*, 142, 111
- Boquien, M., Buat, V., & Perret, V. 2014, *A&A*, 571, AA72
- Brinchmann, J., & Ellis, R. S. 2000, *ApJ*, 536, L77
- Brinchmann, J., Charlot, S., White, S. D. M., et al. 2004, *MNRAS*, 351, 1151
- Bruzual, G., & Charlot, S. 2003, *MNRAS*, 344, 1000
- Buat, V., Boselli, A., Gavazzi, G., & Bonfanti, C. 2002, *A&A*, 383, 801
- Buat, V., Heinis, S., Boquien, M., et al. 2014, *A&A*, 561, AA39
- Caldwell, N., Kennicutt, R., Phillips, A. C., & Schommer, R. A. 1991, *ApJ*, 370, 526
- Calzetti, D. 2001, *PASP*, 113, 1449
- Calzetti, D., Kennicutt, R. C., Engelbracht, C. W., et al. 2007, *ApJ*, 666, 870
- Calzetti, D., Wu, S.-Y., Hong, S., et al. 2010, *ApJ*, 714, 1256
- Cappellari, M., & Emsellem, E. 2004, *PASP*, 116, 138
- Chabrier, G. 2003, *PASP*, 115, 763
- Chomiuk, L., & Povich, M. S. 2011, *AJ*, 142, 197
- Ciesla, L., Boselli, A., Smith, M. W. L., et al. 2012, *A&A*, 543, AA161
- Ciesla, L., Boquien, M., Boselli, A., et al. 2014, *A&A*, 565, AA128
- Ciesla, L., Charmandaris, V., Georgakakis, A., et al. 2015, arXiv:1501.03672
- Condon, J. J. 1987, *ApJS*, 65, 485
- Condon, J. J. 1992, *ARA&A*, 30, 575
- Condon, J. J., Yin, Q. F., & Burstein, D. 1987, *ApJS*, 65, 543
- Condon, J. J., Helou, G., Sanders, D. B., & Soifer, B. T. 1990, *ApJS*, 73, 359
- Condon, J. J., Anderson, M. L., & Helou, G. 1991, *ApJ*, 376, 95
- Condon, J. J., Cotton, W. D., Greisen, E. W., et al. 1998, *AJ*, 115, 1693
- Condon, J. J., Cotton, W. D., & Broderick, J. J. 2002, *AJ*, 124, 675
- Conselice, C. J. 2003, *ApJS*, 147, 1
- Conselice, C. J. 2014, *ARA&A*, 52, 291
- Conselice, C. J., Bershad, M. A., & Gallagher, J. S., III 2000, *A&A*, 354, L21
- Cortese, L., & Hughes, T. M. 2009, *MNRAS*, 400, 1225
- Cortese, L., Boselli, A., Franzetti, P., et al. 2008, *MNRAS*, 386, 1157
- Cortese, L., Catinella, B., Boissier, S., Boselli, A., & Heinis, S. 2011, *MNRAS*, 415, 1797
- Cortese, L., Boissier, S., Boselli, A., et al. 2012a, *A&A*, 544, A101
- Cortese, L., Ciesla, L., Boselli, A., et al. 2012b, *A&A*, 540, AA52
- Cortese, L., Fritz, J., Bianchi, S., et al. 2014, *MNRAS*, 440, 942
- da Cunha, E., Charlot, S., & Elbaz, D. 2008, *MNRAS*, 388, 1595
- Daddi, E., Dickinson, M., Morrison, G., et al. 2007, *ApJ*, 670, 156
- da Silva, R. L., Fumagalli, M., & Krumholz, M. R. 2014, *MNRAS*, 444, 3275
- de Jong, T., Klein, U., Wielebinski, R., & Wunderlich, E. 1985, *A&A*, 147, L6
- Domingue, D. L., Sulentic, J. W., Xu, C., et al. 2003, *AJ*, 125, 555
- Draine, B. T., & Li, A. 2007, *ApJ*, 657, 810
- Draine, B. T., Dale, D. A., Bendo, G., et al. 2007, *ApJ*, 663, 866
- Dreyer, J. L. E. 1895, *MNRAS*, 51, 185
- Dreyer, J. L. E. 1888, *MNRAS*, 49, 1
- Elbaz, D., Daddi, E., Le Borgne, D., et al. 2007, *A&A*, 468, 33
- Falcón-Barroso, J., Bacon, R., Bureau, M., et al. 2006, *MNRAS*, 369, 529
- Finkelman, I., Brosch, N., Funes, J. G., Kniazev, A. Y., Vaumlisänen, P. 2010, *MNRAS*, 407, 2475
- Fitzpatrick, E. L., & Massa, D. 2007, *ApJ*, 663, 320
- Fossati, M., Gavazzi, G., Savorgnan, G., et al. 2013, *A&A*, 553, A91
- Fumagalli, M., da Silva, R. L., & Krumholz, M. R. 2011, *ApJ*, 741, LL26
- Gallego, J., Zamorano, J., Aragon-Salamanca, A., & Rego, M. 1995, *ApJ*, 455, L1
- Gavazzi, G., & Boselli, A. 1999, *A&A*, 343, 93
- Gavazzi, G., & Boselli, A. 1999, *A&A*, 343, 86
- Gavazzi, G., Boselli, A., & Kennicutt, R. 1991, *AJ*, 101, 1207
- Gavazzi, G., Catinella, B., Carrasco, L., Boselli, A., & Contursi, A. 1998, *AJ*, 115, 1745
- Gavazzi, G., Boselli, A., Scodreggio, M., Pierini, D., & Belsole, E. 1999, *MNRAS*, 304, 595
- Gavazzi, G., Boselli, A., Pedotti, P., Gallazzi, A., & Carrasco, L. 2002, *A&A*, 386, 114
- Gavazzi, G., Boselli, A., Donati, A., Franzetti, P., & Scodreggio, M. 2003, *A&A*, 400, 451
- Gavazzi, G., Boselli, A., Cortese, L., et al. 2006, *A&A*, 446, 839
- Gavazzi, G., Fumagalli, M., Galardo, V., et al. 2012, *A&A*, 545, A16
- Gavazzi, G., Fumagalli, M., Fossati, M., et al. 2013a, *A&A*, 553, AA89
- Gavazzi, G., Savorgnan, G., Fossati, M., et al. 2013b, *A&A*, 553, AA90
- Gavazzi, G., Consolandi, G., Dotti M., et al. 2015a, *A&A*, submitted
- Gavazzi, G., Consolandi, G., Viscardi E., et al. 2015b, *A&A*, in press
- Groves, B., Brinchmann, J., & Walcher, C. J. 2012, *MNRAS*, 419, 1402
- Gunawardhana, M. L. P., Hopkins, A. M., Bland-Hawthorn, J., et al. 2013, *MNRAS*, 433, 2764
- Guzmán, R., Gallego, J., Koo, D. C., et al. 1997, *ApJ*, 489, 559
- James, P. A., Shane, N. S., Beckman, J. E., et al. 2004, *A&A*, 414, 23
- Hameed, S., & Devereux, N. 2005, *AJ*, 129, 2597
- Hao, C.-N., Kennicutt, R. C., Johnson, B. D., et al. 2011, *ApJ*, 741, 124
- Haynes, M. P., & Giovanelli, R. 1984, *AJ*, 89, 758
- Helmholtz, J. F., Waltherbos, R. A. M., Bothun, G. D., & O'Neil, K. 2005, *ApJ*, 630, 824
- Hollenbach, D., & Salpeter, E. E. 1971, *ApJ*, 163, 155
- Hollenbach, D. J., & Tielens, A. G. G. M. 1997, *ARA&A*, 35, 179
- Hughes, T. M., & Cortese, L. 2009, *MNRAS*, 396, L41
- Hughes, T. M., Cortese, L., Boselli, A., Gavazzi, G., & Davies, J. I. 2013, *A&A*, 550, AA115
- Karim, A., Schinnerer, E., Martínez-Sansigre, A., et al. 2011, *ApJ*, 730, 61
- Kennicutt, R. C., Jr. 1998, *ARA&A*, 36, 189
- Kennicutt, R. C., Jr., & Kent, S. M. 1983, *AJ*, 88, 1094
- Kennicutt, R. C., & Evans, N. J. 2012, *ARA&A*, 50, 531
- Kennicutt, R. C., Jr., Roettiger, K. A., Keel, W. C., van der Hulst, J. M., & Hummel, E. 1987, *AJ*, 93, 1011
- Kennicutt, R. C., Jr., Edgar, B. K., & Hodge, P. W. 1989, *ApJ*, 337, 761
- Kennicutt, R. C., Jr., Tamblyn, P., & Congdon, C. E. 1994, *ApJ*, 435, 22
- Kennicutt, R. C., Jr., Calzetti, D., Walter, F., et al. 2007, *ApJ*, 671, 333
- Kennicutt, R. C., Jr., Lee, J. C., Funes, S. J., José G., Sakai, S., & Akiyama, S. 2008, *ApJS*, 178, 247
- Kennicutt, R. C., Jr., Hao, C.-N., Calzetti, D., et al. 2009, *ApJ*, 703, 1672
- Kim, D.-W. 1989, *ApJ*, 346, 653
- Koopmann, R. A., & Kenney, J. D. P. 2006, *ApJS*, 162, 97
- Koopmann, R. A., Kenney, J. D. P., & Young, J. 2001, *ApJS*, 135, 125
- Kroupa, P. 2001, *MNRAS*, 322, 231
- Iglesias-Páramo, J., Boselli, A., Cortese, L., Vilchez, J. M., & Gavazzi, G. 2002, *A&A*, 384, 383
- Isobe, T., Feigelson, E. D., Akritas, M. G., & Babu, G. J. 1990, *ApJ*, 364, 104
- Lauger, S., Burgarella, D., & Buat, V. 2005, *A&A*, 434, 77
- Lee, J. C., Gil de Paz, A., Tremonti, C., et al. 2009, *ApJ*, 706, 599
- Lequeux, J. 1971, *A&A*, 15, 42
- Lequeux, J., Maucherat-Joubert, M., Deharveng, J. M., & Kunth, D. 1981, *A&A*, 103, 305
- Liu, G., Calzetti, D., Kennicutt, R. C., Jr., et al. 2013, *ApJ*, 772, 27
- Macchetto, F., Pastoriza, M., Caon, N., et al. 1996, *A&AS*, 120, 463
- Martel, A. R., Ford, H. C., Bradley, L. D., et al. 2004, *AJ*, 128, 2758
- Massey, P., Strobel, K., Barnes, J. V., & Anderson, E. 1988, *ApJ*, 328, 315
- Momcheva, I. G., Lee, J. C., Ly, C., et al. 2013, *AJ*, 145, 47
- Nilson, P. 1973, *Acta Universitatis Upsaliensis. Nova Acta Regiae Societatis Scientiarum Upsaliensis - Uppsala Astronomiska Observatoriums Annaler*, Uppsala: Astronomiska Observatorium, 1973,
- Noeske, K. G., Weiner, B. J., Faber, S. M., et al. 2007, *ApJ*, 660, L43
- Noll, S., Burgarella, D., Giovannoli, E., et al. 2009, *A&A*, 507, 1793
- Nothenius, R. 1993, *ApJS*, 85, 1
- O'Connell, R. W. 1999, *ARA&A*, 37, 603
- Osterbrock, D. E., & Ferland, G. J. 2006, *Astrophysics of gaseous nebulae and active galactic nuclei*, 2nd. ed. by D.E. Osterbrock and G.J. Ferland. Sausalito, CA: University Science Books, 2006,
- Pannella, M., Carilli, C. L., Daddi, E., et al. 2009, *ApJ*, 698, L116
- Papovich, C., Moustakas, L. A., Dickinson, M., et al. 2006, *ApJ*, 640, 92
- Peng, Y.-j., Lilly, S. J., Kovač, K., et al. 2010, *ApJ*, 721, 193
- Pérez-González, P. G., Zamorano, J., Gallego, J., Aragón-Salamanca, A., & Gil de Paz, A. 2003, *ApJ*, 591, 827
- Pettini, M., & Pagel, B. E. J. 2004, *MNRAS*, 348, L59
- Pförr, J., Maraston, C., & Tonini, C. 2012, *MNRAS*, 422, 3285
- Reddy, N. A., Steidel, C. C., Fadda, D., et al. 2006, *ApJ*, 644, 792
- Rodighiero, G., Cimatti, A., Gruppioni, C., et al. 2010, *A&A*, 518, LL25
- Rodighiero, G., Daddi, E., Baronchelli, I., et al. 2011, *ApJ*, 739, LL40
- Rodighiero, G., Renzini, A., Daddi, E., et al. 2014, *MNRAS*, 443, 19
- Romanishin, W. 1990, *AJ*, 100, 373
- Salim, S., & Lee, J. C. 2012, *ApJ*, 758, 134
- Salim, S., Rich, R. M., Charlot, S., et al. 2007, *ApJS*, 173, 267
- Salim, S., Dickinson, M., Michael Rich, R., et al. 2009, *ApJ*, 700, 161
- Sánchez-Gallego, J. R., Knapen, J. H., Wilson, C. D., et al. 2012, *MNRAS*, 422, 3208
- Sarzi, M., Falcón-Barroso, J., Davies, R. L., et al. 2006, *MNRAS*, 366, 1151
- Schimminovich, D., Catinella, B., Kauffmann, G., et al. 2010, *MNRAS*, 408, 919
- Schlegel, D. J., Finkbeiner, D. P., & Davis, M. 1998, *ApJ*, 500, 525

- Schombert, J., McGaugh, S., & Maciel, T. 2013, *AJ*, 146, 41
 Shields, J. C. 1991, *AJ*, 102, 1314
 Silva, L., Granato, G. L., Bressan, A., & Danese, L. 1998, *ApJ*, 509, 103
 Singh, K. P., Bhat, P. N., Prabhu, T. P., & Kembhavi, A. K. 1995, *A&A*, 302, 658
 Speagle, J. S., Steinhardt, C. L., Capak, P. L., & Silverman, J. D. 2014, *ApJS*, 214, 15
 Spector, O., Finkelman, I., & Brosch, N. 2012, *MNRAS*, 419, 2156
 Tacconi, L. J., Neri, R., Genzel, R., et al. 2013, *ApJ*, 768, 74
 Taylor-Mager, V. A., Conselice, C. J., Windhorst, R. A., & Jansen, R. A. 2007, *ApJ*, 659, 162
 Thilker, D. A., Braun, R., & Walterbos, R. A. M. 2000, *AJ*, 120, 3070
 Thilker, D. A., Walterbos, R. A. M., Braun, R., & Hoopes, C. G. 2002, *AJ*, 124, 3118
 Tremonti, C. A., Heckman, T. M., Kauffmann, G., et al. 2004, *ApJ*, 613, 898
 Tresse, L., & Maddox, S. J. 1998, *ApJ*, 495, 691
 Trinchieri, G., & di Serego Alighieri, S. 1991, *AJ*, 101, 1647
 Tully, R. B. 1987, *ApJ*, 321, 280
 Usui, T., Saito, M., & Tomita, A. 1998, *AJ*, 116, 2166
 Valiante, R., Schneider, R., Bianchi, S., & Andersen, A. C. 2009, *MNRAS*, 397, 1661
 Young, J. S., Allen, L., Kenney, J. D. P., Lesser, A., & Rownd, B. 1996, *AJ*, 112, 1903
 Youngblood, A. J., & Hunter, D. A. 1999, *ApJ*, 519, 55
 Yun, M. S., Reddy, N. A., & Condon, J. J. 2001, *ApJ*, 554, 803
 Weisz, D. R., Johnson, B. D., Johnson, L. C., et al. 2012, *ApJ*, 744, 44
 Whitaker, K. E., van Dokkum, P. G., Brammer, G., & Franx, M. 2012, *ApJ*, 754, LL29
 Whitaker, K. E., Franx, M., Leja, J., et al. 2014, *ApJ*, 795, 104
 Waller, W. H. 1990, *PASP*, 102, 1217
 Wolfire, M. G., Hollenbach, D., McKee, C. F., Tielens, A. G. G. M., & Bakes, E. L. O. 1995, *ApJ*, 443, 152
 Wolfire, M. G., Tielens, A. G. G. M., Hollenbach, D., & Kaufman, M. J. 2008, *ApJ*, 680, 384
 Wuyts, S., Franx, M., Cox, T. J., et al. 2009, *ApJ*, 696, 348
 Zhu, Y.-N., Wu, H., Cao, C., & Li, H.-N. 2008, *ApJ*, 686, 155
 Zibetti, S., Charlot, S., & Rix, H.-W. 2009, *MNRAS*, 400, 1181
 Zwicky, F., Herzog, E., & Wild, P. 1968, Pasadena: California Institute of Technology (CIT), 1961-1968,

Appendix A: GANDALF spectroscopy

The comparison of the $H\alpha$ luminosity corrected for dust attenuation using the Balmer decrement measured in Boselli et al. (2013) and the $H\alpha$ luminosity corrected using the $24\ \mu\text{m}$ emission, or the 20 cm radio continuum luminosity (Fig. A.1) shows a systematic shift of ~ 0.5 dex in the relations between galaxies with strong ($H\beta\text{E.W.} > 5\ \text{\AA}$) and weak ($H\beta\text{E.W.} < 5\ \text{\AA}$) $H\beta$ emission. Given that the three variables are roughly equivalent, the observed shift probably results from a systematic bias in the spectroscopic data used to correct $L(H\alpha)_{BD}$. We recall that in Boselli et al. (2013) the intensity of the $H\beta$ line has been measured by fitting the spectra with a double Gaussian, one for the emission line and the other for the underlying stellar absorption. The observed shift can thus be explained if the Balmer decrement is overestimated, or the $H\beta$ emission is underestimated by $\sim 60\%$. To test whether the observed shift in the relations shown in Fig. A.1 results from a systematic bias introduced by the extraction procedure adopted in Boselli et al. (2013) we have extracted the emission line fluxes of all the HRS galaxies with available spectra (Gavazzi et al. 2004; Boselli et al. 2013; 264/323 objects) using the GANDALF fitting code (Sarzi et al. 2006; Falcon-Barroso et al. 2006). GANDALF is a simultaneous emission and absorption lines fitting algorithm designed to separate the relative contribution of the stellar continuum and of nebular emission in the spectra of galaxies. This code implements the pPXF method (Cappellari & Emsellem 2004) which combines and adjusts the observed spectra of several stars of all spectral type to the stellar continuum to first quantify and remove the underlying absorption contaminating the emission of the most important emission lines, including $H\beta$ and $H\alpha$. With

this procedure, the code is expected to correctly account for the underlying stellar absorption that contaminates several emission lines, in particular the Balmer lines which are crucial for the determination of the dust attenuation of the $H\alpha$ line. Figures 4 and 5 show the same relationships between $L(H\alpha)_{24\mu\text{m}}$, $L(20\text{cm})$, and $L(H\alpha)_{BD}$ as those plotted in Fig. A.1 but using GANDALF data for the Balmer decrement and [NII] contamination corrections. Most of the systematic differences observed between galaxies with high and low $H\beta\text{E.W.}$, or high and low signal-to-noise, are removed using this new set of data. We thus use in the analysis presented in this work the spectroscopic dataset extracted using GANDALF. The fluxes of the different emission lines are given in Table 7, arranged as follows:

- Column 1: *Herschel* Reference Sample (HRS) name.
- Columns 2-8: observed line intensities normalised to $H\alpha$. The GANDALF fitting code assumes that $[\text{OIII}]\lambda 4958 = 0.3 \times [\text{OIII}]\lambda 5007$ and that $[\text{NII}]\lambda 6548 = 0.3 \times [\text{NII}]\lambda 6584$.
- Column 9-10: signal-to-noise SN measured empirically from the spectrum as the amplitude of the $H\alpha$ and $H\beta$ lines divided by the noise in the nearby continuum.
- Column 11: Balmer decrement $C(H\beta)$. The contribution of the Milky Way is subtracted using the Galactic extinction map of Schlegel et al. (1998) combined with the Fitzpatrick & Massa (2007) Galactic extinction law.
- Column 12: uncertainty on the Balmer decrement $\sigma[C(H\beta)]$ obtained from standard error propagation of the uncertainties on the line fluxes.

The uncertainty on the Balmer decrement $\sigma[C(H\beta)]$ is tightly correlated with the signal-to-noise measured at the $H\alpha$ and $H\beta$ lines, as depicted in Fig. A.2. For the typical spectral resolution of $R \sim 1000$ of the spectroscopic data used in this work (Boselli et al. 2013), the required limiting uncertainty of $\sigma[C(H\beta)] = 0.1$ is reached for a signal-to-noise of ≈ 50 for $H\alpha$ and ≈ 15 for $H\beta$. A spectral resolution of $R \gtrsim 1000$ is required for an accurate deblending of the $H\alpha$ line from the nearby [NII] lines and for an accurate determination of the underlying Balmer absorption.

Appendix B: Radio continuum data

We have collected radio continuum data at 1.49 GHz (20 cm) obtained at the VLA for 191 HRS galaxies. These data have been taken, in order of preference, from the pointed survey of *IRAS* bright galaxies of Condon et al. (1990), from the survey of optically selected galaxies of Condon (1987), or from the survey of galaxies with H-band magnitudes of Condon et al. (1987). The data presented in these papers have been obtained under similar VLA configurations (generally D and C/D) and thus have a comparable angular resolution (~ 45 arcsec). The typical rms noise level of these observations is 0.1-0.2 mJy per beam. Flux densities of the remaining galaxies have been taken from the NVSS survey of Condon et al. (1998) and published in Condon et al. (2002) whenever available, or extracted by ourselves from the NVSS survey catalogue assuming a search radius of 15 arcsec. These data have been homogeneously taken in VLA-D configuration, and have a typical resolution of 45 arcsec and a sensitivity of 0.45 mJy rms. For three galaxies, we adopt the integrated flux densities obtained by the FIRST survey (Becker et al. 1995). The FIRST survey has been completed using the VLA in B configuration, and thus have an angular resolution of $\lesssim 5$ arcsec. Because of the adopted configuration, this survey is sensitive to compact sources and might miss some of the low surface brightness extended emission. Its typical sensitivity is 0.15 mJy rms.

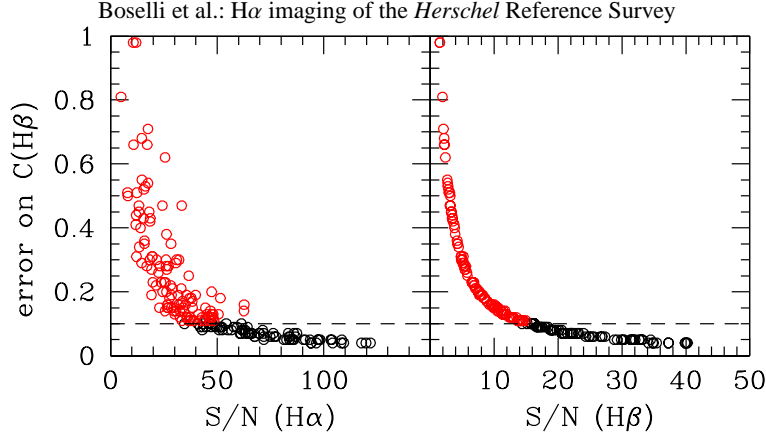


Fig. A.2. Relationship between the uncertainty on the Balmer decrement $\sigma[C(H\beta)]$ and the $H\alpha$ and $H\beta$ signal to noise. The horizontal dashed line shows the $\sigma[C(H\beta)] = 0.1$ limit adopted in this work to identify good quality objects (black symbols) from uncertain measurements (red symbols).

Table C.1. Calibrations of the different star formation tracers

λ	K_λ
$H\alpha$	8.79×10^{-42}
FUV	6.21×10^{-44}

Note: for a Salpeter IMF in the stellar mass range $0.1 < m < 100 M_\odot$, from Hao et al. (2011).

Table 5 gives the radio data for all the HRS galaxies. Table 5 is arranged as follows:

- Column 1: *Herschel* Reference Sample (HRS) name.
- Column 2: sign indicating detections (1) and undetections (0)
- Column 3: flux density $S(20\text{cm})$, or upper limit, in mJy. For the undetected objects we estimate an upper limit to the flux density $S_{ul}(20\text{cm}) = 4 \times \text{rms}$, and assuming for all galaxies the same typical rms noise of the NVSS survey of 0.45 mJy.
- Column 4: logarithm of the 20 cm radio luminosity, or upper limit, in W Hz^{-1} .
- Column 5: flag to the data, as indicated in the original papers. 1 stands for galaxies with good quality observations, 2 for uncertain values.
- Column 6: references to the data: 1: Condon et al. (1990); 2: Condon (1987); 3: Condon et al. (1987); 4: Condon et al. (2002); 5: extracted as described in the text from the NVSS survey (Condon et al. 1998); 6: extracted from the FIRST survey (Becker et al. 1995).

Appendix C: Adopted calibrations of the different star formation tracers

The $H\alpha$ and FUV star formation rates used in this work have been determined using the relation:

$$SFR_\lambda \text{ [} M_\odot \text{yr}^{-1} \text{]} = K_\lambda L(\lambda)_{\text{cor}} \text{ [erg s}^{-1} \text{]} \quad (\text{C.1})$$

where the different values of K_λ used in this work are given in Table C.1 (adapted from Hao et al. 2011).

The attenuation corrected $H\alpha$ luminosity have been determined using either the Balmer decrement or the following relation (from Calzetti et al. 2010):

$$\log(L(H\alpha)_{\text{cor}}) = \log(L(H\alpha)_{\text{obs}}) + 0.020 \times \log(L(24\mu\text{m})) \text{ for } L(24\mu\text{m}) < 10^{41} \text{ erg s}^{-1} \quad (\text{C.2})$$

and

$$\log(L(H\alpha)_{\text{cor}}) = \log(L(H\alpha)_{\text{obs}}) + 0.031 \times \log(L(24\mu\text{m})) \text{ for } L(24\mu\text{m}) \geq 10^{41} \text{ erg s}^{-1} \quad (\text{C.3})$$

where the observed ($L(H\alpha)_{\text{obs}}$)¹¹ and corrected ($L(H\alpha)_{\text{cor}}$) $H\alpha$ luminosities and the $24 \mu\text{m}$ luminosity ($L(24\mu\text{m})$) are expressed in erg s^{-1} .

The corrected UV luminosities are determined using the recipes of Hao et al. (2011):

$$L(FUV)_{24\mu\text{m}} = L(FUV)_{\text{obs}} + 3.89 \times L(24\mu\text{m}) \quad (\text{C.4})$$

Star formation rates from radio continuum luminosities at 1.49 GHz (20 cm) have been determined using the calibration of Bell (2003):

$$SFR_{\text{radio}} \text{ [} M_\odot \text{yr}^{-1} \text{]} = 5.52 \times 10^{-22} L(20\text{cm}) \text{ for } L(20\text{cm}) > L_c \quad (\text{C.5})$$

$$SFR_{\text{radio}} \text{ [} M_\odot \text{yr}^{-1} \text{]} = \frac{5.52 \times 10^{-22}}{0.1 + 0.9(L(20\text{cm})/L_c)^{0.3}} L(20\text{cm}) \text{ for } L(20\text{cm}) \leq L_c \quad (\text{C.6})$$

where the radio luminosity is expressed in W Hz^{-1} , and $L_c = 6.4 \times 10^{21} \text{ W Hz}^{-1}$.

The different estimates of the star formation rate are listed in Table 6, arranged as follows:

- Column 1: *Herschel* Reference Sample (HRS) name.
- Column 2: $SFR_{H\alpha+BD}$ determined by correcting the $H\alpha$ luminosity using the Balmer decrement derived using the GANDALF code for galaxies with $\text{SN} > 50$.
- Column 3: $SFR_{H\alpha+24\mu\text{m}}$ determined by correcting the $H\alpha$ luminosity using the $24 \mu\text{m}$ emission and eq. C.2 and C.3.
- Column 4: $SFR_{FUV+24\mu\text{m}}$ determined by correcting the FUV luminosity using the $24 \mu\text{m}$ emission and eq. C.4.
- Column 5: SFR_{radio} determined using the relation C.5 and C.6. This value has been determined only in galaxies with high-quality radio data (flag = 1 in Table 5).

¹¹ The observed $H\alpha$ luminosity must be also corrected for Galactic extinction and [NII] contamination.

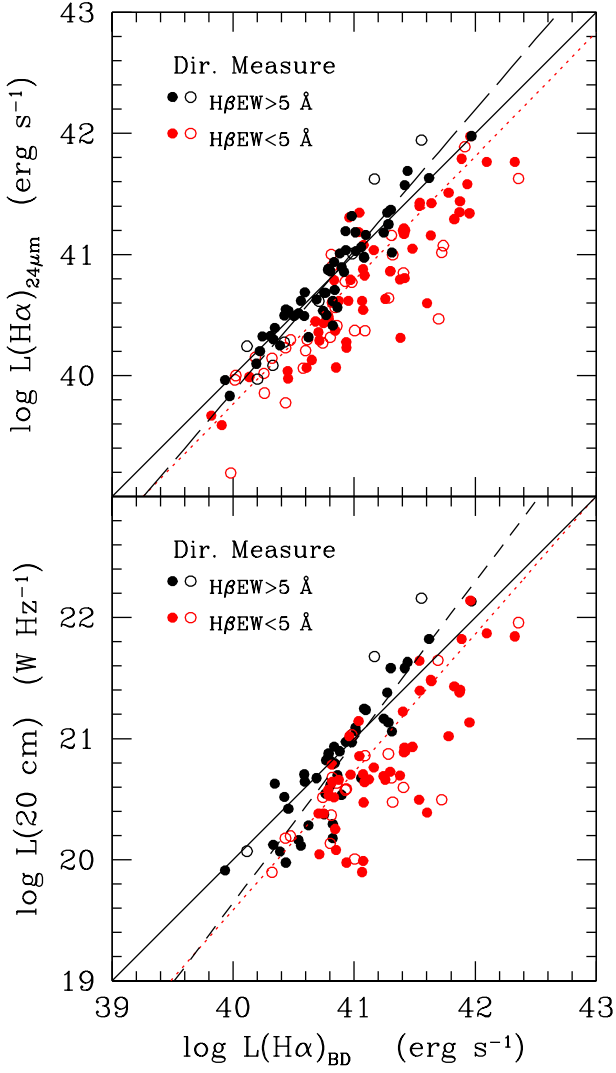


Fig. A.1. Relationship between the $H\alpha$ luminosity corrected for dust attenuation using the $24\ \mu\text{m}$ emission (upper panel), the 20 cm radio continuum luminosity (lower panel) and the $H\alpha$ luminosity corrected for Balmer decrement using the spectroscopic set of data published in Boselli et al. (2013), where the line emission is directly measured on the data. Filled dots are for HI-normal ($HI - def \leq 0.4$) galaxies, empty symbols for HI-deficient ($HI - def > 0.4$) objects. Black symbols indicate galaxies with an $H\beta E.W. > 5\ \text{\AA}$, red symbols those with $H\beta E.W. < 5\ \text{\AA}$. The black solid line shows the 1:1 relation, the black long dashed line the bisector fit to the high-quality data (black symbols), the red dotted line the best fit to the whole dataset.

– Column 9: SFR_{del} derived by fitting the SED with the CIGALE code using a delayed exponentially declining star formation history.

The star formation rates determined using the CIGALE fitting code have been measured only whenever FUV data are available. All galaxies are assumed coeval, with an age of 13 Gyr. We recall that these SFR have been measured assuming consistently a Salpeter IMF in the stellar mass range $0.1 < m_{star} < 100 M_{\odot}$. These values of SFR can be converted into SFR measured using a Chabrier (2003) or Kroupa (2001) IMF by dividing them by a factor of ~ 1.58 . This value slightly changes with the assumed population synthesis model, and might vary from reference to reference (Brinchmann et al. 2004; Salim et al. 2007; Bigiel et al. 2008; Argence & Lamareille 2009; Schiminovich et al. 2010; Peng et al. 2010; Chomiuk & Povich 2011).

- Column 6: SFR_{MED} , mean value of the different monochromatic estimates given in columns 2-5.
- Column 7: SFR_{1exp} derived by fitting the SED with the CIGALE code using one exponentially declining star formation history.
- Column 8: SFR_{2exp} derived by fitting the SED with the CIGALE code using two exponentially declining star formation histories.

Table 1. *Herschel* Reference Survey.

HRS	CGCG	VCC	UGC	NGC	IC	RA(2000)	dec	type	<i>D</i>	<i>M</i> _{star}	<i>D</i> _{24.5(g)}	incl	vel	memb	H α +[[NII]]
(1)	(2)	(3)	(4)	(5)	(6)	h m s	° ' "	(9)	Mpc	M _⊙	'	deg	km s ⁻¹	(15)	(16)
1	123035	-	-	-	-	101739.66	224835.9	Pec	16.79	8.72	0.92	67.09	1175	Leo Cl.	1
2	124004	-	5588	-	-	102057.13	252153.4	S?	18.44	8.77	0.73	44.82	1291	Leo Cl.	1
3	94026	-	5617	3226	-	102327.01	195354.7	E2;pec;LINER;Sy3	16.70	10.21	3.15	34.97	1169	Leo Cl.	1
4	94028	-	5620	3227	-	102330.58	195154.2	SAB(s)pec;Sy1.5	16.40	10.26	4.80	61.37	1148	Leo Cl.	1
5	94052	-	-	-	610	102628.37	201341.5	Sc	16.71	9.62	1.96	77.41	1170	Leo Cl.	1
6	154016	-	5662	3245A	-	102701.16	283821.9	SB(s)b	18.89	8.94	2.21	90.00	1322	Leo Cl.	1
7	154017	-	5663	3245	-	102718.39	283026.6	SA(r)0?:?;HII;LINER	18.77	10.29	3.13	55.29	1314	Leo Cl.	0
8	154020	-	5685	3254	-	102919.92	292929.2	SA(s)bc;Sy2	19.37	9.88	3.92	70.43	1356	Leo Cl.	1
9	154026	-	5731	3277	-	103255.45	283042.2	SA(r)ab;HII	20.21	10.08	2.60	49.22	1415	Leo Cl.	1
10	183028	-	5738	-	-	103429.82	351524.4	S?	21.66	8.71	0.92	46.50	1516	Leo Cl.	1
11	124038	-	5742	3287	-	103447.31	213854.0	SB(s)d	18.93	9.45	2.40	62.51	1325	Leo Cl.	1
12	124041	-	-	-	-	103542.07	260733.7	cI	19.89	8.47	0.74	49.03	1392	Leo Cl.	1
13	183030	-	5753	3294	-	103616.25	371928.9	SA(s)c	22.47	10.17	3.59	63.21	1573	Leo Cl.	1
14	124045	-	5767	3301	-	103656.04	215255.7	(R')SB(rs)0/a	19.16	10.12	2.80	70.35	1341	Leo Cl.	0
15	65087	-	5826	3338	-	104207.54	134449.2	SA(s)c	18.57	10.00	4.82	55.69	1300	Leo Cl.	1
16	94116	-	5842	3346	-	104338.91	145218.7	SB(rs)cd	18.00	9.61	2.65	27.27	1260	Leo Cl.	1
17	95019	-	5887	3370	-	104704.05	171625.3	SA(s)c	18.30	9.46	2.68	58.49	1281	Leo Cl.	1
18	155015	-	5906	3380	-	104812.17	283606.5	(R')SBa?	22.91	9.77	1.51	18.71	1604	Leo Cl.	1
19	184016	-	5909	3381	-	104824.82	344241.1	SB pec	23.29	9.39	1.79	21.68	1630	Leo Cl.	1
20	184018	-	5931	3395	2613	104950.11	325858.3	SAB(rs)ed pec:	23.10	9.17	2.31	61.85	1617	Leo Cl.	1
21	155028	-	5958	-	-	105115.81	275054.9	Sbc	16.89	8.82	1.56	80.13	1182	Leo Cl.	1
22	155029	-	5959	3414	-	105116.23	275830.0	S0 pec;LINER	20.20	10.48	3.31	43.72	1414	Leo Cl.	1
23	184028	-	5972	3424	-	105146.33	325402.7	SB(s)b?:?;HII	21.44	9.90	2.91	78.74	1501	Leo Cl.	1
24	184029	-	5982	3430	-	105211.41	325701.5	SAB(rs)c	22.64	9.88	3.48	60.53	1585	Leo Cl.	1
25	125013	-	5995	3437	-	105235.75	225602.9	SAB(rs)c:	18.24	9.69	2.39	68.42	1277	Leo Cl.	1
26	184031	-	5990	-	-	105238.34	342859.3	Sab	22.41	8.94	1.26	90.00	1569	Leo Cl.	0
27	184034	-	6001	3442	-	105308.11	335437.3	Sa?	24.77	8.94	0.72	29.21	1734	Leo Cl.	1
28	155035	-	6023	3451	-	105420.86	271422.9	Sd	19.03	9.16	1.66	60.50	1332	Leo Cl.	1
29	95060	-	6026	3454	-	105429.45	172038.3	SB(s)c? sp;HII	15.73	9.06	2.46	80.08	1101	Leo Cl.	1
30	95062	-	6028	3455	-	105431.07	171704.7	(R')SAB(rs)b	15.79	8.87	2.20	61.59	1105	Leo Cl.	1
31	267027	-	6024	3448	-	105439.24	541818.8	I0	19.63	9.27	2.97	70.30	1374	Ursa Maj. S S	1
32	95065	-	6030	3457	-	105448.63	173716.3	S?	16.54	9.46	1.05	18.49	1158	Leo Cl.	1
33	95085	-	6077	3485	-	110002.38	145029.7	SB(r)b:	20.46	9.62	2.08	18.49	1432	Leo Cl.	1
34	95097	-	6116	3501	-	110247.32	175922.2	Scd	16.14	9.58	3.36	79.98	1130	Leo Cl.	1
35	267037	-	6115	3499	-	110311.03	561318.2	I0	21.74	9.69	0.83	30.85	1522	Ursa Maj. S S	0
36	155049	-	6118	3504	-	110311.21	275821.0	(R)SAB(s)ab;HII	21.94	10.24	2.60	19.92	1536	Leo Cl.	1
37	155051	-	6128	3512	-	110402.98	280212.5	SAB(rs)c	19.61	9.53	1.54	28.52	1373	Leo Cl.	1
38	38129	-	6167	3526	-	110656.63	071026.1	SAC pec sp	20.27	9.10	2.32	77.41	1419	Leo Cl.	1
39	66115	-	6169	-	-	110703.35	120336.2	Sb:	22.24	9.08	1.46	72.78	1557	Leo Cl.	1
40	67019	-	6209	3547	-	110955.94	104315.0	Sb:	22.63	9.18	1.62	60.18	1584	Leo Cl.	1
41	96011	-	6267	3592	-	111427.25	171536.5	Sc? sp	18.61	9.25	2.06	77.41	1303	Leo Cl.	1
42	96013	-	6277	3596	-	111506.21	144713.5	SAB(rs)c	17.04	9.77	2.75	28.52	1193	Leo Cl.	1
43	96022	-	6299	3608	-	111658.96	180854.9	E2;LINER:	15.83	10.27	3.21	37.06	1108	Leo Cl.	0
44	96026	-	6320	-	-	111817.24	185049.0	S?	16.01	8.70	1.10	18.49	1121	Leo Cl.	1
45	291054	-	6330	3619	-	111921.60	574527.8	(R)SA(s)0+:	22.06	10.25	2.79	30.44	1544	Ursa Major Cl.	0
46	96029	-	6343	3626	-	112003.80	182124.5	(R)SA(rs)0+:	21.34	10.28	2.92	48.89	1494	Leo Cl.	0
47	156064	-	6352	3629	-	112031.82	265748.2	SA(s)cd:	21.53	9.11	1.90	39.89	1507	Leo Cl.	1
48	268021	-	6360	3631	-	112102.85	531011.0	SA(s)c	16.50	9.92	4.16	25.99	1155	Ursa Major Cl.	1
49	39130	-	6368	3640	-	112106.85	031405.4	E3	17.87	10.70	3.96	30.44	1251	Leo Cl.	0

Continued on next page...

Table 1. *Herschel* Reference Survey.

HRS	CGCG	VCC	UGC	NGC	IC	RA(2000)	dec	type	<i>D</i>	<i>M</i> _{star}	<i>D</i> _{24.5(g)}	incl	vel	memb	H α + [NII]
(1)	(2)	(3)	(4)	(5)	(6)	h m s	° ' "	(9)	Mpc	M _⊙	'	deg	km s ⁻¹	(15)	(16)
50	96037	-	6396	3655	-	112254.62	163524.5	SA(s)c::HII	21.43	9.87	1.95	49.05	1500	Leo Cl.	1
51	96038	-	6405	3659	-	112345.49	174906.8	SB(s)m?	18.56	9.21	1.71	53.52	1299	Leo Cl.	1
52	268030	-	6406	3657	-	112355.57	525515.5	SAB(rs)c pec	17.20	9.11	1.20	31.98	1204	Ursa Major Cl.	1
53	67071	-	6420	3666	-	112426.07	112032.0	SA(rs)c:	15.14	9.49	3.64	73.54	1060	Leo Cl.	1
54	96045	-	6445	3681	-	112629.80	165147.5	SAB(r)bc;LINER	17.77	9.87	2.08	18.38	1244	Leo Cl.	1
55	96047	-	6453	3684	-	112711.18	170149.0	SA(rs)bc;HII	16.54	9.54 ^a	2.69	43.65	1158	Leo Cl.	1
56	291072	-	6458	3683	-	112731.85	565237.4	SB(s)c?;HII	24.40	10.2	2.10	60.53	1708	Ursa Major Cl.	1
57	96049	-	6460	3686	-	112743.95	171326.8	SB(s)bc	16.51	9.81	3.12	40.12	1156	Leo Cl.	1
58	96050	-	6464	3691	-	112809.41	165513.7	SBB?	15.24	8.94	1.43	43.09	1067	Leo Cl.	1
59	67084	-	6474	3692	-	112824.01	092427.5	Sb;LINER;HII	24.53	9.96	3.11	82.22	1717	Leo Cl.	1
60	268051	-	6547	3729	-	113349.34	530731.8	SB(r)a pec	15.14	9.93	2.80	47.21	991	Ursa Major Cl.	1
61	292009	-	6575	-	-	113626.47	581129.0	Scd;HII	17.39	8.54	1.73	72.21	1217	Ursa Major Cl.	1
62	186012	-	6577	3755	-	113633.37	362437.2	SAB(rs)c pec	22.44	9.11	3.29	70.35	1571	Ursa Maj. S S	1
63	268063	-	6579	3756	-	113648.02	541736.8	SAB(rs)bc	18.41	9.94	3.81	61.00	1289	Ursa Major Cl.	1
64	292017	-	6629	3795	-	114006.84	583647.2	Sc;HII	17.33	9.06	1.89	72.27	1213	Ursa Major Cl.	1
65	292019	-	6640	3794	-	114053.42	561207.3	SAB(s)d	19.76	9.04	2.27	57.07	1383	Ursa Major Cl.	1
66	186024	-	6651	3813	-	114118.65	363248.3	SA(rs)b:	20.97	9.77	2.57	65.10	1468	Ursa Maj. S S	1
67	268076	-	6706	-	-	114414.83	550205.9	SB(s)m:	20.51	8.99	2.01	50.56	1436	Ursa Major Cl.	1
68	186045	-	-	-	-	114625.96	345109.2	S?	20.17	8.93	0.53	18.49	1412	Ursa Maj. S S	1
69	268088	-	6787	3898	-	114915.37	565053.7	SA(s)ab;LINE;HII	16.73	10.47	4.12	61.76	1171	Ursa Major Cl.	1
70	-	-	-	-	2969	115231.27	-035220.1	SB(r)bc?;HII	23.10	9.01 ^a	1.27	50.90	1617	Crater Cl.	1
71	292042	-	6860	3945	-	115313.73	604032.0	SB(rs)0+;LINER	17.99	10.55	4.84	56.83	1259	Ursa Major Cl.	0
72	-	-	-	3952	2972	115340.63	-035947.5	IBm: sp;HII	22.53	8.85 ^a	1.58	59.15	1577	Crater Cl.	1
73	269013	-	6870	3953	-	115348.92	521936.4	SB(r)bc;HII/LINER	15.00	10.60	6.19	61.69	1050	Ursa Major Cl.	1
74	269019	-	6918	3982	-	115628.10	550730.6	SAB(r)b::HII;Sy2	15.83	9.52	1.94	34.51	1108	Ursa Major Cl.	1
75	269020	-	6919	-	-	115637.51	553759.5	Sdm:	18.33	9.00	1.33	71.57	1283	Ursa Major Cl.	1
76	269022	-	6923	-	-	115649.43	530937.3	Im:	15.27	8.72	1.94	67.09	1069	Ursa Major Cl.	1
77	13033	-	6993	4030	-	120023.64	-010600.0	SA(s)bc;HII	20.83	10.54	3.86	40.12	1458	Crater Cl.	1
78	98019	-	6995	4032	-	120032.82	200426.0	Im:	18.13	9.20	1.63	33.05	1269	Coma I Cl.	1
79	69024	-	7001	4019	755	120110.39	140616.2	SBB? sp	21.54	8.62	1.94	84.36	1508	Virgo Out.	1
80	69027	-	7002	4037	-	120123.67	132403.7	SB(rs)b:	17.00	9.51	2.57	28.84	932	Virgo Out.	1
81	13046	-	7021	4045	-	120242.26	015836.4	SAB(r)a;HII	17.00	9.94	2.73	52.14	2011	Virgo Out.	1
82	98037	-	-	-	-	120335.94	160320.0	Sab	17.00	8.69	0.87	56.01	931	Virgo Out.	1
83	41031	-	7035	-	-	120340.14	023828.4	SB(r)a::HII	17.60	8.53	1.38	75.09	1232	Crater Cl.	1
84	69036	-	7048	4067	-	120411.55	105115.8	SA(s)b:	17.00	9.39	1.23	39.46	2424	Virgo Out.	1
85	243044	-	7095	4100	-	120608.60	493456.3	(R')SA(rs)bc;HII	15.31	10.07	4.88	72.43	1072	Ursa Major Cl.	1
86	41041	-	7111	4116	-	120736.82	024132.0	SB(rs)dm	17.00	9.23	3.40	54.24	1309	Virgo Out.	1
87	69058	-	7117	4124	-	120809.64	102243.4	SA(r)0+	17.00	10.01	4.19	72.67	1652	Virgo Out.	0
88	41042	-	7116	4123	-	120811.11	025241.8	SB(r)c;Sbrst;HII	17.00	9.63	3.57	47.49	1326	Virgo Out.	1
89	69088	66	7215	4178	-	121246.45	105157.5	SB(rs)dm;HII	17.00	9.61	5.02	71.57	369	Virgo N Cl.	1
90	13104	-	7214	4179	-	121252.11	011758.9	S0 edge-on	17.00	10.26	4.11	80.56	1279	Virgo Out.	0
91	98108	92	7231	4192	-	121348.29	145401.2	SAB(s)ab;HII;Sy	17.00	10.65	9.83	90.00	-135	Virgo N Cl.	1
92	69101	131	7255	-	3061	121504.44	140144.3	SBC? sp	17.00	9.10	1.91	77.41	2317	Virgo N Cl.	1
93	187029	-	7256	4203	-	121505.06	331150.4	SAB0-;LINER;Sy3	15.59	10.44	3.47	23.75	1091	Coma I Cl.	1
94	69104	145	7260	4206	-	121516.81	130126.3	SA(s)bc:	17.00	9.54	4.45	81.71	702	Virgo N Cl.	1
95	69107	152	7268	4207	-	121530.50	093505.6	Scd	17.00	9.66	1.71	55.67	592	Virgo N Cl.	1
96	69110	157	7275	4212	-	121539.36	135405.4	SAC::HII	17.00	10.01	2.99	50.58	-83	Virgo N Cl.	1
97	69112	167	7284	4216	-	121554.44	130857.8	SAB(s)b::HII/LINER	17.00	11.00	8.16	81.28	140	Virgo N Cl.	1
98	69119	187	7291	4222	-	121622.52	131825.5	Sc	17.00	9.31	3.03	81.47	226	Virgo N Cl.	1
99	69123	213	7305	-	3094	121656.00	133731.0	S;BCD	17.00	8.82	0.76	18.49	-162	Virgo N Cl.	1

Continued on next page...

Table 1. *Herschel* Reference Survey.

HRS	CGCG	VCC	UGC	NGC	IC	RA(2000)	dec	type	<i>D</i>	<i>M</i> _{star}	<i>D</i> _{24.5(g)}	incl	vel	memb	H α + [NII]
(1)	(2)	(3)	(4)	(5)	(6)	h m s	° ' "	(9)	Mpc	M _⊙	'	deg	km s ⁻¹	(15)	(16)
100	98130	226	7315	4237	-	121711.42	151926.3	SAB(rs)bc;HII	17.00	9.98	2.27	49.35	864	Virgo N Cl.	1
101	158060	-	7338	4251	-	121808.31	281031.1	SB0? sp	15.30	10.20	3.45	55.29	1014	Coma I Cl.	0
102	98144	307	7345	4254	-	121849.63	142459.4	SA(s)c	17.00	10.39	5.64	39.90	2405	Virgo N Cl.	1
103	42015	341	7361	4260	-	121922.24	060555.2	SB(s)a	23.00	10.35	3.51	72.67	1935	Virgo B	1
104	99015	-	7366	-	-	121928.66	171349.4	Spiral	17.00	8.80	1.05	55.09	925	Virgo Out.	1
105	99014	355	7365	4262	-	121930.58	145239.8	SB(s)0-?	17.00	9.88	1.82	25.22	1369	Virgo A	1
106	42032	393	7385	4276	-	122007.50	074131.2	S(s)c II	23.00	9.37	1.62	28.52	2617	Virgo B	1
107	42033	404	7387	-	-	122017.35	041205.1	Sd(f)	17.00	8.98	1.87	79.98	1733	Virgo S Cl.	1
108	42037	434	-	4287	-	122048.49	053823.5	Sc(f)	23.00	9.25	1.29	71.63	2155	Virgo B	1
109	42038	449	7403	4289	-	122102.25	034319.7	SA(s)cd: sp	17.00	9.39	3.13	83.55	2541	Virgo S Cl.	1
110	70024	465	7407	4294	-	122117.79	113040.0	SB(s)cd	17.00	9.23	2.59	60.50	357	Virgo N Cl.	1
111	99024	483	7412	4298	-	122132.76	143622.2	SA(rs)c	17.00	10.10	3.62	57.10	1136	Virgo A	1
112	42044	492	7413	4300	-	122141.47	052305.4	Sa	23.00	10.04	1.81	61.37	2310	Virgo B	1
113	99027	497	7418	4302	-	122142.48	143553.9	Sc: sp	17.00	10.44	7.05	81.47	1150	Virgo A	1
114	42045	508	7420	4303	-	122154.90	042825.1	SAB(rs)bc;HII;Sy2	17.00	10.51	5.81	26.12	1568	Virgo S Cl.	1
115	42047	517	7422	-	-	122201.30	050600.2	SBab(s)	17.00	9.24	1.11	78.46	1864	Virgo S Cl.	1
116	70031	522	7432	4305	-	122203.60	124427.3	SA(r)a	17.00	9.62	2.08	58.36	1888	Virgo A	1
117	70029	524	7431	4307	-	122205.63	090236.8	Sb	23.00	10.35	3.19	74.94	1035	Virgo B	1
118	42053	552	7439	-	-	122227.25	043358.7	SAB(s)cd	17.00	8.67	1.73	45.87	1296	Virgo S Cl.	1
119	99029	559	7442	4312	-	122231.36	153216.5	SA(rs)ab: sp	17.00	9.92	3.98	90.00	153	Virgo A	1
120	70034	570	7445	4313	-	122238.55	114803.4	SA(rs)ab: sp	17.00	10.08	4.12	90.00	1443	Virgo A	1
121	70035	576	7447	4316	-	122242.24	091956.9	Sbc	23.00	10.09	2.50	76.52	1254	Virgo B	1
122	99030	596	7450	4321	-	122254.90	154920.6	SAB(s)bc;LINER;HII	17.00	10.71	6.74	23.32	1575	Virgo A	1
123	42063	613	7451	4324	-	122306.18	051501.5	SA(r)0+	17.00	10.14	2.60	68.83	1670	Virgo S Cl.	1
124	70039	630	7456	4330	-	122317.25	112204.7	Scd	17.00	9.52	4.73	83.55	1564	Virgo A	1
125	42068	648	7461	4339	-	122334.94	060454.2	E0;Sy2	23.00	10.30	2.38	25.22	1298	Virgo B	0
126	99036	654	7467	4340	-	122335.31	164319.9	SB(r)0+	17.00	10.24	2.93	47.21	930	Virgo A	0
127	42070	656	7465	4343	-	122338.70	065714.7	SA(rs)b:	23.00	10.24	2.18	58.74	1014	Virgo B	1
128	42072	667	7469	-	3259	122348.52	071112.6	SAB(s)dm?	23.00	9.31	1.79	61.85	1420	Virgo B	1
129	99038	685	7473	4350	-	122357.81	164136.1	SA0;LINER	17.00	10.29	2.85	55.29	1241	Virgo A	0
130	70045	692	7476	4351	-	122401.56	121218.1	SB(rs)ab pec:	17.00	9.17	2.10	54.09	2324	Virgo A	1
131	42079	697	7474	-	3267	122405.53	070228.6	SA(s)cd	23.00	9.41	1.26	18.29	1231	Virgo B	1
132	42080	699	7477	-	3268	122407.44	063626.9	Sm/Im	23.00	9.13	1.15	21.68	727	Virgo B	1
133	158099	-	7483	4359	-	122411.06	313117.8	SB(rs)c? sp	17.90	9.26	2.62	68.42	1253	Coma I Cl.	1
134	70048	713	7482	4356	-	122414.53	083208.9	Sc	23.00	9.96	3.07	76.76	1137	Virgo B	1
135	42083	731	7488	4365	-	122428.23	071903.1	E3	23.00	11.48	6.71	48.89	1240	Virgo B	1
136	42089	758	7492	4370	-	122454.93	072640.4	Sa	23.00	10.14	1.68	48.89	784	Virgo B	1
137	70057	759	7493	4371	-	122455.43	114215.4	SB(r)0+	17.00	10.58	4.44	64.35	943	Virgo A	0
138	70058	763	7494	4374	-	122503.78	125313.1	E1;LERG;LINER;Sy2	17.00	11.18	7.58	18.71	910	Virgo A	1
139	42093	787	7498	4376	-	122518.06	054428.3	Im	23.00	9.00	1.54	53.52	1136	Virgo B	1
140	42092	785	7497	4378	-	122518.09	045530.2	(R)SA(s)a;Sy2	17.00	10.03	3.33	39.05	2557	Virgo S Cl.	1
141	70061	792	7503	4380	-	122522.17	100100.5	SA(rs)b:?	23.00	10.32	3.58	59.46	971	Virgo B	1
142	99044	801	7507	4383	-	122525.50	162812.0	Sa? pec;HII	17.00	9.42	2.17	56.06	1710	Virgo A	1
143	42095	827	7513	-	-	122542.63	071300.1	SB(s)cd: sp	23.00	9.60	2.82	77.33	992	Virgo B	1
144	70068	836	7520	4388	-	122546.82	123943.5	SA(s)b: sp;Sy2	17.00	10.14	6.10	79.55	2515	Virgo A	1
145	70067	849	7519	4390	-	122550.67	102732.6	Sbc(s) II	23.00	9.31	1.76	46.16	1103	Virgo B	1
146	42098	851	7518	-	3322	122554.12	073317.4	SAB(s)cd: sp	23.00	9.38	2.27	75.40	1195	Virgo B	1
147	42099	859	7522	-	-	122558.30	032547.3	Sd(f)	17.00	9.45	2.58	80.66	1428	Virgo S Cl.	1
148	99049	865	7526	4396	-	122558.80	154017.3	SAD: sp	17.00	9.25	3.49	75.40	-124	Virgo A	1
149	70071	873	7528	4402	-	122607.56	130646.0	Sb	17.00	10.04	4.12	75.67	234	Virgo A	1

Continued on next page...

Table 1. *Herschel* Reference Survey.

HRS	CGCG	VCC	UGC	NGC	IC	RA(2000)	dec	type	D	M_{star}	$D_{24.5(g)}$	incl	vel	memb	H α + [NII]
(1)	(2)	(3)	(4)	(5)	(6)	h m s	° ' "	(9)	Mpc	M_{\odot}	'	deg	km s $^{-1}$	(15)	(16)
150	70072	881	7532	4406	-	122611.74	125646.4	S0(3)/E3	17.00	11.22	12.37	54.51	-221	Virgo A	1
151	70076	912	7538	4413	-	122632.25	123639.5	(R')SB(rs)ab:	17.00	9.68	2.35	55.05	105	Virgo A	1
152	42104	921	7536	4412	-	122636.10	035752.7	SB(r)b? pec;LINER	17.00	9.30	1.63	23.46	2289	Virgo S Cl.	1
153	42105	938	7541	4416	-	122646.72	075508.4	SB(rs)cd::Sbrst	17.00	9.34	1.67	27.27	1395	Virgo S Cl.	1
154	70082	939	7546	-	-	122647.23	085304.6	SAB(s)cd	23.00	9.49	2.50	18.29	1271	Virgo B	1
155	70080	944	7542	4417	-	122650.62	093503.0	SB0: s	23.00	10.65	3.31	68.83	832	Virgo B	0
156	99054	958	7551	4419	-	122656.43	150250.7	SB(s)a;LINER;HII	17.00	10.24	3.29	74.27	-273	Virgo A	1
157	42106	957	7549	4420	-	122658.48	022939.7	SB(r)bc:	17.00	9.28	2.03	61.69	1695	Virgo S Cl.	1
158	42107	971	7556	4423	-	122708.97	055248.6	Sdm:	23.00	9.04	2.71	81.35	1120	Virgo B	1
159	70090	979	7561	4424	-	122711.59	092514.0	SB(s)a;HII	23.00	10.17	3.66	62.11	438	Virgo B	1
160	42111	1002	7566	4430	-	122726.41	061546.0	SB(rs)b:	23.00	9.83	2.44	27.59	1450	Virgo B	1
161	70093	1003	7568	4429	-	122726.56	110627.1	SA(r)0+;LINER;HII	17.00	10.79	6.22	65.09	1130	Virgo A	1
162	70098	1030	7575	4435	-	122740.49	130444.2	SB(s)0;LINER;HII	17.00	10.30	3.37	45.49	775	Virgo A	0
163	70097	1043	7574	4438	-	122745.59	130031.8	Sb(tides);LINER	17.00	10.66	8.68	68.57	70	Virgo A	1
164	70099	1047	7581	4440	-	122753.57	121735.6	SB(rs)a	17.00	9.91	1.87	26.61	724	Virgo A	1
165	42117	1048	7579	-	-	122755.39	054316.4	Sdm:	23.00	8.86	1.33	74.76	2252	Virgo B	1
166	70100	1062	7583	4442	-	122803.89	094813.0	SB(s)0	23.00	10.67	4.32	68.83	517	Virgo B	0
167	70104	1086	7587	4445	-	122815.94	092610.7	Sab: sp	23.00	9.96	2.51	90.00	328	Virgo B	1
168	70108	1091	7590	-	-	122818.77	084346.1	Sbc	23.00	8.64	1.26	61.00	1119	Virgo B	1
169	99063	-	7595	-	3391	122827.28	182455.1	Scd:	24.30	9.28	1.58	44.22	1701	Coma I Cl.	1
170	99062	1110	7594	4450	-	122829.63	170505.8	SA(s)ab;LINER;Sy3	17.00	10.70	5.59	56.97	1954	Virgo A	1
171	70111	1118	7600	4451	-	122840.55	091532.2	Sbc:	23.00	9.69	1.62	49.35	865	Virgo B	1
172	99065	1126	7602	-	3392	122843.26	145958.2	SAb:	17.00	9.77	2.57	65.79	1687	Virgo A	1
173	42124	1145	7609	4457	-	122859.01	033414.2	(R)Sb(rs)II;LINER	17.00	10.43	3.38	18.49	884	Virgo S Cl.	1
174	70116	1154	7614	4459	-	122900.03	135842.9	SA(r)0+;HII;LINER	17.00	10.78	4.11	41.90	1210	Virgo A	1
175	70115	1158	7613	4461	-	122903.01	131101.5	SB(s)0+:	17.00	10.40	3.31	68.83	1919	Virgo A	1
176	70121	1190	7622	4469	-	122928.03	084459.7	SB(s)0/a? sp	23.00	10.64	4.20	76.78	508	Virgo B	1
177	42132	1205	7627	4470	-	122937.78	074927.1	Sa?;HII	17.00	9.20	1.52	50.53	2339	Virgo S Cl.	1
178	42134	1226	7629	4472	-	122946.76	080001.7	E2/S0;Sy2;LINER	17.00	11.59	11.29	40.97	868	Virgo S Cl.	1
179	70125	1231	7631	4473	-	122948.87	132545.7	E5	17.00	10.71	4.69	54.51	2236	Virgo A	1
180	70129	1253	7638	4477	-	123002.17	133811.2	SB(s)0?:;Sy2	17.00	10.58	3.56	23.75	1353	Virgo A	1
181	70133	1279	7645	4478	-	123017.42	121942.8	E2	17.00	10.09	1.83	33.89	1370	Virgo A	0
182	42139	1290	7647	4480	-	123026.78	041447.3	SAB(s)c	17.00	9.38	2.10	59.17	2438	Virgo S Cl.	1
183	70139	1316	7654	4486	-	123049.42	122328.0	E+0-1 pec;NLRG;Sy	17.00	11.36	9.42	41.90	1292	Virgo A	1
184	70140	1326	7657	4491	-	123057.13	112900.8	SB(s)a:	17.00	9.55	1.95	61.37	497	Virgo A	1
185	42141	1330	7656	4492	-	123059.74	080440.6	SA(s)a?	17.00	10.06	2.48	18.71	1777	Virgo S Cl.	1
186	129005	-	7662	4494	-	123124.03	254629.9	E1-2;LINER	18.71	10.88	4.59	30.44	1310	Coma I Cl.	0
187	42144	1375	7668	4505	-	123139.21	035622.1	SB(rs)m	17.00	9.41	3.36	38.04	1732	Virgo S Cl.	1
188	99075	1379	7669	4498	-	123139.57	165110.1	SAB(s)d	17.00	9.37	2.86	60.50	1505	Virgo A	1
189	99077	1393	7676	-	797	123154.76	150726.2	SB(s)c II.5	17.00	8.94	1.71	50.58	2100	Virgo A	1
190	99076	1401	7675	4501	-	123159.22	142513.5	SA(rs)b;HII;Sy2	17.00	10.98	6.78	61.59	2284	Virgo A	1
191	99078	1410	7677	4502	-	123203.35	164115.8	Scd:	17.00	8.56	1.14	53.52	1629	Virgo A	1
192	70152	1419	7682	4506	-	123210.53	132510.6	Sa pec?	17.00	9.39	1.69	41.90	737	Virgo A	1
193	70157	1450	7695	-	3476	123241.88	140301.8	IB(s)m:	17.00	9.03	2.13	49.80	-173	Virgo A	1
194	14063	-	7694	4517	-	123245.59	000654.1	SA(s)cd: sp	17.00	10.46	9.92	82.79	1129	Virgo Out.	1
195	99087	1479	7703	4516	-	123307.56	143429.8	SB(rs)ab?	17.00	9.66	1.97	72.01	958	Virgo A	1
196	70167	1508	7709	4519	-	123330.25	083917.1	SB(rs)d	17.00	9.21	2.80	46.67	1212	Virgo S Cl.	1
197	70168	1516	7711	4522	-	123339.66	091029.5	SB(s)cd: sp	17.00	9.38	3.62	74.76	2330	Virgo S Cl.	1
198	159016	-	7714	4525	-	123351.19	301639.1	Scd:	16.77	9.29	2.31	57.77	1174	Coma I Cl.	1
199	99090	1532	7716	-	800	123356.66	152117.4	SB(rs)c pec?	17.00	9.07	1.69	45.89	2335	Virgo A	1

Continued on next page...

Table 1. *Herschel* Reference Survey.

HRS	CGCG	VCC	UGC	NGC	IC	RA(2000)	dec	type	<i>D</i>	<i>M</i> _{star}	<i>D</i> _{24.5(g)}	incl	vel	memb	H α + [NII]
(1)	(2)	(3)	(4)	(5)	(6)	h m s	° ' "	(9)	Mpc	M _⊙	'	deg	km s ⁻¹	(15)	(16)
200	42155	1535	7718	4526	-	123403.03	074156.9	SAB(s)0:	17.00	10.96	7.94	75.93	448	Virgo S Cl.	1
201	42156	1540	7721	4527	-	123408.50	023913.7	SAB(s)bc;HII;LINER	17.00	10.67	6.23	71.76	1736	Virgo S Cl.	1
202	70173	1549	7728	-	3510	123414.79	110417.7	dE3,N	17.00	9.02	0.81	18.71	1357	Virgo A	0
203	42158	1554	7726	4532	-	123419.33	062803.7	IBm;HII	17.00	9.21	2.95	66.45	2021	Virgo S Cl.	1
204	42159	1555	7727	4535	-	123420.31	081151.9	SAB(s)c;HII	17.00	10.45	6.76	48.27	1962	Virgo S Cl.	1
205	14068	1562	7732	4536	-	123427.13	021116.4	SAB(rs)bc;HII;Sbrst	17.00	10.26	7.50	69.76	1807	Virgo S Cl.	1
206	42162	1575	7736	-	3521	123439.42	070936.0	SBm pec;BCD	17.00	9.24	1.51	44.22	597	Virgo S Cl.	1
207	99093	1588	7742	4540	-	123450.87	153305.2	SAB(rs)cd;LINER;Sy1	17.00	9.69	2.31	30.85	1288	Virgo A	1
208	99096	1615	7753	4548	-	123526.43	142946.8	SBb(rs);LINER;Sy	17.00	10.74	5.44	40.39	484	Virgo A	1
209	-	-	-	4546	-	123529.51	-034735.5	SB(s)0-	15.00	10.48 ^a	3.08	67.33	1050	Virgo Out.	0
210	70182	1619	7757	4550	-	123530.61	121315.4	SB0: sp;LINER	17.00	9.98	2.45	70.35	381	Virgo A	1
211	70184	1632	7760	4552	-	123539.88	123321.7	E;LINER;HII;Sy2	17.00	10.80	5.60	32.77	322	Virgo A	1
212	99098	-	7768	4561	-	123608.14	191921.4	SB(rs)dm	20.14	9.14	1.65	38.04	1410	Coma I Cl.	1
213	129010	-	7772	4565	-	123620.78	255915.6	SA(s)b? sp;Sy3;Sy1.9	17.61	11.12	11.97	87.55	1233	Coma I Cl.	1
214	70186	1664	7773	4564	-	123626.99	112621.5	E6	17.00	10.25	3.23	65.09	1165	Virgo A	0
215	70189	1673	7777	4567	-	123632.71	111528.8	SA(rs)bc	17.00	9.92	3.41	44.50	2277	Virgo A	1
216	70188	1676	7776	4568	-	123634.26	111420.0	SA(rs)bc	17.00	10.33	4.97	67.76	2255	Virgo A	1
217	70192	1690	7786	4569	-	123649.80	130946.3	SAB(rs)ab;LINER;Sy	17.00	10.66	9.23	90.00	-216	Virgo A	1
218	42178	1692	7785	4570	-	123653.40	071448.0	S0(7)/E7	17.00	10.48	3.84	77.67	1730	Virgo S Cl.	0
219	70195	1720	7793	4578	-	123730.55	093318.4	SA(r)0:	17.00	10.19	2.93	46.35	2284	Virgo E Cl.	0
220	70197	1727	7796	4579	-	123743.52	114905.5	SAB(rs)b;LINER;Sy1.9	17.00	10.94	5.91	39.46	1520	Virgo A	1
221	42183	1730	7794	4580	-	123748.40	052206.4	SAB(rs)a pec	17.00	9.99	2.33	44.61	1032	Virgo S Cl.	1
222	70199	1757	7803	4584	-	123817.89	130635.5	SAB(s)a?	17.00	9.30	1.55	48.89	1783	Virgo A	1
223	42186	1758	7802	-	-	123820.82	075328.7	Sdm	17.00	8.62	1.84	79.98	1788	Virgo S Cl.	1
224	42187	1760	7804	4586	-	123828.44	041908.8	SA(s)a: sp	17.00	10.22	3.78	76.78	792	Virgo S Cl.	1
225	70202	1778	7817	-	3611	123904.14	132148.7	S?	17.00	8.72	1.47	63.00	2750	Virgo E Cl.	1
226	42191	1780	7821	4591	-	123912.44	060044.3	Sb	17.00	9.31	1.57	59.46	2424	Virgo S Cl.	1
227	14091	-	7819	4592	-	123918.74	0-3155.2	SA(s)dm:	15.27	9.16	4.25	73.48	1069	Virgo Out.	1
228	-	-	-	-	-	123922.26	-053953.3	Pec	171.43	-	0.58	37.09	12000	Background	0
229	70204	1809	7825	-	3631	123948.02	125826.1	S?	17.00	8.89	1.09	54.34	2839	Virgo E Cl.	0
230	99106	1811	7826	4595	-	123951.91	151752.1	SAB(rs)b?	17.00	9.15	1.95	52.84	632	Virgo E Cl.	1
231	70206	1813	7828	4596	-	123955.94	101033.9	SB(r)0+;LINER:	17.00	10.62	4.35	39.05	1834	Virgo E Cl.	1
232	70213	1859	7839	4606	-	124057.56	115443.6	SB(s)a:	17.00	9.77	3.01	67.33	1645	Virgo E Cl.	1
233	70216	1868	7843	4607	-	124112.41	115311.9	SBb? sp	17.00	9.60	3.01	81.28	2255	Virgo E Cl.	1
234	70214	1869	7842	4608	-	124113.29	100920.9	SB(r)0:	17.00	10.33	3.40	32.77	1864	Virgo E Cl.	0
235	42205	1883	7850	4612	-	124132.76	071853.2	(R)SAB0	17.00	9.93	2.70	38.06	1875	Virgo S Cl.	0
236	70223	1903	7858	4621	-	124202.32	113848.9	E5	17.00	10.99	5.26	26.61	444	Virgo E Cl.	0
237	42208	1923	7871	4630	-	124231.15	035737.3	IB(s)m?	17.00	9.51	1.97	41.66	742	Virgo S Cl.	1
238	14109	-	7869	4629	-	124232.67	-012102.4	SAB(s)m pec	15.94	8.46	1.33	38.97	1116	Virgo Out.	0
239	99112	1932	7875	4634	-	124240.96	141745.0	SBcd: sp	17.00	9.57	3.59	79.98	116	Virgo E Cl.	1
240	70229	1938	7880	4638	-	124247.43	112632.9	S0-	17.00	10.13	2.36	44.61	1147	Virgo E Cl.	0
241	43002	1939	7878	4636	-	124249.87	024116.0	E/S0/1;LINER;Sy3	17.00	10.98	8.71	48.89	1094	Virgo S Cl.	1
242	70230	1943	7884	4639	-	124252.37	131526.9	SAB(rs)bc;Sy1.8	17.00	9.85	2.92	54.63	1048	Virgo E Cl.	1
243	15008	-	7895	4643	-	124320.14	015842.1	SB(rs)0/a;LINER	17.00	10.57	3.97	34.97	1346	Virgo Out.	1
244	71015	1972	7896	4647	-	124332.45	113457.4	SAB(rs)c	17.00	10.19	4.16	44.24	1422	Virgo E Cl.	1
245	71016	1978	7898	4649	-	124340.01	113309.4	E2	17.00	11.34	8.33	37.06	1095	Virgo E Cl.	1
246	100004	-	7901	4651	-	124342.63	162336.2	SA(rs)c;LINER	17.00	10.13	3.84	49.05	797	Virgo Out.	1
247	71019	1987	7902	4654	-	124356.58	130736.0	SAB(rs)cd;HII	17.00	10.14	5.18	54.96	1039	Virgo E Cl.	1
248	71023	2000	7914	4660	-	124431.97	111125.9	E5	17.00	10.05	2.19	43.72	1115	Virgo E Cl.	0
249	71026	2006	7920	-	3718	124445.99	122105.2	S	17.00	9.01	2.19	72.78	844	Virgo E Cl.	1

Continued on next page...

Table 1. *Herschel* Reference Survey.

HRS	CGCG	VCC	UGC	NGC	IC	RA(2000)	dec	type	D	M_{star}	$D_{24.5(g)}$	incl	vel	memb	H α + [NII]
(1)	(2)	(3)	(4)	(5)	(6)	h m s	° ' "	(9)	Mpc	M_{\odot}	'	deg	km s $^{-1}$	(15)	(16)
250	43018	-	7924	4665	-	124505.96	030320.5	SB(s)0/a	17.00	10.58	3.99	20.52	785	Virgo Out.	0
251	15015	-	7926	4666	-	124508.59	-002742.8	SABc::HII;LINER	21.61	10.71	4.93	70.35	1513	Virgo Out.	1
252	15016	-	7931	4668	-	124532.14	-003205.0	SB(s)d::NLGN	23.13	9.13	1.57	55.67	1619	Virgo Out.	1
253	15019	-	7951	4684	-	124717.52	-024338.6	SB(r)0+;HII	21.29	10.26	2.94	70.35	1490	Virgo Out.	0
254	71043	2058	7965	4689	-	124745.56	134546.1	SA(rs)bc	17.00	10.19	4.05	41.02	1620	Virgo E Cl.	1
255	43028	-	7961	4688	-	124746.46	042009.9	SB(s)cd	17.00	8.97	2.31	25.98	984	Virgo Out.	1
256	15023	-	-	4691	-	124813.63	-031957.8	Aa pec::HII	15.99	9.98	3.38	40.02	1119	Virgo Out.	1
257	71045	2070	7970	4698	-	124822.92	082914.3	SA(s)ab;Sy2	17.00	10.52	6.03	90.00	1008	Virgo E Cl.	1
258	-	-	-	4697	-	124835.91	-054803.1	E6;AGN	17.73	11.10	7.93	48.05	1241	Virgo Out.	1
259	43034	-	7975	4701	-	124911.56	032319.4	SA(s)cd	17.00	9.27	2.17	38.04	727	Virgo Out.	1
260	100011	-	7980	4710	-	124938.96	150955.8	SA(r)0+? sp::HII	17.00	10.45	4.30	74.27	1129	Virgo Out.	1
261	43040	-	7982	-	-	124950.19	025110.4	Sd(f)	16.54	9.42	2.89	79.30	1158	Virgo Out.	1
262	43041	-	7985	4713	-	124957.87	051841.1	SAB(rs)d;LINER	17.00	9.22	2.43	40.78	652	Virgo Out.	1
263	129027	-	7989	4725	-	125026.61	253002.7	SAB(r)ab pec::Sy2	17.27	10.92	9.34	51.19	1209	Coma I Cl.	1
264	15027	-	7991	-	-	125038.96	012752.3	Sd(f)	18.17	9.06	2.04	79.98	1272	Virgo Out.	1
265	-	-	-	4720	-	125042.78	-040921.0	Pec	21.49	9.05 ^a	0.77	40.78	1504	Virgo Out.	1
266	-	-	-	4731	-	125101.09	-062335.0	SB(s)cd	21.30	9.52 ^a	5.96	44.22	1491	Virgo Out.	1
267	129028	-	8005	4747	-	125145.96	254638.3	SBcd? pec sp	16.84	9.50	4.12	71.57	1179	Coma I Cl.	1
268	71060	-	8007	4746	-	125155.37	120458.9	Sb: sp	17.00	9.42	1.96	69.97	1779	Virgo Out.	1
269	71062	2092	8010	4754	-	125217.56	111849.2	SB(r)0-	17.00	10.62	4.40	61.37	1377	Virgo E Cl.	0
270	15029	-	8009	4753	-	125222.11	-011158.9	l0	17.70	10.93	6.92	58.46	1239	Virgo Out.	1
271	100015	-	8014	4758	-	125244.04	155055.9	Im::HII	17.00	9.33	3.48	78.64	1240	Virgo Out.	1
272	71065	2095	8016	4762	-	125256.05	111350.9	SB(r)0 sp::LINER	17.00	10.59	7.99	85.96	985	Virgo E Cl.	0
273	15031	-	8020	4771	-	125321.27	011609.0	SAd? sp::NLGN	17.00	9.88	3.58	76.04	1119	Virgo Out.	1
274	15032	-	8021	4772	-	125329.17	021006.0	SA(s)a;LINER;Sy3	17.00	10.25	4.25	61.37	1038	Virgo Out.	1
275	-	-	-	4775	-	125345.70	-063719.8	SA(s)d	22.37	9.61 ^a	2.06	23.20	1566	Virgo Out.	1
276	71068	-	8022	4779	-	125350.86	094235.7	SB(rs)bc;Sbrst	17.00	9.35	1.96	37.30	2832	Virgo Out.	1
277	43060	-	-	4791	-	125443.97	080310.7	cI	17.00	8.91	0.71	50.56	2529	Virgo Out.	1
278	71071	-	8032	-	-	125444.19	131414.2	S	16.01	9.31	2.46	81.28	1121	Virgo Out.	1
279	15037	-	8041	-	-	125512.68	000700.0	SB(s)d	17.00	9.24	3.09	61.18	1321	Virgo Out.	1
280	43066	-	8043	4799	-	125515.53	025347.9	S?	17.00	9.48	1.44	63.00	2802	Virgo Out.	1
281	43068	-	8045	-	-	125523.62	075434.0	IBm:	17.00	8.77	0.90	18.29	2801	Virgo Out.	1
282	43069	-	-	4803	-	125533.67	081425.8	Comp	17.00	9.30	0.89	45.87	2664	Virgo Out.	0
283	43071	-	8054	4808	-	125548.94	041814.7	SA(s)cd::HII	17.00	9.49	2.54	65.15	760	Virgo Out.	1
284	-	-	-	-	3908	125640.62	-073346.1	SB(s)d?;HII	18.51	9.71 ^a	1.79	69.02	1296	Virgo Out.	1
285	15049	-	8078	4845	-	125801.19	013433.0	SA(s)ab sp::HII	17.00	10.46	4.65	90.00	1097	Virgo Out.	1
286	71092	-	8102	4866	-	125927.14	141015.8	SA(r)0+ : sp::LINER	17.00	10.45	4.49	84.22	1986	Virgo Out.	1
287	15055	-	8121	4904	-	130058.67	-000138.8	SB(s)cd;Sbrst	17.00	9.53	2.24	45.05	1174	Virgo Out.	1
288	-	-	-	4941	-	130413.14	-053305.8	(R)SAB(r)ab::Sy2	15.91	10.04 ^a	3.36	81.97	1114	Virgo Out.	1
289	-	-	-	4981	-	130848.74	-064639.1	SAB(r)bc;LINER	23.97	10.31 ^a	2.60	53.16	1678	Virgo Out.	1
290	189037	-	8271	5014	-	131131.16	361654.9	Sa? sp	16.23	9.23	1.52	70.35	1136	Canes Ven. Spur	1
291	217031	-	8388	5103	-	132030.08	430502.3	Sab	18.53	9.86	1.56	48.22	1297	Canes Ven. Spur	0
292	218010	-	8439	5145	-	132513.92	431602.2	S?;HII;Sbrst	17.50	9.80	1.30	41.31	1225	Canes Ven. Spur	1
293	16069	-	8443	5147	-	132619.71	020602.7	SB(s)dm	15.60	9.07	1.97	36.11	1092	Virgo Out.	1
294	246017	-	8593	-	902	133601.22	495739.0	Sb	22.97	9.56	2.09	79.55	1608	Canes Ven. Spur	1
295	73054	-	8616	5248	-	133732.07	085306.2	(R)SB(rs)bc;Sy2;HII	16.46	10.43	5.50	42.79	1152	Virgo-Libra Cl.	1
296	190041	-	8675	5273	-	134208.34	353915.2	SA(s)0;Sy1.9	15.20	9.95	2.43	31.62	1064	Canes Ven. Spur	1
297	246023	-	8711	5301	-	134624.61	460626.7	SA(s)bc: sp	21.54	9.99	3.69	76.52	1508	Canes Ven. Spur	1
298	218047	-	8725	5303	-	134744.97	381816.4	Pec	20.27	9.11	1.05	49.80	1419	Canes Ven. Spur	1
299	45108	-	8727	5300	-	134816.04	035703.1	SAB(r)c	16.73	9.63	3.30	49.82	1171	Virgo-Libra Cl.	1

Continued on next page...

Table 1. *Herschel* Reference Survey.

HRS	CGCG	VCC	UGC	NGC	IC	RA(2000)	dec	type	D	M_{star}	$D_{24.5}(g)$	incl	vel	memb	$H\alpha+[NII]$
(1)	(2)	(3)	(4)	(5)	(6)	h m s	° ' ''	(9)	Mpc	M_{\odot}	'	deg	$km\ s^{-1}$	(15)	(16)
300	218058	-	8756	-	-	135035.89	423229.5	Sab	19.34	9.47	1.54	90.00	1354	Canes Ven. Spur	1
301	17088	-	8790	5334	4338	135254.46	-010652.7	SB(rs)c:	19.71	9.75	3.64	45.89	1380	Virgo-Libra Cl.	1
302	45137	-	8821	5348	-	135411.27	051338.8	SBbc: sp	20.61	9.24	3.00	82.55	1443	Virgo-Libra Cl.	1
303	295024	-	8843	5372	-	135446.01	583959.4	S?	24.53	9.23	0.81	37.55	1717	Canes Ven-Came. Cl.	1
304	46001	-	8831	5356	-	135458.46	052001.4	SABbc: sp;HII	19.57	10.01	3.07	75.82	1370	Virgo-Libra Cl.	1
305	46003	-	8838	5360	958	135538.75	045906.2	I0	16.73	9.13	1.74	66.45	1171	Virgo-Libra Cl.	1
306	46007	-	8847	5363	-	135607.21	051517.2	I0?	16.23	10.78	5.81	49.03	1136	Virgo-Libra Cl.	1
307	46009	-	8853	5364	-	135612.00	050052.1	SA(rs)bc pec;HII	17.74	10.25	6.20	50.13	1242	Virgo-Libra Cl.	1
308	46011	-	8857	-	-	135626.61	042348.0	Sb(f)	15.59	8.61	1.02	72.07	1091	Virgo-Libra Cl.	1
309	272031	-	9036	5486	-	140724.97	550611.1	SA(s)m:	19.76	8.70	1.63	52.79	1383	Canes Ven-Came. Cl.	1
310	47010	-	9172	5560	-	142005.42	035928.4	SB(s)b pec	24.54	9.94	2.51	68.57	1718	Virgo-Libra Cl.	1
311	47012	-	9175	5566	-	142019.95	035600.9	SB(r)ab;LINER	21.31	10.81	5.75	90.00	1492	Virgo-Libra Cl.	1
312	47020	-	9183	5576	-	142103.68	031615.6	E3	21.17	10.60	3.78	46.35	1482	Virgo-Libra Cl.	0
313	47022	-	9187	5577	-	142113.11	032608.8	SA(rs)bc:	21.29	9.64	3.05	75.14	1490	Virgo-Libra Cl.	1
314	19012	-	9215	-	-	142327.12	014334.7	SB(s)d	19.84	9.07	2.64	63.18	1389	Virgo-Libra Cl.	1
315	220015	-	9242	-	-	142521.02	393222.5	Sc	20.57	8.76	4.07	90.00	1440	Canes Ven. Spur	1
316	47063	-	9308	5638	-	142940.39	031400.2	E1	23.94	10.52	2.62	30.44	1845	Virgo-Libra Cl.	0
317	47066	-	9311	-	1022	143001.85	034622.3	S?	24.51	8.94	1.22	72.07	1716	Virgo-Libra Cl.	1
318	47070	-	9328	5645	-	143039.35	071630.3	SB(s)d	19.57	9.43	2.54	55.67	1370	Virgo-Libra Cl.	1
319	75064	-	9353	5669	-	143243.88	095330.5	SAB(rs)cd	19.54	9.47	3.26	42.53	1368	Virgo-Libra Cl.	1
320	47090	-	9363	5668	-	143324.34	042701.6	SA(s)d	22.61	9.60	2.85	21.68	1583	Virgo-Libra Cl.	1
321	47123	-	9427	5692	-	143818.12	032437.2	S?	22.59	9.11	1.03	48.94	1581	Virgo-Libra Cl.	1
322	47127	-	9436	5701	-	143911.06	052148.8	(R')SBa;LINER	21.50	10.45	4.12	18.71	1505	Virgo-Libra Cl.	1
323	48004	-	9483	-	1048	144257.88	045324.5	S	23.43	9.88	2.15	72.07	1640	Virgo-Libra Cl.	1

Table 2. *H α* observational parameters of the 138 target galaxies.

HRS	Filter Å	Tel	CCD	Pixel "	Year	N. exp	T. exp s	AM	Phot	Z. point erg cm ⁻² s ⁻¹	Norm
(1)	(2)	(3)	(4)	(5)	(6)	(7)	(8)	(9)	(10)	(11)	(12)
1	6603	2.1	E2V	0.35	2011	3	300.0	1.02	1	-15.36	0.190
2	6603	2.1	E2V	0.35	2011	3	300.0	1.02	1	-15.36	0.130
3	6603	2.1	E2V	0.35	2012	4	300.0	1.06	0	-	0.438
4	6603	2.1	E2V	0.35	2012	4	300.0	1.06	0	-	0.438
5	6603	2.1	sit3	0.31	2008	3	420.0	1.04	1	-15.45	0.153
6	6607	1.5	e2vm	0.28	2010	2	720.0	1.00	0	-	0.166
8	6603	2.1	sit3	0.31	2006	1	900.0	1.00	1	-15.52	0.460
9	6603	2.1	sit3	0.31	2008	1	900.0	1.05	1	-15.45	0.446
10	6603	2.1	E2V	0.35	2011	3	300.0	1.02	1	-15.36	0.160
11	6603	2.1	sit3	0.31	2008	1	900.0	1.04	1	-15.45	0.482
12	6603	2.1	E2V	0.35	2011	3	240.0	1.01	1	-15.36	0.124
13	6603	2.1	sit3	0.31	2006	1	900.0	1.03	1	-15.52	0.468
15	6603	2.1	E2V	0.35	2011	3	600.0	1.07	1	-15.49	0.137
16	6603	2.1	sit3	0.31	2006	1	900.0	1.04	1	-15.52	0.482
17	6603	2.1	sit3	0.31	2006	1	900.0	1.03	1	-15.52	0.490
18	6603	2.1	E2V	0.35	2011	3	300.0	1.02	1	-15.36	0.160
19	6603	2.1	sit3	0.31	2006	1	900.0	1.00	1	-15.52	0.454
20	6603	2.1	sit3	0.31	2006	1	900.0	1.02	1	-15.52	0.470
21	6603	2.1	sit3	0.31	2008	1	900.0	1.13	1	-15.45	0.458
23	6603	2.1	sit3	0.31	2006	1	900.0	1.00	1	-15.52	0.458
24	6603	2.1	sit3	0.31	2006	1	900.0	1.02	1	-15.52	0.480
25	6603	2.1	sit3	0.31	2006	1	900.0	1.01	1	-15.52	0.524
27	6603	2.1	E2V	0.35	2012	3	300.0	1.02	0	-	0.438
28	6603	2.1	sit3	0.31	2008	1	900.0	1.08	1	-15.45	0.458
29	6603	2.1	sit3	0.31	2009	3	300.0	1.03	1	-15.40	0.167
29	6603	2.1	E2V	0.35	2011	3	300.0	1.04	1	-15.36	0.155
30	6603	2.1	E2V	0.35	2011	3	300.0	1.04	1	-15.36	0.155
31	6603	2.1	sit3	0.31	2008	3	900.0	1.10	1	-15.45	0.600
32	6603	2.1	sit3	0.31	2008	1	900.0	1.13	1	-15.45	0.458
33	6603	2.1	sit3	0.31	2007	1	900.0	1.12	1	-15.46	0.468
34	6603	2.1	sit3	0.31	2008	3	420.0	1.05	1	-15.45	0.165
36	6603	2.1	E2V	0.35	2011	3	300.0	1.01	1	-15.38	0.162
37	6603	2.1	sit3	0.31	2006	1	900.0	1.15	1	-15.52	0.480
38	6603	2.1	sit3	0.31	2008	1	900.0	1.36	1	-15.45	0.458
39	6603	2.1	E2V	0.35	2012	3	360.0	1.18	1	-15.33	0.511
40	6603	2.1	sit3	0.31	2006	1	900.0	1.07	1	-15.52	0.458
41	6603	2.1	sit3	0.31	2008	1	900.0	1.19	1	-15.45	0.458
42	6603	2.1	sit3	0.31	2006	1	900.0	1.04	1	-15.52	0.480
44	6603	2.1	E2V	0.35	2011	3	300.0	1.02	1	-15.36	0.094
47	6603	2.1	sit3	0.31	2006	1	900.0	1.00	1	-15.52	0.468
48	6603	2.1	sit3	0.31	2008	1	900.0	1.21	1	-15.45	0.458
50	6603	2.1	sit3	0.31	2008	1	900.0	1.22	1	-15.45	0.458
51	6603	2.1	sit3	0.31	2008	1	900.0	1.23	1	-15.45	0.458
52	6603	2.1	E2V	0.35	2012	3	420.0	1.11	1	-15.33	0.614
53	6603	2.1	sit3	0.31	2006	1	900.0	1.06	1	-15.52	0.473
54	6603	2.1	sit3	0.31	2008	1	900.0	1.10	1	-15.45	0.458
55	6603	2.1	sit3	0.31	2006	1	900.0	1.04	1	-15.52	0.480
56	6603	2.1	sit3	0.31	2008	3	600.0	1.12	1	-15.45	0.188
57	6603	2.1	sit3	0.31	2008	1	900.0	1.06	1	-15.45	0.458
58	6603	2.1	sit3	0.31	2008	1	900.0	1.47	1	-15.45	0.458
59	6603	2.1	sit3	0.31	2008	1	900.0	1.17	1	-15.45	0.458
60	6603	2.1	sit3	0.31	2009	3	300.0	1.08	1	-15.40	0.470
61	6603	2.1	E2V	0.35	2012	3	300.0	1.18	1	-15.33	0.428
62	6603	2.1	sit3	0.31	2008	1	900.0	1.02	1	-15.45	0.482
63	6603	2.1	sit3	0.31	2008	3	600.0	1.13	1	-15.45	0.183
64	6603	2.1	E2V	0.35	2012	3	300.0	1.16	1	-15.33	0.437
65	6603	2.1	E2V	0.35	2012	3	360.0	1.15	1	-15.33	0.513
66	6603	2.1	sit3	0.31	2008	1	900.0	1.17	1	-15.45	0.482
67	6603	2.1	E2V	0.35	2012	3	360.0	1.20	1	-15.33	0.525
68	6603	2.1	E2V	0.35	2012	4	300.0	1.14	1	-15.33	0.423
69	6603	2.1	sit3	0.31	2009	3	300.0	1.12	1	-15.40	0.146
70	6603	2.1	sit3	0.31	2008	1	900.0	1.26	1	-15.45	0.482
72	6603	2.1	E2V	0.35	2012	3	300.0	1.22	1	-15.33	0.401
73	6603	2.1	sit3	0.31	2008	3	420.0	1.09	1	-15.45	0.161
74	6603	2.1	sit3	0.31	2008	3	600.0	1.16	1	-15.45	0.188
75	6603	2.1	E2V	0.35	2012	3	300.0	1.13	1	-15.33	0.465
76	6603	2.1	E2V	0.35	2012	3	360.0	1.20	1	-15.33	0.542
77	6603	2.1	sit3	0.31	2008	4	300.0	1.20	1	-15.45	0.360
78	6603	2.1	sit3	0.31	2009	3	300.0	1.04	1	-15.40	0.165

Continued on next page...

Table 2. $H\alpha$ observational parameters of the 138 target galaxies.

HRS	Filter Å	Tel	CCD	Pixel "	Year	N. exp	T. exp s	AM	Phot	Z. point erg cm ⁻² s ⁻¹	Norm
(1)	(2)	(3)	(4)	(5)	(6)	(7)	(8)	(9)	(10)	(11)	(12)
79	6603	2.1	sit3	0.31	2007	1	900.0	1.05	1	-15.46	0.455
80	6603	2.1	sit3	0.31	2007	1	900.0	1.05	1	-15.46	0.469
80	6603	2.1	E2V	0.35	2012	3	300.0	1.12	0	-	0.420
82	6603	2.1	E2V	0.35	2012	3	300.0	1.12	1	-15.33	0.433
83	6603	2.1	E2V	0.35	2012	3	300.0	1.14	1	-15.33	0.414
84	6603	2.1	sit3	0.31	2007	1	900.0	1.07	1	-15.46	0.420
85	6603	2.1	sit3	0.31	2008	3	600.0	1.17	1	-15.45	0.188
104	6603	2.1	sit3	0.31	2009	3	300.0	1.06	1	-15.40	0.162
105	6603	2.1	sit3	0.31	2007	1	600.0	1.05	1	-15.46	1.800
120	6603	2.1	sit3	0.31	2007	1	900.0	1.06	1	-15.46	0.441
120	6603	2.1	sit3	0.31	2006	1	900.0	1.06	1	-15.52	0.440
133	6603	2.1	sit3	0.31	2006	1	900.0	1.03	1	-15.52	0.475
133	6603	2.1	sit3	0.31	2006	1	900.0	1.23	1	-15.52	0.458
136	6603	2.1	sit3	0.31	2008	3	420.0	1.12	1	-15.45	0.165
169	6603	2.1	sit3	0.31	2006	2	900.0	1.35	1	-15.52	0.420
173	6603	2.1	sit3	0.31	2006	1	900.0	1.24	1	-15.52	0.480
177	6603	2.1	E2V	0.35	2011	3	600.0	1.10	1	-15.36	0.190
195	6603	2.1	sit3	0.31	2008	3	420.0	1.11	1	-15.45	0.161
198	6603	2.1	sit3	0.31	2006	1	900.0	1.28	1	-15.52	0.460
207	6603	2.1	sit3	0.31	2006	1	900.0	1.06	1	-15.52	0.404
212	6603	2.1	E2V	0.35	2012	4	300.0	1.37	0	-	0.410
213	6603	2.1	sit3	0.31	2008	1	900.0	1.20	1	-15.45	0.458
221	6603	2.1	sit3	0.31	2006	1	900.0	1.11	1	-15.52	0.570
227	6603	2.1	sit3	0.31	2008	3	420.0	1.39	1	-15.45	0.165
246	6603	2.1	E2V	0.35	2012	3	300.0	1.29	0	-	0.430
249	6603	2.1	sit3	0.31	2006	1	900.0	1.06	1	-15.52	0.460
251	6603	2.1	E2V	0.35	2012	3	300.0	1.17	1	-15.33	0.483
252	6603	2.1	E2V	0.35	2012	3	300.0	1.18	1	-15.33	0.419
256	6603	2.1	E2V	0.35	2012	3	300.0	1.21	1	-15.33	0.440
261	6603	2.1	E2V	0.35	2012	5	180.0	1.14	1	-15.33	0.261
262	6603	2.1	E2V	0.35	2011	3	240.0	1.12	1	-15.36	0.165
264	6603	2.1	E2V	0.35	2012	3	300.0	1.15	1	-15.33	0.406
265	6603	2.1	E2V	0.35	2012	3	300.0	1.23	1	-15.33	0.425
266	6603	2.1	sit3	0.31	2008	1	900.0	1.26	1	-15.45	0.458
267	6603	2.1	sit3	0.31	2006	1	900.0	1.06	1	-15.52	0.460
267	6603	2.1	sit3	0.31	2008	5	180.0	1.36	1	-15.45	0.101
275	6603	2.1	E2V	0.35	2012	3	300.0	1.26	1	-15.34	0.437
277	6603	2.1	E2V	0.35	2012	3	420.0	1.20	0	-	0.557
278	6603	2.1	sit3	0.31	2006	1	900.0	1.08	1	-15.52	0.440
278	6603	2.1	sit3	0.31	2009	3	300.0	1.05	1	-15.40	0.156
281	6603	2.1	sit3	0.31	2008	1	900.0	1.09	1	-15.45	0.470
283	6570	1.5	e2vm	0.28	2010	1	900.0	1.46	1	-15.08	0.238
283	6570	1.5	e2vm	0.28	2010	3	900.0	1.13	0	-	0.246
284	6603	2.1	E2V	0.35	2012	3	300.0	1.28	1	-15.33	0.454
286	6603	2.1	sit3	0.31	2006	1	900.0	1.31	1	-15.52	0.463
288	6570	1.5	e2vm	0.28	2010	3	900.0	1.44	1	-15.12	0.247
289	6603	2.1	sit3	0.31	2008	3	420.0	1.68	1	-15.45	0.636
290	6603	2.1	sit3	0.31	2009	3	300.0	1.01	1	-15.40	0.154
292	6603	2.1	sit3	0.31	2008	3	600.0	1.13	1	-15.45	0.188
293	6603	2.1	sit3	0.31	2008	3	420.0	1.49	1	-15.45	0.161
294	6603	2.1	sit3	0.31	2009	3	300.0	1.06	1	-15.40	0.180
295	6603	2.1	sit3	0.31	2006	1	900.0	1.13	1	-15.52	0.474
295	6603	2.1	sit3	0.31	2007	1	600.0	1.59	1	-15.46	0.300
297	6603	2.1	sit3	0.31	2008	1	900.0	1.27	1	-15.45	0.458
298	6603	2.1	sit3	0.31	2008	3	420.0	1.16	1	-15.45	0.165
299	6603	2.1	sit3	0.31	2006	1	900.0	1.36	1	-15.52	0.466
300	6603	2.1	sit3	0.31	2009	3	300.0	1.02	1	-15.40	0.148
302	6603	2.1	sit3	0.31	2008	1	900.0	1.24	1	-15.45	0.458
303	6603	2.1	sit3	0.31	2009	3	300.0	1.13	1	-15.40	0.179
304	6603	2.1	sit3	0.31	2008	1	900.0	1.13	1	-15.45	0.458
305	6603	2.1	sit3	0.31	2008	5	180.0	1.45	1	-15.45	0.092
306	6570	1.5	e2vm	0.28	2010	3	900.0	1.27	1	-15.12	0.255
307	6603	2.1	sit3	0.31	2006	1	900.0	1.33	1	-15.52	0.460
308	6603	2.1	sit3	0.31	2009	3	300.0	1.15	1	-15.40	0.191
309	6603	2.1	sit3	0.31	2008	1	1200.0	1.25	1	-15.45	0.446
310	6603	2.1	sit3	0.31	2006	1	900.0	1.45	1	-15.52	0.422
311	6603	2.1	sit3	0.31	2009	3	300.0	1.13	1	-15.40	0.155
313	6603	2.1	sit3	0.31	2006	1	900.0	1.39	1	-15.52	0.466
314	6603	2.1	sit3	0.31	2006	1	900.0	1.25	1	-15.52	0.454

Continued on next page...

Table 2. $H\alpha$ observational parameters of the 138 target galaxies.

HRS	Filter Å	Tel	CCD	Pixel "	Year	N. exp	T. exp s	AM	Phot	Z. point erg cm ⁻² s ⁻¹	Norm
(1)	(2)	(3)	(4)	(5)	(6)	(7)	(8)	(9)	(10)	(11)	(12)
315	6603	2.1	sit3	0.31	2008	1	900.0	1.20	1	-15.45	0.458
317	6607	1.5	e2vm	0.28	2010	2	600.0	1.16	1	-14.65	0.193
318	6603	2.1	sit3	0.31	2006	1	900.0	1.25	1	-15.52	0.472
319	6603	2.1	sit3	0.31	2006	1	900.0	1.28	1	-15.52	0.485
320	6603	2.1	sit3	0.31	2008	1	900.0	1.17	1	-15.45	0.443
321	6607	1.5	e2vm	0.28	2010	3	600.0	1.19	1	-15.12	0.188
321	6607	1.5	e2vm	0.28	2010	3	600.0	1.76	1	-14.67	0.096
322	6603	2.1	sit3	0.31	2008	1	900.0	1.34	1	-15.45	0.458
322	6603	2.1	Tho	0.31	2010	3	300.0	1.12	1	-15.80	0.229
323	6603	2.1	sit3	0.31	2006	1	900.0	1.29	1	-15.52	0.461

Table 3. $H\alpha$ + $[NII]$ fluxes and equivalent widths.

HRS	$H\alpha$ + $[NII]$ E.W. Å	err Å	log F($H\alpha$ + $[NII]$) erg cm ⁻² s ⁻¹	err erg cm ⁻² s ⁻¹	Ref	Alt. Ref.	Notes
(1)	(2)	(3)	(4)	(5)	(6)	(7)	(8)
1	41	4	-12.80	0.04	TW		
2	41	3	-12.40	0.03	TW		
3	8	4	-12.82	0.21	TW	14,17	c
4	34	5	-11.90	-	TW,7	22	
5	3	3	-13.27	0.40	TW		
6	0	36	-	-	TW		
7	-	-	-	-	-		
8	11	4	-12.16	0.14	TW	22	
9	11	3	-12.21	0.13	TW		
10	31	3	-12.58	0.04	TW		
11	20	3	-12.16	0.07	TW		
12	28	3	-12.91	0.05	TW		
13	23	3	-11.65	0.06	TW		
14	-	-	-	-	-		
15	38	16	-11.62	0.17	TW	21	
16	14	3	-12.06	0.10	TW		
17	28	4	-11.86	0.05	TW		
18	10	3	-12.59	0.15	TW		
19	32	4	-12.06	0.05	TW		
20	63	4	-11.58	0.02	TW	7	
21	5	3	-13.56	0.26	TW		
22	1	2	-12.89	0.40	11		
23	23	3	-12.11	0.06	TW		
24	17	4	-11.91	0.10	TW	7,21	
25	40	3	-11.79	0.03	TW		
26	-	-	-	-	-		
27	70	4	-12.10	-	TW,12		
28	46	4	-12.03	0.03	TW		
29	33	4	-12.37	0.06	TW		m
30	43	5	-12.07	0.05	TW	TW	
31	25	4	-11.92	0.07	TW		
32	-2	3	-	-	TW		
33	17	1	-12.15	0.10	TW		
34	6	4	-12.76	0.24	TW		
35	-	-	-	-	-		
36	37	4	-11.46	0.04	TW,20	6,10	
37	23	3	-12.11	0.06	TW		
38	30	4	-12.42	0.05	TW		
39	28	3	-12.67	0.05	TW	TW	
40	38	3	-12.11	0.04	TW		
41	8	4	-13.04	0.19	TW		
42	22	4	-11.75	0.08	TW		
43	-	-	-	-	-		
44	78	4	-12.05	0.02	TW	TW	
45	-	-	-	-	-		
46	-	-	-	-	-		
47	21	4	-12.30	0.09	TW	21	

Continued on next page...

Table 3. $H\alpha$ + $[NII]$ fluxes and equivalent widths.

HRS	$H\alpha$ + $[NII]$ E.W.	err	$\log F(H\alpha+[NII])$	err	Ref	Alt. Ref.	Notes
(1)	\AA	\AA	$\text{erg cm}^{-2} \text{s}^{-1}$	$\text{erg cm}^{-2} \text{s}^{-1}$	(6)	(7)	(8)
48	32	5	-11.33	0.06	TW	6,20	
49	-	-	-	-	-		
50	34	3	-11.68	0.04	TW		
51	28	4	-12.16	0.06	TW		
52	19	3	-12.43	0.07	TW		
53	25	3	-11.92	0.05	TW		
54	11	3	-12.18	0.13	TW		
55	22	3	-11.91	0.06	TW	21	
56	30	3	-11.86	0.04	TW		
57	31	4	-11.54	0.05	TW		
58	23	3	-12.34	0.06	TW		
59	17	3	-12.21	0.08	TW		
60	18	6	-12.01	0.14	TW	12	
61	44	4	-12.46	0.03	TW		
62	71	8	-11.83	0.04	TW		
63	9	4	-12.12	0.19	TW		
64	17	3	-12.64	0.08	TW		
65	27	3	-12.12	0.05	TW		
66	28	3	-11.72	0.05	TW		
67	35	5	-12.42	0.06	TW		
68	44	3	-12.65	0.03	TW		
69	13	4	-11.84	0.13	TW	10	
70	31	4	-12.33	0.05	TW		
71	-	-	-	-	-		
72	64	4	-12.07	0.02	TW		
73	13	4	-11.47	0.13	TW		
74	33	4	-11.62	0.04	TW		
75	3	3	-13.81	0.48	TW		
76	26	4	-12.54	0.06	TW	21	
77	17	3	-11.40	0.09	TW		
78	29	8	-12.21	0.11	TW		
79	43	1	-12.47	0.03	TW		
80	17	5	-12.58	0.21	TW	9	m
81	11	2	-12.24	0.11	4	12	
82	41	3	-12.50	0.03	TW		
83	32	3	-12.68	0.04	TW		
84	20	3	-12.31	0.07	3,TW		m
85	18	4	-11.67	0.09	TW		
86	40	6	-11.77	0.07	3		
87	-	-	-	-	-		
88	26	4	-11.73	0.07	4		
89	33	1	-11.72	-	1,20	5,6,9	
90	-	-	-	-	-		
91	9	1	-11.53	0.06	1	5,6	
92	23	2	-12.68	0.05	3		
93	-	-	-12.78	0.18	18	18	
94	28	2	-12.07	0.05	4	1,6	
95	9	1	-12.63	0.26	1		
96	20	3	-11.70	-	20	5,6	
97	3	1	-11.52	-	1,6		
98	20	1	-12.54	0.05	42		
99	24	2	-12.67	0.05	2	29	
100	9	1	-12.27	0.05	4	5,6,9,20	
101	-	-	-	-	-		
102	32	1	-10.96	0.05	1	5,6,20,22	
103	2	1	-12.86	0.16	1		
104	-1	10	-	-	TW		
105	3	3	-12.67	0.48	TW	22	
106	25	3	-12.34	0.06	3		
107	8	1	-13.22	0.07	2		
108	18	1	-13.25	0.06	4		
109	14	2	-12.76	0.06	3		
110	57	3	-11.63	0.04	3	5,6,20	
111	31	7	-11.61	0.07	1	5,20,21,22	
112	6	1	-12.74	0.06	3		
113	15	8	-11.86	0.14	1		
114	36	6	-10.85	-	1,20	5,6	
115	13	1	-12.98	0.05	4		
116	-1	8	-	-	3		
117	5	1	-12.52	0.09	1		

Continued on next page...

Table 3. $H\alpha$ + $[NII]$ fluxes and equivalent widths.

HRS	$H\alpha$ + $[NII]$ E.W.	err	$\log F(H\alpha+[NII])$	err	Ref	Alt. Ref.	Notes
(1)	\AA	\AA	$\text{erg cm}^{-2} \text{s}^{-1}$	$\text{erg cm}^{-2} \text{s}^{-1}$	(6)	(7)	(8)
118	48	7	-12.19	0.06	3		
119	2	1	-12.86	0.15	1		
120	6	3	-12.41	0.21	TW	1	m
121	14	1	-12.49	0.05	3		
122	18	1	-11.01	0.05	1	5,6,20,22	
123	6	1	-12.40	0.07	3	22	
124	7	2	-12.62	0.12	1		
125	-	-	-	-	-		
126	-	-	-	-	-		
127	9	1	-	-	1		
128	9	3	-12.97	0.09	3		
129	-	-	-	-	-		
130	18	4	-12.45	0.10	4	5,6	
131	14	4	-12.81	0.21	1		
132	42	7	-12.27	0.06	3		
133	12	4	-12.62	0.14	TW		m
134	8	1	-12.72	0.06	3		
135	2	3	-	-	20		
136	-2	3	-	-	TW	15	
137	-	-	-	-	-		
138	3	2	-12.42	-	20,14	15,16,18	
139	22	1	-12.48	0.04	2	22	
140	8	2	-12.19	0.10	3		
141	10	2	-12.64	-	1,5	6	
142	65	1	-11.63	0.04	4	1,5,22	
143	26	1	-12.25	0.05	3		
144	15	1	-11.67	0.13	1		
145	28	4	-12.31	0.08	4	21,22	
146	20	3	-12.55	0.05	3		
147	13	2	-12.82	0.06	3		
148	34	2	-12.12	0.05	1		
149	12	1	-12.09	0.05	2		
150	-1	3	-12.02	-	20,14	20	
151	13	1	-12.56	0.31	1	5,6	
152	38	3	-12.03	0.05	3		
153	16	3	-12.40	0.08	4	21	
154	24	5	-12.37	-	21	5	
155	-	-	-	-	-		
156	7	1	-12.70	-	1,5	6	
157	44	1	-11.84	0.04	4	20	
158	29	2	-12.52	0.05	3	22	
159	9	1	-12.22	-	1,5	6,9	
160	9	1	-12.10	1.00	1	22	
161	5	2	-11.72	0.13	1	5	
162	-	-	-	-	-		
163	7	3	-11.77	-	1,5	6	
164	-1	2	-	-	1		
165	31	1	-12.84	0.05	4		
166	-	-	-	-	-		
167	26	2	-12.31	0.06	4		
168	59	2	-12.33	0.04	3	22	
169	17	3	-12.69	0.08	TW		
170	2	10	-12.30	-	1,5	6	
171	17	2	-12.34	0.05	3		
172	11	5	-12.55	0.13	3	5	
173	7	3	-11.93	0.18	TW	1,5	
174	-1	0	-12.32	-	5	6,18	
175	-1	1	-	-	1		
176	3	1	-12.49	0.08	1	9	
177	24	3	-12.17	0.06	TW	22	
178	0	2	-12.76	-	20,8		
179	0	0	-13.58	-	8		
180	-	-	-12.90	0.13	18		
181	-	-	-	-	-		
182	30	1	-12.09	0.04	3		
183	2	3	-12.05	0.63	2	8,20	
184	-1	2	-	-	1		
185	4	1	-12.68	0.13	3		
186	-	-	-	-	-		
187	28	3	-11.69	-	1,20		

Continued on next page...

Table 3. $H\alpha$ + $[NII]$ fluxes and equivalent widths.

HRS	$H\alpha$ + $[NII]$ E.W.	err	$\log F(H\alpha+[NII])$	err	Ref	Alt. Ref.	Notes
(1)	\AA	\AA	$\text{erg cm}^{-2} \text{s}^{-1}$	$\text{erg cm}^{-2} \text{s}^{-1}$	(6)	(7)	(8)
188	36	3	-11.92	0.05	3	5,6	
189	38	3	-12.30	0.05	3		
190	6	1	-11.48	0.07	1	5,6,20	
191	35	9	-12.71	0.07	3		
192	5	1	-13.06	0.79	1		
193	69	22	-11.89	0.08	1		
194	32	2	-11.24	0.10	1		
195	-2	4	-	-	TW		
196	40	5	-11.78	0.06	3	5,6	
197	17	3	-12.38	0.10	4	5,6,22	
198	11	3	-12.55	0.13	TW		
199	17	2	-12.55	0.07	3		
200	0	2	-11.23	-	20,6		
201	20	1	-11.35	-	1,5	6	
202	-	-	-	-	-		
203	75	1	-11.40	-	1,5	6	
204	17	4	-11.26	0.11	1	5,6,20	
205	20	2	-11.37	0.06	1	5,6,20	
206	13	1	-12.73	0.06	1		
207	8	3	-12.43	0.16	TW	1	
208	17	1	-11.96	-	1,5	6,9,20	
209	-	-	-	-	-		
210	6	1	-12.35	0.07	22		
211	-	-	-13.01	-	14	8	
212	47	4	-12.29	-	TW,20	5,6,22	
213	9	3	-11.33	0.14	TW		
214	-	-	-	-	-		
215	15	1	-12.00	0.05	1	5,22	
216	19	1	-11.74	0.05	1	5,22	
217	2	1	-12.02	0.25	1	5,6,20,22	
218	-	-	-	-	-		
219	-	-	-	-	-		
220	4	1	-11.49	-	1,20	5,6,22	
221	7	3	-12.40	0.19	TW	1,5	
222	7	5	-12.98	0.19	3		
223	17	3	-13.07	0.07	3		
224	5	2	-12.46	0.16	1		
225	6	2	-13.35	0.17	4		
226	17	1	-12.51	0.05	4		
227	28	7	-11.86	0.10	TW		
228	-	-	-	-	-		
229	-	-	-	-	-		
230	16	1	-12.50:	-	1,20	9,22	
231	-1	1	-	-	1		
232	1	6	-13.28	0.29	4	1,5	
233	16	3	-12.51	0.07	4	1	
234	-	-	-	-	-		
235	-	-	-	-	-		
236	-	-	-	-	-		
237	36	4	-11.93	0.05	3		
238	-	-	-	-	-		
239	16	1	-12.32	0.49	1		
240	-	-	-	-	-		
241	-	-	-12.67	-	8	18,19	
242	24	2	-11.94	-	1,5	6,22	
243	0	0	-12.30	-	5		
244	16	1	-11.71	-	1,21	5,6,22	
245	-	-	-12.56	-	14		
246	29	3	-11.54	-	TW,20	5,6,9,22	
247	31	2	-11.34	-	1,21	5,6	
248	-	-	-	-	-		
249	-1	3	-	-	1		
250	-	-	-	-	-		
251	27	3	-11.29	0.05	TW	20	
252	43	4	-12.21	0.03	TW		
253	-	-	-	-	-		
254	14	2	-11.85	-	1,20	5,6	
255	60	21	-11.82	0.14	3		
256	40	3	-11.36	0.03	TW		
257	6	2	-11.98	-	21	1,5	

Continued on next page...

Table 3. $H\alpha$ + $[NII]$ fluxes and equivalent widths.

HRS	$H\alpha$ + $[NII]$ E.W. Å	err Å	$\log F(H\alpha+[NII])$ $\text{erg cm}^{-2} \text{s}^{-1}$	err $\text{erg cm}^{-2} \text{s}^{-1}$	Ref	Alt. Ref.	Notes
(1)	(2)	(3)	(4)	(5)	(6)	(7)	(8)
258	-	-	-13.33	-	14		
259	51	11	-11.77	0.09	3		
260	19	10	-11.39	-	6		
261	15	4	-12.60	0.10	TW		
262	74	7	-11.46	0.04	TW	5,6,9,20,21	
263	6	-	-11.42	0.11	10	22	
264	31	3	-12.65	0.04	TW		
265	49	3	-12.18	0.03	TW		
266	16	5	-11.91	0.14	TW		
267	20	5	-12.20	0.14	TW		m
268	44	1	-11.97	0.04	1		
269	-	-	-	-	-		
270	-	-	-12.27	-	19	18	
271	37	5	-12.06	0.05	3		
272	-	-	-	-	-		
273	15	1	-12.19	0.05	4	3	
274	9	1	-12.09	0.05	4	5,22	
275	48	4	-11.57	0.03	TW	20	
276	23	2	-12.21	0.06	4		
277	12	4	-	-	TW		v
278	7	6	-13.12	0.40	TW		m
279	17	2	-12.30	0.06	4	4	
280	22	1	-12.41	0.05	4		
281	15	5	-13.08	0.14	TW		
282	-	-	-	-	-		
283	49	4	-11.56	0.03	TW	5,6,9,20	m
284	24	3	-12.19	0.05	TW		
285	11	3	-11.89	0.14	3		
286	4	3	-12.36	0.32	20		
287	28	4	-11.89	0.06	3		
288	14	4	-11.92	0.11	TW	20,22	
289	20	4	-11.77	0.08	TW		
290	41	5	-12.25	0.05	TW		
291	-	-	-	-	-		
292	27	4	-12.08	0.06	TW		
293	42	4	-11.73	0.03	TW		
294	16	6	-12.68	0.16	TW		
295	25	4	-11.23	0.06	TW	6,20,21	m
296	3	2	-12.82	0.40	11	16	
297	21	3	-12.00	0.07	TW		
298	59	4	-11.90	0.02	TW		
299	18	3	-11.98	0.07	TW	21	
300	13	7	-12.90	0.21	TW		
301	27	2	-11.82	0.04	11		
302	22	5	-12.44	0.09	TW		
303	51	4	-12.13	0.03	TW		
304	8	3	-12.55	0.17	TW		
305	9	7	-13.04	0.31	TW		
306	8	3	-11.63	0.13	TW	15	
307	17	4	-11.49	0.10	TW	20	
308	20	8	-13.13	0.18	TW		
309	38	5	-12.39	0.05	TW	22	
310	24	3	-12.12	0.06	TW		
311	19	6	-11.56	0.13	TW	10	
312	-	-	-	-	-		
313	12	3	-12.43	0.12	TW		
314	34	4	-12.13	0.04	TW		
315	30	5	-12.55	0.07	TW		
316	-	-	-	-	-		
317	7	7	-13.39	0.42	TW		
318	21	3	-12.06	0.07	TW		
319	23	4	-11.90	0.08	TW		
320	38	5	-11.65	0.05	TW	21	
321	43	5	-12.20	0.04	TW		m
322	5	4	-12.33	0.50	TW	20,22	
323	11	3	-12.54	0.11	TW		

Table 4. CAS parameters for HRS galaxies

HRS	$r_c(r)$ arcsec	$r_c(H\alpha)$ arcsec	$r_c(EW_{H\alpha})$ arcsec	C_r	A_r	S_r	$C_{H\alpha}$	$A_{H\alpha}$	$S_{H\alpha}$
(1)	(2)	(3)	(4)	(5)	(6)	(7)	(8)	(9)	(10)
1	8.37	7.80	9.54	2.66	0.21	0.08	2.10	0.21	0.16
2	8.01	9.00	11.09	2.31	0.10	0.14	1.76	0.47	0.68
5	25.00	21.27	20.72	2.30	0.04	0.74	2.39	0.08	0.47
6	35.88	27.52	31.11	2.82	-0.09	-0.10	2.94	-0.17	-1.10
8	46.10	71.12	82.15	3.96	0.08	0.14	1.76	0.19	0.54
9	12.89	9.52	24.43	3.66	0.06	-0.04	4.24	0.34	0.71
10	9.56	11.48	17.80	2.81	0.10	0.11	2.44	0.47	1.01
11	27.87	27.07	30.30	2.37	0.19	0.17	1.83	0.38	1.47
12	6.46	5.40	7.03	2.94	0.17	0.10	2.13	0.40	0.35
13	39.59	37.91	40.94	2.37	0.22	0.44	1.42	0.70	1.92
15	52.50	71.73	97.78	2.91	0.17	0.44	2.35	0.48	0.95
16	39.24	49.30	54.91	2.20	0.12	0.25	1.51	0.42	1.41
17	24.45	29.19	45.98	3.17	0.14	0.31	2.23	0.63	1.71
18	14.87	16.37	16.29	3.43	0.07	0.11	0.97	0.38	1.40
19	21.36	15.51	22.05	2.85	0.19	0.24	4.85	0.52	1.33
21	-	-	-	2.35	0.05	0.18	-	-	-
23	29.75	29.39	34.40	2.49	0.33	0.49	2.35	0.43	0.99
24	35.36	40.44	49.15	2.64	0.21	0.33	1.93	0.46	1.39
25	24.21	20.65	32.51	2.61	0.24	0.37	2.32	0.82	1.31
27	6.40	6.03	11.73	2.60	0.21	0.21	2.34	0.74	0.71
28	19.62	21.13	24.68	2.47	0.18	0.31	1.55	0.75	1.69
29	28.29	28.23	27.46	2.19	0.13	0.57	1.73	0.13	0.60
30	20.14	21.23	24.17	2.42	0.14	0.28	1.84	0.44	1.08
31	33.09	20.63	31.77	2.67	0.30	0.10	2.77	0.61	0.59
33	25.68	30.92	31.81	2.35	0.20	0.38	0.93	0.40	1.25
34	45.31	45.46	48.92	2.66	0.13	0.71	1.90	0.15	1.01
36	21.43	37.63	42.05	5.16	0.12	0.28	2.03	0.47	1.53
37	16.00	19.12	21.98	3.03	0.21	0.25	1.59	0.56	1.31
38	27.08	21.66	22.45	2.23	0.12	0.38	1.80	0.26	1.00
40	17.25	14.68	20.86	2.38	0.19	0.28	2.27	0.72	1.22
41	20.55	15.43	15.37	2.63	0.07	0.11	2.63	0.13	0.57
42	32.03	34.92	38.95	2.78	0.17	0.34	1.79	0.69	1.90
44	11.09	6.47	9.19	2.59	0.20	0.16	2.39	1.00	1.12
47	26.74	31.70	35.92	2.62	0.17	0.29	2.10	0.37	0.94
48	51.13	54.35	71.50	3.77	0.15	0.37	3.64	0.48	1.57
50	14.80	18.74	22.96	3.04	0.19	0.15	1.50	0.52	0.94
51	18.05	13.86	16.44	2.56	0.22	0.18	1.98	0.43	0.89
52	5.85	13.11	19.70	3.48	0.09	0.06	0.85	0.59	0.71
53	24.25	23.79	37.33	2.79	0.15	0.37	2.42	0.42	0.95
54	18.24	25.47	25.93	3.54	0.05	0.08	1.43	0.32	1.02
55	24.41	28.23	37.79	2.90	0.13	0.24	2.21	0.66	1.50
56	18.43	18.77	22.78	2.76	0.25	0.49	1.83	0.65	1.25
57	37.27	41.04	52.58	2.59	0.18	0.27	2.22	0.46	1.37
58	17.71	18.09	19.06	2.08	0.08	0.15	1.16	0.29	0.93
59	29.80	33.34	49.11	2.68	0.12	0.45	1.72	0.27	0.87
60	31.25	23.64	25.84	2.63	0.10	0.12	4.42	0.18	0.42
61	25.21	24.81	29.09	2.34	0.09	0.21	1.91	0.32	0.51
62	30.52	52.93	53.96	3.35	0.15	0.29	2.54	0.30	1.32
63	46.45	48.37	52.84	2.27	0.12	0.19	1.52	0.16	0.73
64	22.15	24.28	28.28	2.45	0.08	0.33	1.90	0.23	0.55
65	26.34	24.80	32.99	2.84	0.13	0.18	2.40	0.38	1.15
66	24.53	27.62	34.38	2.47	0.20	0.35	1.78	0.58	1.38
67	18.96	17.00	18.57	3.12	0.24	0.11	1.31	0.32	0.54
68	3.60	2.69	5.32	3.17	0.19	-0.02	3.34	0.16	0.10
70	15.24	16.03	18.65	2.45	0.15	0.21	1.94	0.55	1.35
72	17.48	16.15	18.75	2.67	0.24	0.29	2.46	0.78	1.51
73	66.49	84.00	102.00	3.29	0.15	0.29	1.65	0.32	1.07
74	17.27	16.77	20.43	2.56	0.13	0.28	1.27	0.53	1.65
75	18.54	16.09	14.94	2.42	0.09	0.17	2.40	0.08	0.29
76	20.96	13.01	26.40	2.97	0.12	0.06	3.33	0.42	0.60
77	32.48	38.20	51.32	3.36	0.12	0.25	2.44	0.43	1.26
78	16.41	15.88	27.49	2.99	0.17	0.10	3.40	0.35	0.71
79	20.94	15.03	19.90	2.58	0.12	0.39	2.29	0.40	0.94
81	20.63	24.15	31.26	3.68	0.09	0.06	1.61	0.13	0.54
82	8.73	7.63	9.08	2.31	0.12	0.14	1.80	0.55	0.67
83	15.29	9.68	12.41	2.36	0.10	0.06	2.23	0.35	0.23
84	12.22	15.92	18.30	3.50	0.08	0.18	1.80	0.35	0.86
85	54.48	52.39	59.45	2.25	0.14	0.45	3.12	0.32	1.26
86	41.27	45.95	49.91	2.81	0.24	0.36	2.22	0.45	1.16
88	47.12	62.92	69.72	2.92	0.14	0.42	1.35	0.17	0.73
89	68.21	89.95	90.87	2.61	0.09	0.06	2.05	0.24	0.84

Continued on next page...

Table 4. CAS parameters for HRS galaxies

HRS	$r_e(r)$ arcsec	$r_e(H\alpha)$ arcsec	$r_e(EW_{H\alpha})$ arcsec	C_r	A_r	S_r	$C_{H\alpha}$	$A_{H\alpha}$	$S_{H\alpha}$
(1)	(2)	(3)	(4)	(5)	(6)	(7)	(8)	(9)	(10)
91	98.35	120.80	130.50	2.92	0.22	0.64	1.24	0.36	1.30
92	26.88	22.22	22.56	2.50	0.06	0.25	2.27	0.11	0.19
94	60.26	73.75	84.28	2.59	0.08	0.34	2.04	0.09	0.33
95	19.78	11.95	12.65	2.49	0.14	0.24	3.13	0.13	0.33
97	69.02	92.36	95.73	4.21	0.21	0.41	2.28	0.15	0.45
98	42.42	32.00	39.89	2.24	0.12	1.16	2.46	0.18	0.69
99	7.34	8.02	9.43	2.88	0.15	0.19	1.37	0.94	1.55
100	23.60	24.90	27.63	2.55	0.16	0.22	1.63	0.24	0.77
102	50.73	57.25	79.18	3.24	0.31	0.48	2.52	0.83	2.10
106	18.02	20.81	22.00	2.93	0.16	-0.01	1.71	0.33	0.82
107	25.85	26.25	27.43	2.37	0.10	0.97	1.74	0.06	0.17
109	36.49	33.01	37.61	2.60	0.19	0.29	2.38	0.14	0.32
110	36.28	27.55	35.20	2.37	0.19	0.35	2.00	0.63	1.51
111	40.87	43.47	33.00	2.49	0.10	0.00	2.47	0.10	0.22
113	-	-	-	2.58	-0.02	-0.03	-	-	-
114	53.85	63.65	72.96	2.83	0.25	0.59	1.16	0.85	2.21
117	45.33	27.81	25.92	2.47	0.11	0.33	2.03	0.08	0.38
118	17.40	20.98	21.61	2.96	0.17	0.29	0.85	0.72	1.62
119	48.92	14.55	14.28	2.56	0.08	0.20	2.34	0.09	0.34
120	-	-	-	2.66	0.16	0.38	-	-	-
121	26.13	28.47	30.28	2.65	0.18	0.71	1.66	0.35	0.71
122	87.62	95.82	109.20	2.94	0.16	0.38	1.73	0.55	1.72
124	57.55	35.48	37.45	2.47	0.05	0.37	2.29	0.11	0.46
127	18.93	25.33	20.10	3.72	0.10	0.12	1.91	0.11	0.20
128	21.31	9.98	16.32	2.71	0.11	0.02	3.29	0.10	0.20
130	27.45	10.76	11.76	3.02	0.18	0.00	3.28	0.11	-0.10
131	18.46	18.01	20.10	2.56	0.01	-0.02	1.65	0.12	0.45
132	12.95	11.45	15.06	2.77	0.18	0.13	2.58	0.80	1.41
133	33.93	32.01	37.16	2.71	0.08	0.24	1.81	0.15	0.53
134	39.69	20.14	14.22	2.26	0.08	0.73	3.51	0.10	-0.02
139	21.06	16.54	19.90	2.53	0.18	0.16	2.56	0.77	1.43
140	17.14	43.84	52.84	4.01	0.03	-0.05	2.23	0.19	0.38
141	47.22	46.65	65.30	2.87	0.03	0.01	2.17	0.12	0.43
142	15.07	6.58	27.59	3.48	0.13	0.08	3.40	0.36	0.44
143	49.54	52.19	53.73	1.99	0.17	1.02	1.02	0.25	1.11
145	20.54	23.30	24.32	2.45	0.11	0.16	0.99	0.22	0.46
146	28.15	13.66	16.29	2.49	0.12	0.35	2.75	0.15	0.46
147	41.60	43.90	49.04	2.04	0.09	0.90	1.91	0.08	0.34
148	44.10	45.58	52.36	2.62	0.13	0.25	2.40	0.37	0.84
149	49.99	39.69	42.45	2.13	0.21	0.73	1.90	0.27	0.78
151	28.02	28.81	31.37	3.02	0.08	0.17	5.07	0.27	0.73
152	19.43	17.81	19.08	2.39	0.17	0.27	1.17	0.32	1.22
154	34.15	40.91	14.28	3.06	0.06	0.14	2.27	0.14	0.37
156	26.10	24.88	25.35	3.41	0.14	0.12	1.83	0.37	0.75
157	22.15	23.21	27.58	2.11	0.18	0.35	1.54	0.42	0.94
158	34.20	25.51	33.74	2.51	0.19	0.58	3.06	0.22	0.58
159	23.80	8.68	8.33	3.23	0.09	0.15	2.69	0.14	0.29
160	30.61	26.26	27.17	2.84	0.11	0.06	1.54	0.08	0.25
164	-	-	-	4.30	0.05	0.11	-	-	-
165	19.66	14.74	14.75	2.28	0.08	0.27	1.93	0.05	0.10
167	35.86	31.19	24.49	2.22	0.11	0.55	1.97	0.04	0.06
168	15.26	20.08	24.46	3.20	0.28	0.26	2.26	0.47	1.05
169	18.62	20.62	21.15	2.20	0.16	0.27	0.82	0.68	1.93
170	46.55	43.91	61.13	3.79	0.05	0.00	2.31	0.23	0.91
171	13.97	11.19	12.27	2.37	0.07	0.12	1.42	0.35	0.73
172	26.51	16.30	14.30	2.66	0.07	0.08	2.25	0.07	0.14
173	19.13	21.71	22.85	3.87	0.07	0.05	1.40	0.68	1.75
177	16.81	12.94	12.95	2.14	0.18	0.27	1.72	0.41	1.30
182	24.68	29.75	33.77	2.56	0.14	0.30	1.36	0.50	1.48
187	51.05	44.92	50.49	2.44	0.27	0.38	2.40	0.65	1.74
188	32.03	32.28	37.44	2.69	0.16	0.30	2.25	0.43	1.31
189	17.94	13.41	14.27	2.61	0.08	0.03	1.57	0.41	0.34
190	65.55	69.39	80.01	3.06	0.16	0.21	2.03	0.34	0.89
191	14.51	14.86	15.30	2.39	0.08	0.07	1.54	0.24	0.78
193	22.47	22.66	22.00	2.80	0.21	0.37	2.16	0.32	0.88
194	131.00	116.70	120.20	2.29	0.14	0.66	1.82	0.21	0.67
196	32.61	43.30	46.64	2.76	0.23	0.45	1.50	0.70	2.00
197	43.02	23.82	18.26	2.51	0.14	0.16	2.76	0.03	-0.08
198	30.63	29.56	31.65	2.52	0.10	0.09	1.10	0.25	0.79
199	22.06	11.85	13.88	2.51	0.03	0.03	2.40	0.17	0.40
201	59.26	76.93	87.55	3.44	0.12	0.16	1.79	0.47	1.25

Continued on next page...

Table 4. CAS parameters for HRS galaxies

HRS	$r_e(r)$ arcsec	$r_e(H\alpha)$ arcsec	$r_e(EW_{H\alpha})$ arcsec	C_r	A_r	S_r	$C_{H\alpha}$	$A_{H\alpha}$	$S_{H\alpha}$
(1)	(2)	(3)	(4)	(5)	(6)	(7)	(8)	(9)	(10)
203	27.55	23.41	30.97	2.25	0.23	0.51	2.73	0.62	0.81
204	81.31	84.74	89.39	2.46	0.12	0.31	2.00	0.40	1.40
205	73.74	83.39	88.80	3.39	0.13	0.21	3.10	0.28	0.82
206	19.01	13.58	13.86	2.77	0.11	0.20	1.09	0.22	0.60
207	25.88	19.53	21.34	2.67	0.10	0.07	1.77	0.31	0.98
208	52.29	84.98	77.99	3.89	0.07	0.13	1.91	0.10	0.29
212	18.35	18.95	23.21	2.53	0.16	0.25	2.05	0.59	1.36
213	135.80	126.60	210.30	2.94	0.36	0.61	2.11	0.03	-0.59
217	82.06	46.57	52.94	3.60	0.15	0.22	1.77	0.23	1.00
220	44.81	71.31	63.63	4.16	0.06	0.07	1.56	0.19	0.67
221	25.50	17.96	17.87	2.58	0.08	0.09	1.05	0.20	0.66
223	23.02	20.39	21.21	2.50	0.06	0.15	2.48	0.02	-0.09
224	47.64	46.12	27.72	3.07	0.07	0.10	2.68	0.07	0.19
225	17.79	9.78	6.99	2.90	0.08	-0.08	2.43	0.04	0.00
226	16.43	13.42	13.84	2.79	0.05	0.04	2.65	0.15	0.37
227	48.78	51.03	53.98	2.31	0.13	0.29	1.66	0.30	0.84
230	21.04	25.05	29.05	2.49	0.16	0.13	2.06	0.35	0.75
232	35.05	17.10	9.02	2.85	0.08	-0.02	5.04	0.05	-0.26
233	39.95	29.80	22.85	2.11	0.11	0.44	1.90	0.07	0.17
237	21.20	6.13	10.18	3.07	0.17	0.05	2.71	0.60	0.21
239	33.57	22.96	22.07	2.50	0.23	1.01	2.73	0.04	0.05
242	26.75	39.89	44.24	3.16	0.06	0.11	1.10	0.47	1.08
246	28.67	32.94	59.32	3.17	0.14	0.18	2.47	0.56	1.26
247	57.58	57.96	69.98	2.58	0.30	0.41	2.03	0.52	1.33
249	-	-	-	2.53	0.04	0.03	-	-	-
251	44.12	55.06	77.88	3.34	0.20	0.44	2.22	0.54	0.93
252	17.56	17.93	21.16	2.27	0.15	0.26	1.51	0.64	1.41
254	55.67	39.40	43.94	2.73	0.10	0.20	2.16	0.19	0.43
255	38.06	40.00	40.04	2.79	0.18	0.41	2.13	0.45	1.43
256	22.89	9.77	14.69	3.84	0.18	0.02	2.32	0.48	0.08
259	17.64	18.59	26.90	2.88	0.13	0.17	2.61	0.53	0.96
261	36.71	32.38	36.84	2.62	0.11	0.53	2.36	0.08	0.16
262	28.02	35.51	37.65	2.52	0.20	0.30	2.02	0.59	1.25
263	92.07	143.70	164.40	3.88	0.11	0.23	1.05	0.26	0.53
264	25.88	21.78	21.69	2.23	0.08	0.61	2.24	0.06	0.12
265	8.26	7.29	11.28	2.76	0.14	0.14	2.07	0.73	0.70
266	72.54	58.42	94.08	3.04	0.16	0.49	3.78	0.19	0.36
267	42.92	19.69	21.15	2.78	0.22	0.08	1.75	0.18	-0.29
268	21.37	21.14	26.16	2.45	0.06	0.14	2.27	0.36	0.38
271	39.94	30.93	29.79	2.52	0.18	0.24	2.01	0.10	0.15
273	40.10	38.92	39.78	2.42	0.10	0.32	1.99	0.15	0.50
275	25.92	32.27	38.73	2.68	0.28	0.41	1.90	0.75	1.77
276	22.04	14.39	24.52	3.39	0.12	0.30	5.60	0.06	0.20
277	8.07	11.86	11.32	2.64	0.06	0.06	0.53	0.24	0.55
278	27.16	22.42	22.26	2.50	0.04	0.33	2.34	0.12	0.29
279	40.38	39.39	51.17	2.52	0.12	0.24	1.92	0.16	0.28
281	11.82	13.39	14.00	2.59	0.10	0.10	1.35	0.33	0.92
283	25.98	28.87	39.67	2.49	0.20	0.39	1.91	0.74	1.64
284	23.19	15.37	18.96	2.42	0.15	0.38	2.62	0.31	0.57
287	27.45	23.14	33.02	2.74	0.20	0.14	3.04	0.44	0.88
288	37.16	52.33	55.40	3.52	0.07	0.26	1.83	0.23	1.45
289	30.34	36.23	42.92	3.10	0.19	0.24	1.95	0.36	0.98
293	24.58	27.92	29.78	2.30	0.20	0.38	1.07	0.78	1.80
294	25.85	16.62	17.01	2.65	0.16	0.48	2.81	0.11	0.32
295	49.67	64.77	72.91	3.45	0.22	0.42	1.76	0.53	1.38
297	51.60	52.92	62.92	2.56	0.14	0.53	2.13	0.33	1.25
298	11.06	12.01	15.45	2.19	0.30	0.54	1.22	0.96	1.94
299	46.73	54.85	67.84	2.41	0.12	0.23	2.03	0.47	1.75
301	53.32	58.49	75.66	2.45	0.13	0.19	2.00	0.56	1.43
302	43.01	37.96	52.31	2.58	0.07	0.29	3.06	0.10	0.55
303	7.69	6.42	8.87	2.50	0.26	0.24	2.48	0.40	0.84
304	42.30	36.00	35.34	2.31	0.11	0.28	1.96	0.06	0.11
307	74.29	96.75	105.70	3.09	0.15	0.38	2.51	0.25	0.96
308	-	-	-	2.84	0.04	0.08	-	-	-
309	21.59	28.08	30.89	2.80	0.23	0.48	2.16	0.63	1.72
310	32.37	22.68	30.12	2.51	0.14	0.34	1.86	0.36	0.90
313	39.73	38.76	45.85	2.54	0.08	0.13	2.19	0.16	0.63
314	26.24	21.56	29.13	2.97	0.17	0.19	3.31	0.44	0.86
315	63.48	62.18	70.83	2.33	0.10	0.72	2.78	0.06	0.28
317	7.79	5.37	7.23	2.32	0.06	0.21	2.05	0.10	-0.93
318	31.33	36.47	47.01	2.79	0.22	0.19	2.65	0.46	1.26

Continued on next page...

Table 4. CAS parameters for HRS galaxies

HRS	$r_e(r)$ arcsec	$r_e(H\alpha)$ arcsec	$r_e(EW_{H\alpha})$ arcsec	C_r	A_r	S_r	$C_{H\alpha}$	$A_{H\alpha}$	$S_{H\alpha}$
(1)	(2)	(3)	(4)	(5)	(6)	(7)	(8)	(9)	(10)
319	44.46	55.26	64.89	2.98	0.19	0.38	2.56	0.49	1.81
320	31.96	39.69	40.24	3.02	0.19	0.38	1.77	0.67	2.01
321	9.62	8.40	11.68	2.36	0.19	0.18	2.01	0.57	0.71
322	25.10	95.99	97.20	3.72	0.02	-0.01	0.28	0.23	0.69
323	24.98	22.50	23.90	2.44	0.16	0.51	1.94	0.28	0.92

Table 5. Radio continuum data.

HRS	sgn	S(20cm) mJy	log L(20cm) W Hz ⁻¹	flag	ref
(1)	(2)	(3)	(4)	(5)	(6)
1	0	1.8	19.76	-	5
2	1	5.0	20.28	1	4
3	1	6.4	20.30	1	1
4	1	126.0	21.58	1	1
5	1	5.0	20.20	-	5
6	0	1.8	19.86	-	5
7	1	6.7	20.43	1	4
8	0	1.8	19.88	-	5
9	1	4.6	20.33	1	4
10	1	2.2	20.07	1	4
11	1	11.3	20.66	1	4
12	0	1.8	19.91	-	5
13	1	44.2	21.40	1	1
14	1	4.2	20.24	1	4
15	1	28.1	21.04	1	2
16	1	13.8	20.70	1	4
17	1	24.9	20.97	1	4
18	1	2.3	20.14	1	4
19	1	5.6	20.54	1	4
20	1	86.7	21.72	2	1
21	0	1.8	19.76	-	5
22	1	4.4	20.31	1	4
23	1	51.9	21.43	1	1
24	1	28.9	21.22	1	3
25	1	63.7	21.38	1	1
26	0	1.8	20.01	-	5
27	1	12.4	20.93	1	4
28	1	10.8	20.65	1	4
29	0	1.8	19.70	-	5
30	1	7.0	20.30	1	3
31	1	52.5	21.36	2	1
32	0	1.8	19.75	-	5
33	1	6.9	20.51	1	4
34	1	9.2	20.43	1	4
35	0	1.8	19.98	-	5
36	1	265.0	22.16	1	1
37	1	10.1	20.64	1	4
38	1	5.2	20.38	1	4
39	0	1.8	20.00	-	5
40	1	11.4	20.82	1	4
41	0	1.8	19.85	-	5
42	1	17.6	20.76	1	2
43	0	1.8	19.71	-	5
44	1	5.0	20.16	1	4
45	1	5.6	20.49	1	4
46	1	10.0	20.71	1	2
47	1	7.2	20.58	1	4
48	1	80.8	21.40	1	1
49	0	1.8	19.81	-	5
50	1	57.4	21.47	1	1
51	1	12.8	20.70	1	4
52	1	3.6	20.08	1	4
53	1	17.7	20.66	1	3
54	0	1.8	19.81	-	5
55	1	14.1	20.64	1	4

Continued on next page...

Table 5. Radio continuum data.

HRS	sgn	S(20cm) mJy	log L(20cm) W Hz ⁻¹	flag	ref
(1)	(2)	(3)	(4)	(5)	(6)
56	1	98.7	21.82	1	1
57	1	15.4	20.68	1	2
58	1	3.0	19.90	1	4
59	1	7.3	20.70	1	4
60	1	20.6	20.73	1	2
61	0	1.8	19.79	-	5
62	1	8.6	20.69	1	4
63	1	4.2	20.21	1	3
64	0	1.8	19.79	-	5
65	0	1.8	19.90	-	5
66	1	88.3	21.64	1	3
67	1	2.8	20.12	1	4
68	1	3.6	20.22	-	5
69	1	6.3	20.30	2	2
70	0	1.8	20.04	-	5
71	1	1.1	19.60	-	6
72	0	1.8	20.01	-	5
73	1	41.1	21.02	1	1
74	1	61.0	21.24	1	1
75	0	1.8	19.83	-	5
76	1	3.1	19.91	1	4
77	1	151.0	21.87	1	1
78	1	6.5	20.38	1	4
79	1	8.1	20.63	1	4
80	0	1.8	19.77	-	5
81	1	23.0	20.88	1	1
82	1	2.7	19.95	-	5
83	0	1.8	19.80	-	5
84	1	2.9	19.98	1	4
85	1	52.7	21.14	1	1
86	1	14.7	20.68	1	3
87	0	1.8	19.77	-	5
88	1	22.0	20.86	1	1
89	1	23.3	20.88	1	2
90	0	1.8	19.77	-	5
91	1	73.9	21.38	1	1
92	0	1.8	19.77	-	5
93	1	6.1	20.22	1	4
94	0	1.8	19.77	-	5
95	1	18.7	20.79	1	4
96	1	23.7	20.89	1	1
97	1	13.4	20.64	1	2
98	1	3.4	20.05	1	4
99	0	1.8	19.77	-	5
100	1	6.0	20.29	1	4
101	0	1.8	19.68	-	5
102	1	422.0	22.14	1	1
103	0	1.8	20.03	-	5
104	0	1.8	19.77	-	5
105	0	1.8	19.77	-	5
106	0	1.8	20.03	-	5
107	0	1.8	19.77	-	5
108	0	1.8	20.03	-	5
109	1	4.3	20.15	1	4
110	1	24.1	20.90	1	3
111	1	43.6	21.15	1	1
112	0	1.8	20.03	-	5
113	1	38.2	21.10	1	4
114	1	416.0	22.13	1	1
115	0	1.8	19.77	-	5
116	0	1.8	19.77	-	5
117	1	2.5	20.17	1	4
118	0	1.8	19.77	-	5
119	1	11.0	20.56	1	4
120	0	1.8	19.77	-	5
121	1	5.8	20.54	1	4
122	1	340.0	22.05	2	1
123	0	1.8	19.77	-	5
124	1	12.5	20.61	1	4
125	0	1.8	20.03	-	5

Continued on next page...

Table 5. Radio continuum data.

HRS	sgn	S(20cm) mJy	log L(20cm) W Hz ⁻¹	flag	ref
(1)	(2)	(3)	(4)	(5)	(6)
126	0	1.8	19.77	-	5
127	1	3.9	20.37	1	4
128	0	1.8	20.03	-	5
129	0	1.8	19.77	-	5
130	0	1.8	19.77	-	5
131	0	1.8	20.03	-	5
132	1	4.4	20.42	1	4
133	0	1.8	19.81	-	5
134	0	1.8	20.03	-	5
135	0	1.8	20.03	-	5
136	0	1.8	20.03	-	5
137	0	1.8	19.77	-	5
138	1	6094.0	23.30	1	4
139	0	1.8	20.03	-	5
140	0	1.8	19.77	-	5
141	1	0.2	19.08	2	3
142	1	28.5	20.97	1	1
143	1	12.6	20.88	1	4
144	1	146.0	21.68	1	1
145	0	1.8	20.03	-	5
146	1	3.0	20.25	1	4
147	0	1.8	19.77	-	5
148	1	20.3	20.82	1	4
149	1	52.2	21.23	2	1
150	0	1.8	19.77	-	5
151	0	1.8	19.77	-	5
152	1	14.6	20.68	1	4
153	1	4.8	20.20	1	4
154	0	1.8	20.03	-	5
155	0	1.8	20.03	-	5
156	1	49.9	21.21	1	1
157	0	1.8	19.77	-	5
158	1	3.0	20.25	1	4
159	1	3.9	20.37	1	4
160	1	6.6	20.60	1	4
161	0	1.8	19.77	-	5
162	1	2.2	19.85	-	6
163	1	116.0	21.58	2	1
164	0	1.8	19.77	-	5
165	0	1.8	20.03	-	5
166	0	1.8	20.03	-	5
167	0	1.8	20.03	-	5
168	1	3.4	20.31	1	4
169	0	1.8	20.08	-	5
170	1	8.3	20.43	1	2
171	1	6.3	20.58	1	4
172	1	2.9	19.98	1	4
173	1	37.4	21.09	1	2
174	1	1.8	19.78	-	6
175	0	1.8	19.77	-	5
176	0	1.8	20.03	-	5
177	1	15.5	20.70	1	4
178	1	256.0	21.92	1	4
179	0	1.8	19.77	-	5
180	0	1.8	19.77	-	5
181	0	1.8	19.77	-	5
182	1	2.9	19.98	1	4
183	1	266000.0	24.94	1	4
184	0	1.8	19.77	-	5
185	0	1.8	19.77	-	5
186	0	1.8	19.85	-	5
187	0	1.8	19.77	-	5
188	1	4.0	20.12	1	4
189	0	1.8	19.77	-	5
190	1	278.0	21.96	1	1
191	0	1.8	19.77	-	5
192	0	1.8	19.77	-	5
193	1	7.5	20.39	-	5
194	1	32.0	21.02	1	2
195	0	1.8	19.77	-	5

Continued on next page...

Table 5. Radio continuum data.

HRS	sgn	S(20cm) mJy	log L(20cm) W Hz ⁻¹	flag	ref
(1)	(2)	(3)	(4)	(5)	(6)
196	1	9.1	20.47	1	3
197	1	22.1	20.86	1	3
198	0	1.8	19.76	-	5
199	0	1.8	19.77	-	5
200	1	11.1	20.56	1	1
201	1	214.0	21.84	1	1
202	0	1.8	19.77	-	5
203	1	117.0	21.58	1	1
204	1	64.5	21.32	2	1
205	1	203.0	21.82	1	1
206	1	3.6	20.07	1	4
207	1	3.1	20.01	1	4
208	1	4.6	20.18	2	2
209	0	1.8	19.66	-	5
210	0	1.8	19.77	-	5
211	1	100.0	21.51	1	4
212	1	7.2	20.52	1	4
213	1	131.0	21.66	1	1
214	0	1.8	19.77	-	5
215	1	9.6	20.50	1	4
216	1	136.0	21.65	1	1
217	1	83.4	21.44	1	1
218	0	1.8	19.77	-	5
219	0	1.8	19.77	-	5
220	1	103.0	21.53	1	1
221	0	1.8	19.77	-	5
222	0	1.8	19.77	-	5
223	0	1.8	19.77	-	5
224	0	1.8	19.77	-	5
225	0	1.8	19.77	-	5
226	0	1.8	19.77	-	5
227	1	5.7	20.18	1	3
228	0	1.8	21.78	-	5
229	0	1.8	19.77	-	5
230	1	4.6	20.18	1	4
231	1	0.4	19.12	2	2
232	0	1.8	19.77	-	5
233	1	22.9	20.87	1	4
234	0	1.8	19.77	-	5
235	0	1.8	19.77	-	5
236	0	1.8	19.77	-	5
237	1	12.6	20.61	1	4
238	0	1.8	19.71	-	5
239	1	33.0	21.03	1	4
240	0	1.8	19.77	-	5
241	1	77.8	21.41	1	4
242	1	7.5	20.39	1	4
243	0	1.8	19.77	-	5
244	1	35.0	21.06	2	1
245	1	29.1	20.98	1	4
246	1	24.0	20.89	1	1
247	1	117.0	21.58	1	1
248	0	1.8	19.77	-	5
249	0	1.8	19.77	-	5
250	0	1.8	19.77	-	5
251	1	417.0	22.34	1	1
252	0	1.8	20.04	-	5
253	1	7.1	20.56	1	4
254	1	9.6	20.50	1	2
255	0	1.8	19.77	-	5
256	1	47.5	21.14	1	1
257	1	0.6	19.29	2	2
258	0	1.8	19.81	-	5
259	1	18.5	20.78	1	4
260	1	17.2	20.75	1	1
261	0	1.8	19.75	-	5
262	1	37.8	21.09	1	3
263	1	28.2	20.98	2	2
264	0	1.8	19.83	-	5
265	0	1.8	19.97	-	5

Continued on next page...

Table 5. Radio continuum data.

HRS	sgn	S(20cm) mJy	log L(20cm) W Hz ⁻¹	flag	ref
(1)	(2)	(3)	(4)	(5)	(6)
266	1	9.2	20.67	1	2
267	1	7.4	20.38	1	4
268	1	54.1	21.25	1	4
269	0	1.8	19.77	-	5
270	0	1.8	19.80	-	5
271	1	3.0	19.99	1	4
272	0	1.8	19.77	-	5
273	0	1.8	19.77	-	5
274	1	1.0	19.51	-	6
275	1	28.5	21.21	1	2
276	1	8.2	20.43	1	4
277	0	1.8	19.77	-	5
278	0	1.8	19.72	-	5
279	0	1.8	19.77	-	5
280	1	10.0	20.51	1	4
281	0	1.8	19.77	-	5
282	0	1.8	19.77	-	5
283	1	44.8	21.17	1	1
284	1	79.0	21.49	1	1
285	1	39.2	21.11	1	1
286	1	0.2	18.82	2	2
287	1	15.6	20.71	1	4
288	1	19.0	20.74	1	2
289	1	21.0	21.13	1	2
290	1	11.4	20.53	1	4
291	0	1.8	19.84	-	5
292	1	33.2	21.06	1	1
293	1	25.2	20.84	1	4
294	1	7.2	20.63	1	4
295	1	140.0	21.63	1	1
296	1	3.5	19.96	1	4
297	1	16.3	20.93	1	4
298	1	24.9	21.06	1	4
299	1	2.5	19.90	1	2
300	0	1.8	19.88	-	5
301	1	2.1	19.96	2	2
302	0	1.8	19.94	-	5
303	1	15.9	21.03	1	4
304	0	1.8	19.89	-	5
305	0	1.8	19.76	-	5
306	1	160.0	21.68	1	4
307	1	13.9	20.69	2	2
308	0	1.8	19.69	-	5
309	0	1.8	19.90	-	5
310	1	4.4	20.48	1	4
311	1	8.5	20.64	1	2
312	0	1.8	19.96	-	5
313	1	7.5	20.58	1	4
314	1	10.6	20.67	1	4
315	0	1.8	19.93	-	5
316	0	1.8	20.07	-	5
317	0	1.8	20.09	-	5
318	1	14.5	20.80	1	4
319	1	10.7	20.66	1	2
320	1	23.5	21.13	1	4
321	1	6.1	20.55	1	4
322	0	1.8	19.97	-	5
323	1	13.6	20.93	1	4

Table 6. Star formation rates.

HRS	$SFR_{H\alpha+BD}$ M _⊙ yr ⁻¹	$SFR_{H\alpha+24\mu m}$ M _⊙ yr ⁻¹	$SFR_{FUV+24\mu m}$ M _⊙ yr ⁻¹	SFR_{radio} M _⊙ yr ⁻¹	SFR_{MED} M _⊙ yr ⁻¹	SFR_{1exp} M _⊙ yr ⁻¹	SFR_{2exp} M _⊙ yr ⁻¹	SFR_{del} M _⊙ yr ⁻¹
(1)	(2)	(3)	(4)	(5)	(6)	(7)	(8)	(9)
1	-	0.0501	-	-	0.0501	-	-	-

Continued on next page...

Table 6. Star formation rates.

HRS	$SFR_{H\alpha+BD}$ $M_{\odot} \text{ yr}^{-1}$	$SFR_{H\alpha+24\mu\text{m}}$ $M_{\odot} \text{ yr}^{-1}$	$SFR_{FUV+24\mu\text{m}}$ $M_{\odot} \text{ yr}^{-1}$	SFR_{radio} $M_{\odot} \text{ yr}^{-1}$	SFR_{MED} $M_{\odot} \text{ yr}^{-1}$	SFR_{1exp} $M_{\odot} \text{ yr}^{-1}$	SFR_{2exp} $M_{\odot} \text{ yr}^{-1}$	SFR_{del} $M_{\odot} \text{ yr}^{-1}$
(1)	(2)	(3)	(4)	(5)	(6)	(7)	(8)	(9)
2	0.2801	0.1808	0.1661	0.2560	0.2208	0.2169	0.2425	0.2378
4	-	-	-	2.4262	2.4262	-	-	-
5	-	0.0987	-	-	0.0987	-	-	-
6	-	-	0.0393	-	0.0393	0.0357	0.0384	0.0491
8	-	-	0.4053	-	0.4053	0.4002	0.4167	0.4939
9	-	-	0.1838	0.2765	0.2301	0.1798	0.1208	0.1811
10	0.1566	0.1542	-	0.1737	0.1615	-	-	-
11	0.5382	0.3635	0.3696	0.4975	0.4422	0.4893	0.5314	0.4975
12	0.0858	0.0597	0.0631	-	0.0695	0.0765	0.0779	0.0761
13	-	2.3628	1.7414	1.7837	1.9627	2.2441	2.2415	2.3374
15	-	-	1.1530	0.9598	1.0564	1.3780	1.2930	1.1932
16	-	0.5338	0.5321	0.5363	0.5341	0.6061	0.6309	0.6254
17	0.7359	0.9443	0.7930	0.8577	0.8327	0.9711	0.9729	0.9802
18	-	0.1792	0.2072	0.1963	0.1942	0.2257	0.2259	0.1380
19	0.5706	0.6953	0.5814	0.3997	0.5617	0.7622	0.7700	0.7680
20	2.1338	-	-	-	2.1338	1.5248	2.9108	1.8953
21	-	0.0134	-	-	0.0134	-	-	-
23	-	1.7084	1.3503	1.8738	1.6442	0.9027	1.2760	0.7555
24	1.2037	1.3568	1.3212	1.3168	1.2996	1.5853	1.6529	1.5749
25	1.5329	1.9410	1.5027	1.7169	1.6734	1.5590	1.6716	1.6355
26	-	-	0.0600	-	0.0600	0.0959	0.0923	0.0858
27	0.7075	0.7745	0.5857	0.8007	0.7171	0.5235	0.7285	0.6225
28	0.5922	0.4199	0.3434	0.4845	0.4600	0.4280	0.4249	0.4350
29	0.2105	0.1374	0.0931	-	0.1470	0.1289	0.1191	0.1073
30	0.3993	0.2221	0.2109	0.2612	0.2734	0.2428	0.2495	0.2410
31	0.8054	1.3810	1.1478	-	1.1114	1.3318	1.3486	1.3553
33	-	0.5294	0.5542	0.3846	0.4894	0.6249	0.6218	0.6585
34	-	0.1329	0.1723	0.3334	0.2129	0.2703	0.3221	0.2836
36	3.8926	7.7223	6.2515	7.9596	6.4565	3.5936	3.6596	3.5670
37	0.3689	0.3492	0.4060	0.4820	0.4015	0.5024	0.4989	0.4970
38	0.2878	0.2023	-	0.3053	0.2651	-	-	-
39	-	0.1165	0.0936	-	0.1051	0.1185	0.1136	0.1096
40	0.5725	0.6614	0.4783	0.6561	0.5921	0.6622	0.6924	0.7094
41	-	-	0.0412	-	0.0412	0.0639	0.0629	0.0518
42	-	0.9381	-	0.5934	0.7657	-	-	-
44	0.4256	0.2909	0.2016	0.2057	0.2809	0.1836	0.2488	0.2167
47	-	0.2795	0.4243	0.4294	0.3777	0.5578	0.5684	0.6006
48	2.0519	2.3102	2.0328	1.7649	2.0399	2.7152	2.7031	2.7399
50	2.3732	2.3047	1.5871	2.0168	2.0705	1.9495	1.9662	1.9559
51	0.5173	0.3164	-	0.5307	0.4548	-	-	-
52	-	0.0952	0.1636	0.1780	0.1456	0.1054	0.1114	0.1326
53	1.0077	0.3662	0.3458	0.4982	0.5545	0.4988	0.4949	0.4974
54	-	-	0.2572	-	0.2572	0.2659	0.2181	0.1673
55	0.4971	0.5837	0.5280	0.4794	0.5221	0.6638	0.7069	0.6709
56	-	3.7369	2.8221	3.6667	3.4086	0.7723	1.0498	0.7225
57	1.1612	1.2454	0.8707	0.5112	0.9471	0.9886	0.9728	0.9865
58	0.1424	0.1200	0.1344	0.1277	0.1311	0.1682	0.1822	0.1720
59	-	0.5164	0.3692	0.5291	0.4716	0.4271	0.4526	0.5732
60	-	0.6190	0.4953	0.5589	0.5578	0.3644	0.3731	0.3159
61	0.1244	0.1070	0.0951	-	0.1089	0.1209	0.1200	0.1219
62	1.1722	-	-	0.5235	0.8478	0.5570	0.5524	0.5697
63	-	0.5514	0.5257	0.2231	0.4334	0.5488	0.5991	0.6990
64	-	0.0758	-	-	0.0758	-	-	-
65	0.4044	0.2940	0.2595	-	0.3193	0.3272	0.3324	0.3274
66	1.9525	2.1964	1.6592	2.6810	2.1223	2.1948	2.2986	2.3298
67	0.2102	0.1765	0.1830	0.1926	0.1906	0.2249	0.2300	0.2227
68	0.2189	0.1903	0.1550	-	0.1881	0.1396	0.1487	0.1412
69	-	0.3110	0.2428	-	0.2769	0.0846	0.1200	0.0049
70	0.3244	0.3164	0.3628	-	0.3345	0.3570	0.4509	0.4095
72	1.0382	0.8475	0.5999	-	0.8285	0.3621	0.5541	0.4231
73	-	1.7513	-	0.9268	1.3390	-	-	-
74	0.8171	1.2762	-	1.3479	1.1471	-	-	-
76	0.0692	0.0827	-	0.1314	0.0944	-	-	-
77	-	5.0024	3.9616	4.0881	4.3507	4.6335	4.6781	4.7378
78	0.3976	0.2391	0.2867	0.3053	0.3072	0.3413	0.3505	0.3364
79	0.2218	0.2269	0.2480	0.4701	0.2917	0.2361	0.2784	0.2700
80	-	0.1387	0.2054	-	0.1721	0.1958	0.2023	0.2100
81	-	-	0.8056	0.7234	0.7645	0.5814	0.6060	0.6198
82	-	-	0.0933	-	0.0933	0.1312	0.1328	0.1324
83	0.1256	0.0800	0.0734	-	0.0930	0.0763	0.0810	0.0758

Continued on next page...

Table 6. Star formation rates.

HRS	$SFR_{H\alpha+BD}$ $M_{\odot} \text{ yr}^{-1}$	$SFR_{H\alpha+24\mu\text{m}}$ $M_{\odot} \text{ yr}^{-1}$	$SFR_{FUV+24\mu\text{m}}$ $M_{\odot} \text{ yr}^{-1}$	SFR_{radio} $M_{\odot} \text{ yr}^{-1}$	SFR_{MED} $M_{\odot} \text{ yr}^{-1}$	SFR_{1exp} $M_{\odot} \text{ yr}^{-1}$	SFR_{2exp} $M_{\odot} \text{ yr}^{-1}$	SFR_{del} $M_{\odot} \text{ yr}^{-1}$
(1)	(2)	(3)	(4)	(5)	(6)	(7)	(8)	(9)
84	-	0.1425	0.1265	0.1476	0.1389	0.1557	0.1608	0.1670
85	-	1.3293	1.0432	1.1504	1.1743	1.0133	1.0545	1.0479
86	-	0.5771	0.5810	0.5159	0.5580	0.7401	0.7370	0.7628
88	-	1.9248	-	0.6996	1.3122	-	-	-
89	-	0.9720	0.8359	0.7305	0.8461	1.0540	1.0788	1.0398
91	-	1.9228	-	1.7267	1.8248	-	-	-
92	-	0.0838	0.0720	-	0.0779	0.0916	0.0995	0.1003
94	-	0.2641	0.1995	-	0.2318	0.2578	0.2667	0.2737
95	-	0.3467	0.2821	0.6190	0.4159	0.2419	0.2977	0.2941
96	-	1.4283	1.0719	0.7399	1.0801	1.1421	1.1034	1.0866
97	-	1.2143	0.6955	0.4809	0.7969	0.1755	0.2236	0.0046
98	-	0.1705	0.1643	0.1672	0.1673	0.1738	0.1846	0.1859
99	0.0701	0.0800	0.0650	-	0.0717	0.0830	0.0789	0.0715
100	-	-	0.4068	0.2599	0.3333	0.4192	0.4819	0.5548
102	6.5574	8.2892	6.3749	7.6099	7.2078	7.5307	7.5153	7.6073
106	-	-	0.2238	-	0.2238	0.3171	0.3017	0.2763
108	-	0.0623	0.0659	-	0.0641	0.0808	0.0946	0.1027
109	-	0.0774	0.0771	0.2008	0.1184	0.0979	0.1333	0.1268
110	1.0300	0.8975	0.5452	0.7493	0.8055	0.6787	0.6704	0.6929
111	-	-	0.7027	1.1675	0.9351	0.8005	0.8299	0.8458
112	-	0.0772	-	-	0.0772	-	-	-
113	-	-	0.5814	1.0580	0.8197	0.3511	0.2349	0.3542
114	7.1423	8.3402	6.6320	7.5018	7.4041	8.1755	8.1480	8.2527
115	-	0.0655	-	-	0.0655	-	-	-
117	-	-	0.2820	0.2107	0.2464	0.0605	0.0856	0.0015
118	0.2063	-	-	-	0.2063	0.2115	0.2255	0.2321
119	-	0.2963	0.2477	0.4138	0.3193	0.1569	0.1032	0.1682
120	-	-	0.1557	-	0.1557	0.0415	0.0573	0.0012
121	-	0.4956	0.3619	0.4028	0.4201	0.2089	0.2529	0.2113
122	-	6.8213	5.3460	-	6.0837	6.1289	5.9317	5.6317
124	-	0.1464	0.1942	0.4561	0.2656	0.2373	0.2448	0.2509
127	-	-	0.2950	0.2972	0.2961	0.2312	0.2523	0.2338
128	-	-	0.1017	-	0.1017	0.1188	0.1316	0.1392
130	-	0.1259	0.1469	-	0.1364	0.2125	0.2010	0.1959
132	-	0.3454	0.2853	0.3260	0.3189	0.3713	0.3650	0.3750
133	0.1223	0.1014	0.1338	-	0.1192	0.1694	0.1757	0.1808
134	-	-	0.1823	-	0.1823	0.0302	0.0435	0.0569
136	-	-	0.0999	-	0.0999	0.0312	0.0453	0.0020
139	0.2079	-	-	-	0.2079	0.3565	0.3510	0.3594
140	-	-	0.1373	-	0.1373	0.0432	0.1091	0.1483
141	-	0.3691	0.3880	-	0.3786	0.3585	0.4037	0.3617
142	-	1.8442	1.3793	0.8498	1.3578	0.8820	1.3099	1.1313
143	0.5592	0.6651	0.4700	0.7250	0.6048	0.7029	0.7557	0.7015
144	1.1401	3.6780	2.9508	2.8493	2.6545	1.0969	1.1597	1.1749
145	-	0.3255	0.3661	-	0.3458	0.4376	0.4742	0.4480
146	-	0.1983	0.1479	0.2427	0.1963	0.2004	0.2106	0.2131
147	-	0.0783	-	-	0.0783	-	-	-
148	-	0.2799	0.2829	0.6585	0.4071	0.4102	0.4087	0.4120
149	-	1.0203	0.7733	-	0.8968	0.4904	0.4075	0.2975
151	-	0.1749	0.2285	-	0.2017	0.2333	0.2511	0.2592
152	0.4160	0.6982	0.5654	0.5132	0.5482	0.5738	0.5736	0.5767
153	0.1244	0.1735	0.2125	0.2187	0.1823	0.2899	0.2835	0.2996
154	-	0.2539	0.3951	-	0.3245	0.5080	0.5581	0.5206
156	-	-	1.4089	1.2908	1.3499	0.0868	0.1645	0.3253
157	0.6246	0.6264	0.4470	-	0.5660	0.6667	0.6598	0.6719
158	0.2389	-	-	0.2427	0.2408	0.2747	0.2847	0.2812
159	-	0.9111	0.6929	0.2972	0.6337	0.5698	0.4542	0.3626
160	-	0.5988	0.5288	0.4444	0.5240	0.6836	0.6662	0.6453
163	-	0.5014	0.3930	-	0.4472	0.1426	0.2099	0.4782
165	0.1710	0.0995	0.0808	-	0.1171	0.1194	0.1095	0.1236
167	-	0.2251	0.1001	-	0.1626	0.1012	0.0709	0.1014
168	0.4404	0.2637	0.1902	0.2674	0.2904	0.2215	0.2286	0.2313
169	-	0.1620	0.2526	-	0.2073	0.3198	0.3394	0.3242
170	-	0.3340	-	0.3336	0.3338	-	-	-
171	0.5051	0.5238	0.3771	0.4290	0.4587	0.5222	0.4593	0.4367
172	-	0.1534	0.1421	0.1476	0.1477	0.1040	0.0683	0.1053
173	-	0.6748	0.5058	1.0414	0.7407	0.3699	0.2570	0.3752
177	-	0.2592	0.3142	0.5370	0.3702	0.4329	0.4331	0.4350
182	-	0.2686	0.2744	0.1476	0.2302	0.3619	0.3448	0.3629
184	-	-	0.3269	-	0.3269	0.1415	0.0852	0.0724

Continued on next page...

Table 6. Star formation rates.

HRS	$SFR_{H\alpha+BD}$ $M_{\odot} \text{ yr}^{-1}$	$SFR_{H\alpha+24\mu\text{m}}$ $M_{\odot} \text{ yr}^{-1}$	$SFR_{FUV+24\mu\text{m}}$ $M_{\odot} \text{ yr}^{-1}$	SFR_{radio} $M_{\odot} \text{ yr}^{-1}$	SFR_{MED} $M_{\odot} \text{ yr}^{-1}$	SFR_{1exp} $M_{\odot} \text{ yr}^{-1}$	SFR_{2exp} $M_{\odot} \text{ yr}^{-1}$	SFR_{del} $M_{\odot} \text{ yr}^{-1}$
(1)	(2)	(3)	(4)	(5)	(6)	(7)	(8)	(9)
185	-	0.0527	0.0611	-	0.0569	0.0243	0.0424	0.0748
187	0.9393	-	-	-	0.9393	0.9768	1.2149	1.1178
188	-	0.3754	0.3046	0.1898	0.2899	0.4215	0.3996	0.4217
189	0.2375	0.1654	0.1419	-	0.1816	0.2023	0.2152	0.2052
190	-	3.6251	3.1564	5.0132	3.9315	3.1464	2.7981	1.8932
191	0.0869	-	-	-	0.0869	0.0741	0.0827	0.0747
192	-	0.0255	0.0205	-	0.0230	0.0090	0.0125	0.0002
193	0.5029	-	-	-	0.5029	0.3425	0.4156	0.3940
194	-	2.7969	1.5181	0.9268	1.7473	1.5810	1.6775	1.7605
196	-	1.0664	0.9335	0.3580	0.7859	0.8543	1.0738	0.9837
197	-	0.1807	0.2663	0.7020	0.3830	0.3619	0.3579	0.3806
198	-	0.0940	0.1274	-	0.1107	0.1581	0.1641	0.1685
199	0.1103	0.1079	0.1129	-	0.1104	0.1057	0.1113	0.1127
201	-	5.0326	3.7927	3.8591	4.2281	1.6643	1.5091	1.0140
203	2.2193	2.0856	1.3299	2.4222	2.0142	1.0821	1.4982	1.2912
204	-	3.2976	2.8527	-	3.0752	3.2992	3.1697	2.9009
205	-	5.3800	4.5139	3.6607	4.5182	3.9458	4.0266	3.9200
206	0.1266	0.1532	0.1862	0.1748	0.1602	0.1881	0.1756	0.1603
207	-	0.2040	0.2412	0.1555	0.2002	0.2671	0.3031	0.3519
208	-	0.7647	0.7062	-	0.7355	0.6257	0.4325	0.6299
212	0.3272	0.2762	0.4367	0.3879	0.3570	0.4520	0.4727	0.4840
213	-	-	2.4833	2.7713	2.6273	1.8448	1.5393	1.8617
215	-	-	-	0.3730	0.3730	0.8667	0.8012	0.7767
216	-	-	-	2.7050	2.7050	1.1391	1.4582	1.4889
217	-	2.0989	1.8885	1.8880	1.9585	1.0684	0.7286	1.0810
220	-	1.4442	1.1106	2.2056	1.5868	0.2842	0.3999	0.9657
221	-	0.1978	0.1870	-	0.1924	0.1557	0.1787	0.1575
222	-	0.0413	0.0345	-	0.0379	0.0354	0.0234	0.0362
226	-	-	0.1066	-	0.1066	0.1300	0.1359	0.1394
227	0.4492	0.3600	0.5010	0.2115	0.3804	0.5742	0.5975	0.6172
230	-	0.1512	0.2359	0.2116	0.1996	0.3165	0.3022	0.3127
232	-	0.0722	0.0938	-	0.0830	0.0259	0.0354	0.0009
233	-	0.3767	0.2812	0.7211	0.4597	0.1037	0.1210	0.1041
237	0.4141	0.6352	0.4277	0.4589	0.4840	0.5066	0.5184	0.4980
239	-	0.5150	0.4045	0.9484	0.6227	0.4837	0.5411	0.4480
242	-	0.3415	0.3836	0.3087	0.3446	0.4972	0.5136	0.5266
244	-	1.2878	0.9031	-	1.0954	1.1289	1.0948	1.0260
246	-	1.3619	1.0991	0.7470	1.0693	1.1971	1.2506	1.2327
247	-	3.2520	2.5178	2.4222	2.7307	2.9977	3.1036	2.9673
251	-	8.9331	6.6556	12.1511	9.2466	3.7190	6.9103	3.9378
252	0.3830	0.3637	0.3281	-	0.3583	0.4160	0.4216	0.4168
254	-	0.9011	-	0.3730	0.6370	-	-	-
255	-	-	0.4677	-	0.4677	0.4215	0.4481	0.4568
256	-	-	2.4407	1.1359	1.7883	1.9918	2.0173	2.0629
259	-	0.6677	-	0.6140	0.6408	-	-	-
261	-	0.0838	0.0578	-	0.0708	0.0491	0.0593	0.0498
262	0.9063	1.4034	0.9713	1.0497	1.0827	1.0320	1.3799	1.2262
263	-	-	1.9277	-	1.9277	1.6458	1.8489	1.6584
265	0.4744	0.3642	-	-	0.4193	-	-	-
266	0.9434	1.0111	1.5397	0.5090	1.0008	1.5013	1.9207	1.7422
267	0.5886	0.4250	0.3246	0.3011	0.4098	0.3629	0.3381	0.3140
268	-	0.7949	0.5750	1.3707	0.9135	0.6816	0.7245	0.6885
270	-	-	0.2703	-	0.2703	0.0020	0.1318	0.0037
271	0.6544	0.2944	0.1521	0.1516	0.3131	0.1649	0.1743	0.1780
273	-	0.2426	0.2273	-	0.2349	0.2565	0.2243	0.1555
274	-	-	0.1013	-	0.1013	0.0398	0.0539	0.0018
275	-	-	1.6171	1.2802	1.4487	1.5558	2.0678	1.7827
276	-	-	0.3800	0.3305	0.3553	0.3983	0.4321	0.4034
278	-	0.0319	0.0306	-	0.0313	0.0079	0.0126	0.0389
280	-	0.1607	0.1356	0.3848	0.2270	0.1451	0.1625	0.1845
281	-	0.0332	0.0461	-	0.0396	0.0498	0.0454	0.0419
283	-	1.4268	0.9219	1.1914	1.1800	1.1999	1.2353	1.2367
284	-	1.2497	-	2.0565	1.6531	-	-	-
285	-	-	0.7010	1.0786	0.8898	0.0918	0.1984	0.3352
287	-	0.6566	0.4791	0.5397	0.5585	0.5783	0.6052	0.5696
288	-	0.6593	-	0.5667	0.6130	-	-	-
289	-	1.8648	1.5216	1.1304	1.5056	1.7239	1.7703	1.7550
290	0.3094	0.2546	0.2318	0.3962	0.2980	0.2657	0.2467	0.2742
292	-	0.9003	0.6710	0.9949	0.8554	0.3315	0.5824	0.3512
293	0.6056	0.6646	0.5176	0.6809	0.6172	0.5809	0.6079	0.6250

Continued on next page...

Table 6. Star formation rates.

HRS	$SFR_{H\alpha+BD}$ $M_{\odot} \text{ yr}^{-1}$	$SFR_{H\alpha+24\mu\text{m}}$ $M_{\odot} \text{ yr}^{-1}$	$SFR_{FUV+24\mu\text{m}}$ $M_{\odot} \text{ yr}^{-1}$	SFR_{radio} $M_{\odot} \text{ yr}^{-1}$	SFR_{MED} $M_{\odot} \text{ yr}^{-1}$	SFR_{1exp} $M_{\odot} \text{ yr}^{-1}$	SFR_{2exp} $M_{\odot} \text{ yr}^{-1}$	SFR_{del} $M_{\odot} \text{ yr}^{-1}$
(1)	(2)	(3)	(4)	(5)	(6)	(7)	(8)	(9)
294	0.2881	0.2238	0.2179	0.4739	0.3009	0.2390	0.2575	0.2571
295	-	-	3.4111	2.6353	3.0232	3.3584	3.3868	3.4984
297	-	0.9558	0.6690	0.7971	0.8073	0.9366	0.8738	0.7948
298	0.8397	0.9408	0.6422	0.9995	0.8556	0.6687	0.8262	0.7512
299	-	0.3453	0.4293	0.1281	0.3009	0.4308	0.4605	0.4527
300	-	0.0530	-	-	0.0530	-	-	-
301	-	0.6014	0.6001	-	0.6008	0.5431	0.5814	0.5732
302	-	0.1663	0.1099	-	0.1381	0.1526	0.1630	0.1622
303	0.7318	0.8908	0.6296	0.9507	0.8007	0.6302	0.8458	0.7512
304	-	0.1851	0.1726	-	0.1788	0.1213	0.1418	0.1235
305	0.0360	-	-	-	0.0360	0.0225	0.0253	0.0226
306	-	-	0.1812	2.8470	1.5141	0.0016	0.0854	0.0036
307	-	-	1.3541	-	1.3541	1.2425	1.3836	1.5449
309	-	0.1933	0.1865	-	0.1899	0.2088	0.2178	0.2255
310	-	0.8633	0.5789	0.3601	0.6008	0.6881	0.6312	0.6088
311	-	-	-	0.4797	0.4797	0.1613	0.2254	0.0050
313	-	-	-	0.4355	0.4355	0.3182	0.3341	0.3442
314	-	0.3923	0.4538	0.5089	0.4517	0.4602	0.4757	0.4784
315	0.1805	-	-	-	0.1805	0.1766	0.1929	0.1942
317	-	0.0403	0.0794	-	0.0598	0.0727	0.0770	0.0764
318	0.4908	0.4445	0.4778	0.6318	0.5112	0.6950	0.7167	0.6874
319	0.7960	-	-	0.5008	0.6484	0.9920	0.9837	0.9991
320	-	1.5892	1.3583	1.1268	1.3581	1.5643	1.6126	1.6122
321	0.4362	0.4252	0.4080	0.4072	0.4192	0.4985	0.4949	0.5021
323	-	0.5452	0.4144	0.7895	0.5830	0.3362	0.3820	0.4413

Table 7. Fluxes of the emission lines normalised to $H\alpha$ determined using GANDALF.

HRS	[OII] $\lambda 3727$	$H\beta$ $\lambda 4861$	[OIII] $\lambda 5007$	$H\alpha$ $\lambda 6563$	[NII] $\lambda 6584$	[SII] $\lambda 6716$	[SII] $\lambda 6731$	$S/N(H\alpha)$	$S/N(H\beta)$	$C(H\beta)$	$\sigma[C(H\beta)]$
(1)	(2)	(3)	(4)	(5)	(6)	(7)	(8)	(9)	(10)	(11)	(12)
1	0.41	0.17	0.07	1.0	0.37	0.25	0.17	50.64	11.91	1.00	0.13
2	0.48	0.22	0.09	1.0	0.32	0.20	0.14	108.46	31.77	0.64	0.05
4	-	-	-	-	-	-	-	-	-	-	-
5	0.65	0.00	0.00	1.0	0.89	0.62	0.52	12.78	-	-	-
10	0.84	0.28	0.24	1.0	0.24	0.21	0.14	91.33	34.49	0.28	0.05
11	0.40	0.22	0.12	1.0	0.27	0.25	0.18	84.19	25.35	0.64	0.06
12	0.86	0.25	0.32	1.0	0.18	0.24	0.18	97.14	33.10	0.46	0.05
13	0.67	0.20	0.04	1.0	0.39	0.21	0.16	48.13	12.70	0.79	0.12
16	0.19	0.27	0.09	1.0	0.34	0.22	0.18	29.71	11.01	0.34	0.14
17	0.57	0.25	0.21	1.0	0.28	0.18	0.13	60.67	20.61	0.44	0.07
18	0.63	0.26	0.22	1.0	0.43	0.23	0.17	36.03	12.86	0.40	0.12
19	0.63	0.28	0.09	1.0	0.29	0.18	0.12	64.43	23.99	0.29	0.07
20	0.98	0.27	0.40	1.0	0.15	0.15	0.09	47.33	16.93	0.34	0.09
21	0.00	0.19	0.14	1.0	0.27	0.33	0.27	25.12	6.51	0.85	0.23
23	0.35	0.14	0.12	1.0	0.49	0.28	0.22	39.86	7.72	1.30	0.19
24	0.41	0.22	0.07	1.0	0.41	0.19	0.14	63.23	18.96	0.64	0.08
25	0.35	0.19	0.09	1.0	0.35	0.21	0.15	83.29	21.02	0.86	0.07
26	0.75	0.20	0.21	1.0	0.25	0.27	0.20	71.32	19.42	0.79	0.08
27	0.66	0.26	0.16	1.0	0.28	0.17	0.12	93.56	32.79	0.41	0.05
28	0.57	0.24	0.13	1.0	0.28	0.20	0.13	97.68	32.07	0.52	0.05
29	0.62	0.23	0.18	1.0	0.25	0.26	0.20	71.77	22.43	0.56	0.07
30	0.53	0.23	0.12	1.0	0.31	0.25	0.17	61.59	18.88	0.56	0.08
31	1.09	0.26	0.57	1.0	0.11	0.16	0.11	66.24	23.26	0.41	0.07
32	-	-	-	-	-	-	-	1.54	0.09	-	-
33	0.54	0.28	0.09	1.0	0.39	0.24	0.20	38.80	14.53	0.29	0.11
34	0.99	0.07	0.01	1.0	0.42	0.34	0.26	25.60	2.38	2.31	0.62
35	-	-	-	-	-	-	-	-	-	-	-
36	0.23	0.19	0.08	1.0	0.59	0.19	0.15	87.43	21.98	0.85	0.07
37	0.81	0.26	0.07	1.0	0.46	0.20	0.16	49.92	17.58	0.39	0.09
38	1.28	0.25	0.35	1.0	0.14	0.23	0.16	63.14	21.45	0.44	0.07
39	1.16	0.23	0.15	1.0	0.27	0.24	0.17	43.84	13.83	0.59	0.11
40	1.00	0.27	0.29	1.0	0.20	0.19	0.14	54.97	20.17	0.34	0.08
42	0.28	0.22	0.02	1.0	0.40	0.21	0.14	48.46	14.09	0.64	0.11

Continued on next page...

Table 7. Fluxes of the emission lines normalised to $H\alpha$ determined using GANDALF.

HRS	[OII] $\lambda 3727$	H β $\lambda 4861$	[OIII] $\lambda 5007$	H α $\lambda 6563$	[NII] $\lambda 6584$	[SII] $\lambda 6716$	[SII] $\lambda 6731$	S/N($H\alpha$)	S/N(H β)	C(H β)	σ [C(H β)]
(1)	(2)	(3)	(4)	(5)	(6)	(7)	(8)	(9)	(10)	(11)	(12)
44	0.79	0.25	0.56	1.0	0.13	0.14	0.10	184.71	62.81	0.46	0.02
47	1.27	0.27	0.34	1.0	0.16	0.20	0.13	26.73	9.83	0.35	0.16
48	0.24	0.24	0.08	1.0	0.37	0.19	0.14	51.76	16.8	0.52	0.09
50	0.29	0.20	0.04	1.0	0.37	0.16	0.12	86.03	22.87	0.78	0.07
51	0.59	0.22	0.14	1.0	0.27	0.24	0.16	103.86	30.37	0.65	0.05
52	1.38	0.27	0.46	1.0	0.44	0.24	0.17	30.74	11.13	0.35	0.14
53	0.56	0.17	0.07	1.0	0.36	0.23	0.16	61.36	14.40	1.00	0.10
55	0.36	0.25	0.07	1.0	0.36	0.19	0.14	61.08	20.69	0.45	0.07
56	0.26	0.12	0.05	1.0	0.42	0.23	0.18	62.51	10.53	1.53	0.14
57	0.51	0.25	0.02	1.0	0.36	0.16	0.12	51.30	17.45	0.45	0.09
58	1.03	0.27	0.26	1.0	0.27	0.25	0.17	56.72	20.60	0.34	0.08
59	0.76	0.15	0.10	1.0	0.49	0.33	0.27	27.13	5.41	1.19	0.28
60	0.20	0.15	0.26	1.0	0.62	0.23	0.19	26.32	5.45	1.22	0.27
61	1.30	0.30	0.55	1.0	0.15	0.21	0.15	64.89	22.01	0.20	0.07
62	0.55	0.26	0.33	1.0	0.20	0.21	0.14	51.79	18.07	0.40	0.09
63	0.20	0.21	0.02	1.0	0.40	0.21	0.18	28.55	7.93	0.73	0.19
64	0.54	0.12	0.18	1.0	0.31	0.33	0.25	30.60	5.07	1.54	0.29
65	0.45	0.28	0.39	1.0	0.17	0.19	0.13	71.92	26.89	0.30	0.06
66	0.51	0.21	0.11	1.0	0.31	0.21	0.15	86.70	24.84	0.71	0.06
67	1.32	0.29	0.48	1.0	0.13	0.17	0.12	85.58	33.25	0.25	0.05
68	0.79	0.23	0.75	1.0	0.08	0.11	0.08	103.2	31.62	0.58	0.05
69	2.68	0.48	0.31	1.0	0.61	0.38	0.28	4.93	3.19	0.00	-
70	0.63	0.29	0.44	1.0	0.14	0.19	0.13	67.61	26.91	0.23	0.06
72	0.78	0.23	0.75	1.0	0.08	0.11	0.08	98.33	29.88	0.57	0.05
73	0.20	0.18	0.00	1.0	0.45	0.23	0.13	19.51	4.79	0.92	0.31
74	0.49	0.26	0.17	1.0	0.35	0.14	0.10	84.94	30.22	0.41	0.05
75	0.00	0.27	0.09	1.0	0.29	0.28	0.20	14.61	5.29	0.36	0.29
76	1.04	0.33	0.78	1.0	0.08	0.12	0.08	42.95	19.09	0.05	0.08
77	0.50	0.18	0.02	1.0	0.41	0.18	0.14	47.59	11.32	0.93	0.13
78	1.06	0.24	0.30	1.0	0.17	0.24	0.18	62.51	19.84	0.50	0.08
79	0.55	0.29	0.63	1.0	0.07	0.13	0.09	43.39	16.82	0.23	0.09
80	0.59	0.25	0.07	1.0	0.34	0.22	0.14	42.19	14.13	0.45	0.11
81	-	-	-	-	-	-	-	1.54	0.09	-	-
83	1.08	0.24	0.41	1.0	0.18	0.21	0.15	76.77	24.96	0.51	0.06
84	0.00	0.28	0.11	1.0	0.46	0.21	0.16	28.38	10.57	0.29	0.15
85	0.28	0.17	0.06	1.0	0.48	0.24	0.16	37.93	8.48	1.02	0.18
86	0.54	0.26	0.17	1.0	0.20	0.20	0.13	32.54	11.45	0.40	0.14
87	2.81	0.13	0.20	1.0	0.83	0.13	0.12	6.04	1.04	-	1.43
88	0.00	0.22	0.10	1.0	0.50	0.20	0.18	33.90	9.89	0.65	0.15
89	1.91	0.26	0.30	1.0	0.18	0.25	0.18	37.34	12.98	0.39	0.12
90	-	-	-	-	-	-	-	1.60	1.72	-	-
91	0.00	0.15	0.07	1.0	0.53	0.34	0.23	10.80	2.25	1.18	0.66
92	0.00	0.20	0.16	1.0	0.32	0.26	0.17	18.34	4.98	0.76	0.30
94	0.00	0.18	0.16	1.0	0.30	0.20	0.21	12.33	2.93	0.92	0.51
95	0.52	0.12	0.08	1.0	0.38	0.33	0.26	36.67	5.85	1.53	0.25
96	0.06	0.19	0.05	1.0	0.36	0.18	0.11	45.09	11.33	0.84	0.13
97	0.65	0.01	0.12	1.0	0.70	0.15	0.11	5.69	0.06	5.13	22.74
98	0.65	0.17	0.15	1.0	0.24	0.25	0.18	44.43	10.25	1.00	0.15
99	0.20	0.29	0.12	1.0	0.27	0.20	0.13	42.09	16.6	0.22	0.09
100	-	-	-	-	-	-	-	0.50	0.08	-	-
102	0.19	0.22	0.04	1.0	0.32	0.13	0.09	76.25	22.22	0.62	0.07
103	-	-	-	-	-	-	-	0.83	0.10	-	-
106	-	-	-	-	-	-	-	3.31	0.92	-	-
107	0.80	0.20	0.11	1.0	0.42	0.34	0.27	14.10	3.82	0.78	0.40
108	0.17	0.19	0.04	1.0	0.34	0.28	0.19	38.43	10.06	0.86	0.15
109	0.38	0.10	0.13	1.0	0.47	0.41	0.34	17.20	2.22	1.79	0.66
110	1.03	0.27	0.41	1.0	0.15	0.20	0.14	90.44	32.72	0.33	0.05
111	-	-	-	-	-	-	-	2.29	-	-	-
112	0.00	0.25	0.02	1.0	0.90	0.39	0.15	4.09	1.36	0.46	1.13
113	-	-	-	-	-	-	-	1.27	-	-	-
114	0.67	0.23	0.05	1.0	0.39	0.14	0.09	61.74	19.13	0.58	0.08
115	1.25	0.09	0.08	1.0	0.67	0.35	0.29	11.93	1.50	1.95	0.98
116	-	-	-	-	-	-	-	0.11	-	-	-
118	1.36	0.32	0.83	1.0	0.08	0.13	0.08	71.87	31.37	0.09	0.05
119	2.67	0.11	0.06	1.0	0.62	0.28	0.19	14.64	2.19	1.64	0.68
121	2.32	0.09	0.02	1.0	0.53	0.37	0.31	17.54	2.09	1.94	0.71
122	0.00	0.27	0.04	1.0	0.36	0.09	0.06	39.07	14.11	0.34	0.11
124	0.74	0.20	0.06	1.0	0.28	0.20	0.16	15.86	4.31	0.78	0.35
127	0.09	0.14	0.16	1.0	0.49	0.24	0.18	18.66	3.47	1.30	0.43

Continued on next page...

Table 7. Fluxes of the emission lines normalised to H α determined using GANDALF.

HRS	[OII] $\lambda 3727$	H β $\lambda 4861$	[OIII] $\lambda 5007$	H α $\lambda 6563$	[NII] $\lambda 6584$	[SII] $\lambda 6716$	[SII] $\lambda 6731$	S/N(H α)	S/N(H β)	C(H β)	σ [C(H β)]
(1)	(2)	(3)	(4)	(5)	(6)	(7)	(8)	(9)	(10)	(11)	(12)
128	-	-	-	-	-	-	-	3.85	1.12	-	-
129	-	-	-	-	-	-	-	2.27	0.94	-	-
130	0.70	0.33	0.13	1.0	0.24	0.23	0.15	33.41	14.97	0.04	0.11
132	0.95	0.26	0.46	1.0	0.06	0.06	0.20	29.76	10.51	0.40	0.15
133	0.61	0.26	0.23	1.0	0.19	0.25	0.17	52.22	17.98	0.40	0.09
134	-	-	-	-	-	-	-	3.40	-	-	-
135	-	-	-	-	-	-	-	1.50	0.45	-	-
136	-	-	-	-	-	-	-	3.16	-	-	-
137	-	-	-	-	-	-	-	0.59	1.59	-	-
139	1.11	0.30	0.39	1.0	0.15	0.07	0.32	44.84	18.46	0.19	0.09
140	-	-	-	-	-	-	-	0.19	-	-	-
141	1.55	0.20	0.03	1.0	0.50	0.17	0.11	15.95	4.23	0.78	0.36
142	0.61	0.16	0.21	1.0	0.21	0.21	0.29	33.17	7.06	1.10	0.21
143	1.16	0.24	0.44	1.0	0.21	0.22	0.15	77.62	25.61	0.51	0.06
144	0.68	0.22	0.99	1.0	0.45	0.31	0.25	69.56	20.86	0.63	0.07
145	0.94	0.28	0.27	1.0	0.18	0.19	0.12	37.50	14.37	0.28	0.11
146	2.05	0.11	0.10	1.0	0.30	0.32	0.22	32.06	4.87	1.64	0.30
147	0.00	0.10	0.00	1.0	0.52	0.53	0.41	10.66	1.51	1.79	0.98
148	0.66	0.24	0.21	1.0	0.19	0.24	0.16	44.37	14.58	0.51	0.11
149	0.81	0.05	0.02	1.0	0.39	0.22	0.19	18.50	1.22	2.79	1.20
151	0.78	0.24	0.05	1.0	0.30	0.18	0.14	21.37	6.93	0.50	0.22
152	0.63	0.24	0.10	1.0	0.42	0.17	0.13	47.67	15.20	0.52	0.10
153	0.26	0.29	0.05	1.0	0.32	0.20	0.14	40.95	16.29	0.24	0.10
154	0.81	0.32	0.16	1.0	0.20	0.19	0.12	19.25	8.24	0.09	0.19
156	-	-	-	-	-	-	-	3.82	-	-	-
157	0.60	0.26	0.18	1.0	0.25	0.19	0.13	82.53	28.81	0.41	0.05
158	1.24	0.28	0.55	1.0	0.09	0.18	0.11	43.39	16.26	0.29	0.10
159	0.30	0.11	0.05	1.0	0.45	0.21	0.21	26.25	3.93	1.65	0.38
160	0.40	0.15	0.05	1.0	0.48	0.22	0.24	25.99	5.37	1.20	0.28
161	-	-	-	-	-	-	-	2.29	1.00	-	-
162	-	-	-	-	-	-	-	2.36	2.13	-	-
163	1.48	0.05	0.25	1.0	1.30	0.75	0.69	9.62	0.63	2.79	2.32
164	-	-	-	-	-	-	-	0.42	1.74	-	-
165	0.48	0.22	0.16	1.0	0.24	0.27	0.19	54.23	15.90	0.65	0.10
166	-	-	-	-	-	-	-	0.04	1.60	-	-
167	0.13	0.14	0.03	1.0	0.46	0.23	0.16	14.76	2.70	1.30	0.55
168	0.96	0.26	0.67	1.0	0.09	0.18	0.11	74.90	26.60	0.40	0.06
169	0.69	0.25	0.28	1.0	0.34	0.22	0.23	13.43	4.48	0.44	0.34
170	1.31	0.28	0.61	1.0	1.14	0.74	0.63	7.99	3.07	0.28	0.51
171	0.44	0.22	0.05	1.0	0.31	0.19	0.12	57.81	16.87	0.65	0.09
172	0.00	0.05	0.07	1.0	0.42	0.16	0.15	19.14	1.34	2.78	1.09
173	0.67	0.13	0.18	1.0	0.79	0.43	0.33	16.36	2.78	1.41	0.53
174	-	-	-	-	-	-	-	1.17	-	-	-
175	-	-	-	-	-	-	-	0.91	1.66	-	-
177	0.66	0.18	0.10	1.0	0.33	0.15	0.35	31.74	7.79	0.93	0.19
179	-	-	-	-	-	-	-	0.06	1.25	-	-
180	-	-	-	-	-	-	-	2.81	1.70	-	-
182	0.58	0.19	0.14	1.0	0.51	0.15	0.36	22.52	5.78	0.85	0.26
183	-	-	-	-	-	-	-	1.42	1.44	-	-
184	-	-	-	-	-	-	-	3.42	-	-	-
185	0.66	0.05	0.08	1.0	0.83	0.39	0.34	7.68	0.53	2.79	2.74
187	0.32	0.25	0.15	1.0	0.28	0.20	0.16	66.19	22.00	0.45	0.07
188	0.95	0.17	0.10	1.0	0.28	0.24	0.19	21.63	5.04	1.01	0.30
189	0.27	0.25	0.07	1.0	0.25	0.20	0.13	65.45	22.18	0.44	0.07
190	1.03	0.17	0.01	1.0	0.53	0.16	0.11	15.54	3.50	0.99	0.43
191	0.69	0.26	0.37	1.0	0.22	0.26	0.19	46.28	16.32	0.39	0.10
192	0.22	0.00	0.00	1.0	0.52	0.51	0.50	6.97	-	-	-
193	1.23	0.28	0.15	1.0	0.18	0.18	0.11	50.95	19.35	0.27	0.08
194	0.72	0.19	0.18	1.0	0.25	0.26	0.17	25.65	6.51	0.85	0.23
195	-	-	-	-	-	-	-	1.46	-	-	-
196	0.78	0.28	0.26	1.0	0.19	0.17	0.11	36.53	13.86	0.29	0.11
197	0.60	0.14	0.10	1.0	0.72	0.24	0.57	18.46	3.56	1.30	0.42
198	0.55	0.28	0.16	1.0	0.24	0.27	0.20	26.72	10.06	0.29	0.16
199	0.75	0.27	0.07	1.0	0.26	0.21	0.14	52.48	18.80	0.32	0.08
201	0.59	0.10	0.04	1.0	0.51	0.24	0.20	24.29	3.12	1.79	0.47
203	1.02	0.25	0.57	1.0	0.10	0.16	0.11	119.81	39.92	0.46	0.04
204	0.72	0.29	0.01	1.0	0.42	0.18	0.14	26.95	10.62	0.24	0.15
205	0.39	0.17	0.11	1.0	0.43	0.25	0.20	38.34	8.94	1.02	0.17
206	0.47	0.21	0.02	1.0	0.30	0.16	0.11	117.75	34.12	0.71	0.04

Continued on next page...

Table 7. Fluxes of the emission lines normalised to $H\alpha$ determined using GANDALF.

HRS	[OII] $\lambda 3727$	H β $\lambda 4861$	[OIII] $\lambda 5007$	H α $\lambda 6563$	[NII] $\lambda 6584$	[SII] $\lambda 6716$	[SII] $\lambda 6731$	S/N($H\alpha$)	S/N(H β)	C(H β)	σ [C(H β)]
(1)	(2)	(3)	(4)	(5)	(6)	(7)	(8)	(9)	(10)	(11)	(12)
207	0.09	0.22	0.03	1.0	0.34	0.23	0.15	31.90	9.54	0.62	0.16
208	0.12	0.29	0.11	1.0	0.67	0.20	0.23	8.11	3.16	0.22	0.50
210	3.54	0.00	1.16	1.0	0.81	1.19	0.90	5.80	-	-	-
211	-	-	-	-	-	-	-	0.52	0.79	-	-
212	1.11	0.27	0.65	1.0	0.12	0.19	0.14	86.03	31.90	0.34	0.05
215	0.59	0.17	0.02	1.0	0.35	0.13	0.11	35.61	8.03	1.00	0.19
216	0.62	0.12	0.01	1.0	0.40	0.17	0.13	51.55	8.42	1.51	0.18
217	3.19	0.07	0.24	1.0	0.73	0.24	0.29	8.54	0.85	2.27	1.74
220	4.81	0.24	0.34	1.0	1.12	0.56	0.42	11.86	3.79	0.49	0.41
221	0.00	0.18	0.02	1.0	0.35	0.14	0.11	13.32	3.17	0.93	0.47
222	0.09	0.19	0.03	1.0	0.35	0.20	0.17	13.31	3.33	0.83	0.45
223	0.85	0.21	0.34	1.0	0.17	0.15	0.28	19.27	5.53	0.70	0.27
224	-	-	-	-	-	-	-	2.24	-	-	-
225	2.16	0.32	0.56	1.0	0.12	0.14	0.08	12.13	5.19	0.08	0.31
227	1.11	0.28	0.39	1.0	0.15	0.23	0.16	93.98	34.96	0.29	0.04
229	-	-	-	-	-	-	-	2.69	1.97	-	-
230	1.12	0.29	0.16	1.0	0.23	0.18	0.11	30.13	11.64	0.22	0.13
231	-	-	-	-	-	-	-	2.71	2.26	-	-
232	0.11	0.14	0.10	1.0	0.54	0.31	0.23	15.58	2.87	1.29	0.52
233	0.00	0.11	0.06	1.0	0.42	0.29	0.22	28.32	4.25	1.64	0.35
234	-	-	-	-	-	-	-	0.64	1.87	-	-
236	-	-	-	-	-	-	-	0.42	1.10	-	-
237	0.35	0.28	0.05	1.0	0.28	0.17	0.11	83.99	31.34	0.28	0.05
238	1.47	0.34	0.43	1.0	0.14	0.23	0.18	22.95	10.54	0.00	0.15
239	0.42	0.18	0.07	1.0	0.40	0.22	0.15	48.2	11.94	0.93	0.13
240	-	-	-	-	-	-	-	0.84	1.05	-	-
242	0.53	0.23	0.15	1.0	0.45	0.19	0.13	24.47	7.50	0.57	0.20
244	0.37	0.20	0.00	1.0	0.30	0.13	0.08	46.09	12.35	0.78	0.12
245	-	-	-	-	-	-	-	0.62	1.78	-	-
246	0.64	0.29	0.10	1.0	0.42	0.21	0.15	26.67	10.52	0.23	0.15
247	0.27	0.22	0.08	1.0	0.31	0.18	0.11	46.49	13.64	0.64	0.11
248	-	-	-	-	-	-	-	0.64	1.77	-	-
249	-	-	-	-	-	-	-	2.26	-	-	-
251	0.19	0.12	0.08	1.0	0.42	0.23	0.23	47.42	7.55	14.47	0.20
252	1.32	0.30	0.44	1.0	0.17	0.19	0.13	67.59	27.33	0.19	0.06
254	0.39	0.18	0.03	1.0	0.33	0.15	0.13	28.16	6.84	0.93	0.22
257	2.51	0.29	0.93	1.0	1.43	0.77	0.57	4.91	1.94	0.23	0.81
259	0.63	0.22	0.17	1.0	0.26	0.17	0.19	33.00	9.70	0.63	0.16
260	0.25	0.00	0.00	1.0	0.85	0.57	0.63	6.66	-	-	-
261	0.45	0.18	0.11	1.0	0.32	0.29	0.23	29.05	7.26	0.92	0.21
262	1.38	0.34	0.38	1.0	0.13	0.14	0.08	34.65	15.92	0.00	0.10
263	-	-	-	-	-	-	-	3.21	1.50	-	-
264	0.65	0.13	0.08	1.0	0.34	0.39	0.33	18.15	3.31	1.40	0.45
265	0.48	0.27	0.49	1.0	0.13	0.16	0.11	96.55	34.81	0.34	0.04
266	0.59	0.25	0.19	1.0	0.22	0.24	0.16	69.94	23.18	0.44	0.07
267	0.54	0.19	0.30	1.0	0.20	0.18	0.13	153.31	39.88	0.87	0.04
268	0.45	0.14	0.13	1.0	0.45	0.22	0.26	26.04	4.89	1.28	0.30
269	-	-	-	-	-	-	-	0.76	1.33	-	-
270	-	-	-	-	-	-	-	2.00	-	-	-
271	-	0.21	0.20	1.0	0.20	0.29	0.20	59.38	17.18	0.70	0.09
272	-	-	-	-	-	-	-	2.26	0.43	-	-
273	1.39	0.17	0.00	1.0	0.48	0.27	0.20	23.15	5.29	1.02	0.28
274	-	-	-	-	-	-	-	1.12	0.97	-	-
275	-	-	-	-	-	-	-	-	0.97	-	-
277	1.00	0.19	0.02	1.0	0.52	0.30	0.22	19.62	4.91	0.84	0.31
278	0.00	0.03	0.00	1.0	0.51	0.43	0.35	12.29	0.45	3.52	3.24
280	0.24	0.20	0.06	1.0	0.41	0.22	0.17	41.28	11.41	0.76	0.13
281	0.68	0.24	0.15	1.0	0.32	0.27	0.18	34.3	11.07	0.49	0.14
282	-	-	-	-	-	-	-	0.79	1.38	-	-
283	0.49	0.17	0.12	1.0	0.23	0.27	0.15	46.83	10.72	1.00	0.14
284	0.25	0.07	0.03	1.0	0.41	0.31	0.25	33.43	3.15	2.29	0.47
285	-	-	-	-	-	-	-	2.52	-	-	-
286	-	-	-	-	-	-	-	2.35	0.80	-	-
287	0.55	0.23	0.11	1.0	0.32	0.25	0.17	42.94	13.05	0.56	0.12
288	2.80	0.21	0.70	1.0	0.97	0.32	0.35	12.02	3.45	0.69	0.44
289	0.31	0.17	0.05	1.0	0.46	0.23	0.17	37.16	8.55	0.99	0.18
290	0.59	0.22	0.17	1.0	0.31	0.19	0.14	83.62	24.37	0.66	0.06
291	-	-	-	-	-	-	-	2.98	2.93	-	-
292	0.22	0.11	0.01	1.0	0.43	0.18	0.14	62.66	9.30	1.67	0.16

Continued on next page...

Table 7. Fluxes of the emission lines normalised to $H\alpha$ determined using GANDALF.

HRS	[OII] $\lambda 3727$	H β $\lambda 4861$	[OIII] $\lambda 5007$	H α $\lambda 6563$	[NII] $\lambda 6584$	[SII] $\lambda 6716$	[SII] $\lambda 6731$	S/N($H\alpha$)	S/N(H β)	C(H β)	σ [C(H β)]
(1)	(2)	(3)	(4)	(5)	(6)	(7)	(8)	(9)	(10)	(11)	(12)
293	0.12	0.28	0.29	1.0	0.19	0.18	0.12	108.24	40.27	0.28	0.04
294	0.21	0.20	0.09	1.0	0.31	0.29	0.20	64.20	16.93	0.80	0.09
295	-	-	-	-	-	-	-	0.56	0.65	-	-
297	1.04	0.20	0.15	1.0	0.31	0.26	0.20	35.21	9.61	0.79	0.16
298	0.68	0.25	0.23	1.0	0.26	0.15	0.10	109.33	37.28	0.47	0.04
299	1.41	0.21	0.05	1.0	0.35	0.26	0.19	23.67	6.70	0.71	0.23
300	1.42	0.11	0.20	1.0	0.66	0.47	0.38	8.45	1.28	1.66	1.16
301	0.59	0.26	0.15	1.0	0.36	0.29	0.21	19.80	6.83	0.37	0.23
302	0.95	0.22	0.18	1.0	0.18	0.24	0.16	27.70	8.40	0.63	0.18
303	0.35	0.24	0.10	1.0	0.35	0.21	0.15	121.93	40.09	0.53	0.04
304	0.43	0.12	0.00	1.0	0.44	0.29	0.21	17.59	2.74	1.52	0.54
305	1.13	0.26	0.06	1.0	0.31	0.22	0.16	49.20	17.30	0.39	0.09
308	0.20	0.24	0.20	1.0	0.21	0.27	0.20	17.02	5.59	0.50	0.28
309	1.86	0.34	0.50	1.0	0.08	0.15	0.08	25.51	11.75	0.01	0.14
310	0.39	0.20	0.05	1.0	0.38	0.22	0.17	47.31	12.64	0.77	0.12
313	0.29	0.22	0.10	1.0	0.30	0.30	0.23	26.16	7.77	0.62	0.20
314	1.27	0.29	0.51	1.0	0.12	0.16	0.11	32.60	12.71	0.23	0.12
315	0.76	0.28	0.77	1.0	0.08	0.14	0.10	94.19	35.41	0.31	0.04
317	1.08	0.20	0.21	1.0	0.28	0.25	0.16	33.74	8.93	0.77	0.17
318	0.87	0.27	0.37	1.0	0.18	0.24	0.16	81.31	29.25	0.34	0.05
319	0.71	0.25	0.29	1.0	0.24	0.25	0.19	47.61	15.81	0.45	0.10
320	1.56	0.28	0.23	1.0	0.19	0.21	0.15	35.60	13.50	0.27	0.12
321	0.74	0.27	0.19	1.0	0.26	0.20	0.15	104.18	37.28	0.32	0.04
323	1.00	0.12	0.03	1.0	0.42	0.36	0.28	31.02	4.99	1.50	0.30

Table 8. Comparison with the literature

Sample	$H\alpha + [NII]_{E.W.}_{T.W.}/H\alpha + [NII]_{E.W.}_{Lit.}$	N. obj.	$F(H\alpha + [NII]_{T.W.})/F(H\alpha + [NII]_{Lit.})$	N. obj.
All	1.16±0.90	116	1.07±0.82	191
This work	1.22±0.63	8	1.07±0.10	4
Our previous works	1.68±1.02	3	1.21±0.53	3
Kennicutt & Kent (1983) ^a	1.17±0.81	29	1.02±0.39	20
Romanishin (1990)	1.05±0.33	17	0.96±0.25	15
Sanchez-Gallego et al. (2012)	1.05±0.97	29	1.12±0.87	30

Note: ^a the Kennicutt & Kent (1983) fluxes and equivalent widths have been multiplied by a factor of 1.16 to take into account a possible contamination of telluric absorption features in the red continuum as suggested by Kennicutt et al. (1994).

Table 9. Bivariate fit of the luminosity-luminosity relations

x	y	sample	a	b	ρ	σ	N
$\log L(H\alpha)_{BD}$	$\log L(H\alpha)_{24\mu m}$	all	1.02	-1.08	0.90	0.17	152
		$\sigma[C(H\beta)] \leq 0.1$	1.16	-6.45	0.95	0.10	69
$\log L(H\alpha)_{BD}$	$\log L(20cm)$	all	1.18	-27.58	0.80	0.20	93
		$\sigma[C(H\beta)] \leq 0.1$	1.36	-34.80	0.84	0.14	46
$\log L(H\alpha)_{24\mu m}$		all	1.17	-27.09	0.89	0.15	95
		$\sigma[C(H\beta)] \leq 0.1$	1.20	-28.27	0.91	0.11	43

Note: all fits are done using only galaxies with $HI - def \leq 0.4$ (Figs. 4 and 5).

Table 10. Bivariate fit of the relations between the different star formation tracers

x	y	a	b	ρ	σ	N
$\log S FR_{H\alpha+BD}$	$\log S FR_{H\alpha+24\mu m}$	1.14	0.00	0.94	0.09	54
	$\log S FR_{radio}$	1.05	-0.03	0.84	0.13	46
	$\log S FR_{FUV+24\mu m}$	1.10	-0.08	0.87	0.11	49
$\log S FR_{FUV+24\mu m}$	$\log S FR_{H\alpha+24\mu m}$	1.10	0.08	0.97	0.07	109
	$\log S FR_{radio}$	1.00	0.03	0.88	0.13	90

Note: all fits are done using only galaxies with $HI - def \leq 0.4$. *a* determined only on galaxies with GANDALF reduced spectra and $\sigma[C(H\beta)] \leq 0.1$ (Fig. 8).

Table 11. Bivariate fit of the relations between the different $H\alpha$ and FUV attenuations

x	y	sample	a	b	ρ	σ	N	
$A(H\alpha)_{BD}$	$A(H\alpha)_{24\mu m}$	all	Calzetti et al. 2010	0.67	0.08	0.61	0.36	119
		$\sigma[C(H\beta)] \leq 0.1$		1.07	-0.15	0.55	0.24	54
		all	Calzetti et al. 2007	0.60	0.25	0.67	0.31	119
		$\sigma[C(H\beta)] \leq 0.1$		0.97	0.03	0.65	0.20	54
		all	Kennicutt et al. 2009	0.51	0.12	0.67	0.27	119
		$\sigma[C(H\beta)] \leq 0.1$		0.79	-0.05	0.65	0.18	54
$A(FUV)_{24\mu m}$	$A(H\alpha)_{24\mu m}$	all	Calzetti et al. 2010	0.65	0.09	0.86	0.21	109
		$\sigma[C(H\beta)] \leq 0.1$		0.66	0.05	0.79	0.21	49
		all	Calzetti et al. 2007	0.59	0.24	0.86	0.19	109
		$\sigma[C(H\beta)] \leq 0.1$		0.59	0.21	0.83	0.17	49
		all	Kennicutt et al. 2009	0.49	0.12	0.86	0.17	109
		$\sigma[C(H\beta)] \leq 0.1$		0.47	0.11	0.83	0.14	49

Note: all fits are done using only galaxies with $HI - def \leq 0.4$ (Fig. 7).

Table 12. The star formation rate properties as a function of the morphological type

Gas	Sample	Sa	Sab	Sb	Sbc	Sc	Scd
$\log SFR_{H\alpha}$	$HI - def \leq 0.4$	$-10.22 \pm 0.75(8)$	$-10.64 \pm 0.55(4)$	$-9.94 \pm 0.41(20)$	$-10.25 \pm 0.35(19)$	$-10.08 \pm 0.29(32)$	$-9.95 \pm 0.38(22)$
$\log SFR_{H\alpha}$	$HI - def > 0.4$	$-10.70 \pm 0.57(14)$	$-10.71 \pm 0.46(14)$	$-10.51 \pm 0.47(26)$	$-10.34 \pm 0.36(11)$	$-10.41 \pm 0.48(7)$	$-10.16 \pm 0.28(6)$

Note: mean values and standard deviations correspond to the big blue filled dots ($HI - def \leq 0.4$) and big red empty circles ($HI - def > 0.4$) in Fig. 13. For each morphological class, the number in parenthesis gives the number of objects used to determine the mean values.

Table 13. Coefficients of the scaling relations: $y = ax + b$

y	x	fit	sample	a	b	ρ	σ	N.obj
SFR_{MED}	M_{star}	linear	$HI - def \leq 0.4$	0.59	-6.10	0.64	0.30	138
		bisector		0.88	-8.84	0.64	0.29	138
	M_{star}	linear	$HI - def > 0.4$	0.58	-6.44	0.66	0.36	89
		bisector		0.90	-9.55	0.66	0.34	89
$SSFR_{MED}$	M_{star}	bisector	$HI - def \leq 0.4$	-0.79	-2.46	-0.53	0.32	138
	μ_{star}	bisector	$HI - def \leq 0.4$	-0.96	-2.49	-0.29	0.35	138
	$12 + \log(O/H)$	bisector	$HI - def \leq 0.4$	-2.00	7.20	-0.44	0.15	138

Notes: ρ is the Spearman correlation coefficient, σ the dispersion in the relations (solid lines in Figs. 12 and 14).

Table 14. Average scaling relations

y	x	sample	$\langle x \rangle$	$\langle y \rangle$	N	
$\log SFR_{MED}$	$\log M_{star}$	$HI - def \leq 0.4$	10.72 ± 0.21	0.33 ± 0.30	8	
			10.23 ± 0.15	-0.12 ± 0.51	18	
			9.76 ± 0.16	-0.37 ± 0.28	34	
			9.25 ± 0.14	-0.63 ± 0.36	59	
			8.79 ± 0.14	-0.94 ± 0.30	18	
$\log SFR_{MED}$	$\log M_{star}$	$HI - def > 0.4$	10.81 ± 0.13	-0.19 ± 0.44	11	
			10.21 ± 0.14	-0.48 ± 0.56	20	
			9.76 ± 0.16	-0.73 ± 0.31	24	
			9.29 ± 0.12	-1.09 ± 0.43	23	
			8.80 ± 0.15	-1.32 ± 0.33	11	
$\log SSFR_{MED}$	$\log M_{star}$	$HI - def \leq 0.4$	9.01 ± 0.21	-9.77 ± 0.35	52	
			9.47 ± 0.13	-10.01 ± 0.29	42	
			9.99 ± 0.14	-10.28 ± 0.38	30	
			10.58 ± 0.22	-10.33 ± 0.46	14	
			7.02 ± 0.03	-9.52 ± 0.23	4	
	μ_{star}			7.38 ± 0.15	-9.89 ± 0.36	44
				7.84 ± 0.14	-10.01 ± 0.31	52
				8.33 ± 0.12	-10.20 ± 0.50	33
				8.77 ± 0.14	-10.22 ± 0.57	5
	$12 + \log(O/H)$			8.34 ± 0.04	-9.67 ± 0.23	19
				8.52 ± 0.06	-9.88 ± 0.34	49
				8.69 ± 0.05	-10.06 ± 0.29	47
$\log SSFR_{MED}$	$\log M_{star}$	$HI - def > 0.4$	8.97 ± 0.22	-10.16 ± 0.40	20	
			9.47 ± 0.14	-10.43 ± 0.38	25	
			10.01 ± 0.15	-10.67 ± 0.47	26	
			10.64 ± 0.25	-10.86 ± 0.46	18	
			7.46 ± 0.11	-10.17 ± 0.38	15	
	μ_{star}			7.89 ± 0.13	-10.51 ± 0.39	35
				8.34 ± 0.14	-10.60 ± 0.53	27
				8.73 ± 0.13	-11.00 ± 0.42	10
	$12 + \log(O/H)$			8.38 ± 0.03	-10.08 ± 0.41	4
				8.53 ± 0.05	-10.15 ± 0.46	8
			8.69 ± 0.05	-10.25 ± 0.31	34	

Note: mean values and standard deviations for the scaling relations (big symbols in Fig. 12 and 14).